

EXPERIMENTAL INVESTIGATION OF THE THERMAL
EFFECTS OF FROST SUSCEPTIBLE SOILS

by

Zachary Allen Newell

A thesis submitted in partial fulfillment
of the requirements for the degree

of

Master of Science

in

Civil Engineering

MONTANA STATE UNIVERSITY
Bozeman, Montana

August 2005

© COPYRIGHT

by

Zachary Allen Newell

2005

All Rights Reserved

APPROVAL

of a thesis submitted by

Zachary Allen Newell

This thesis has been read by each member of the thesis committee and has been found to be satisfactory regarding content, English usage, format, citations, bibliographic style, and consistency, and is ready for submission to the College of Graduate Studies.

Dr. Robert Mokwa

Approved for the Department of Civil Engineering

Dr. Brett Gunnick

Approved for the College of Graduate Studies

Dr. Joseph Fedock

STATEMENT OF PERMISSION TO USE

In presenting this thesis in partial fulfillment of the requirements for a Master's degree at Montana State University – Bozeman, I agree that the library shall make it available to borrowers under rules of the Library.

If I have indicated my intention to copyright this thesis by including a copyright notice page, copying is allowable only for scholarly purposes, consistent with “fair use” as prescribed in the U.S. Copyright Law. Request for permission for extended quotation from or reproduction of this thesis in whole or in parts may be granted only by the copyright holder.

Zachary Allen Newell

August 2005

ACKNOWLEDGEMENTS

First, I would like to express my utmost appreciation to my father Jim, and my sister Kristin, who have so patiently supported me throughout this merciless endeavor. I would also like to express my deepest appreciation to Dr. Bob Mokwa for his undying faith in me. His encouragement and guidance truly made a very significant impact on my completion of this work.

I would also like to thank Susan Gallagher, Steve Albert, and Suzy Lassacher at the Western Transportation Institute (WTI) for the fellowship and opportunity to complete a Master's program. I would like to thank Wes Harms for his help with the construction of the laboratory-testing device, the use of his tools, and the many hours he devoted to helping with this project. I would also like to thank Renee Hecox in the Department of Civil Engineering, and all those who participated in one way or another, or simply encouraged me along the way.

Lastly, and most importantly, I thank the Good Spirit for keeping my head above water through these most trying times in my life. I miss you very much Mom, and thank you for giving me the strength and courage I needed to get the job done!

TABLE OF CONTENTS

1. INTRODUCTION	1
BACKGROUND	1
FROST ACTION	2
FROST HEAVE	2
INTRODUCTION TO THE SEGREGATION POTENTIAL CONCEPT	4
COMPRESSIBILITY.....	6
SCOPE OF WORK	8
Objectives	8
Experimentation.....	8
Analytical Study.....	9
2. LITERATURE REVIEW	10
INTRODUCTION.....	10
MECHANICS OF FROST HEAVE.....	10
Introduction.....	10
General Observations.....	11
Ice Lens Formation	14
Mass Transfer.....	16
Heat Transfer	18
SEGREGATION POTENTIAL CONCEPT	21
Introduction.....	21
Background.....	22
Fundamental Characteristics of a Freezing Soil	25
Calculation of SP	26
Conclusions.....	29
SUMMARY OF LITERATURE	30
3. EXPERIMENTAL METHODS.....	32
INTRODUCTION.....	32
FIELD FROST HEAVE TEST FACILITY	32
Facility Location	32
Construction of Facility	33
Data Collection	39
LABORATORY FREEZE-THAW TESTS.....	41
Experimental Setup.....	41
Equipment Description	41

TABLE OF CONTENTS - CONTINUED

Soil Test Cylinder	41
Mariotte Tube.....	42
Boundary Conditions	42
Instrumentation and System Controls.....	48
Sample Preparation	49
Data Collection	50
Thaw Process	51
LABORATORY INDEX TESTING	51
Silt-Clay Composition	51
Discussion	52
Post Farm Lean Clay.....	54
Discussion	54
Summary	56
4. EXPERIMENTAL RESULTS.....	58
INTRODUCTION.....	58
EXPERIMENTAL TEST RESULTS	58
Field Frost Heave Test Facility.....	58
Discussion	64
Laboratory Freeze-Thaw Tests	65
Example	66
Results.....	72
Discussion	74
5. PREDICTIVE FROST HEAVE MODEL	81
INTRODUCTION.....	81
THE SSR FROST HEAVE MODEL.....	81
Background.....	81
Heat Balance Equation.....	83
THE SP MODEL	86
Objective	86
Procedure	86
Temperature Profiles.....	87
Temperature Gradient	88
Frost Front.....	90
Water Uptake	92
Heave	92

TABLE OF CONTENTS - CONTINUED

Thermal Conductivity	93
Segregation Potential	93
Numerical Model Application	95
Development of a Predictive Model	95
Discussion	100
6. SUMMARY, CONCLUSIONS AND RECOMMENDATIONS.....	103
SUMMARY	103
CONCLUSION	104
RECOMMENDATIONS FOR CONTINUED RESEARCH	106
Improvements to the Field Facility	106
Laboratory Testing Procedures	108
Interpretation of the Results.....	110
REFERENCES CITED.....	111
APPENDICES	113
APPENDIX A: COMPLETE RESULTS FROM THE FIELD FROST HEAVE TEST FACILITY	114
APPENDIX B: COMPLETE RESULTS FROM THE LABORATORY FREEZING TESTS	121

LIST OF TABLES

Table	Page
3.1: 80% Silt – 20% Clay Geotechnical Parameters.....	51
3.2: Post Farm Clay Geotechnical Parameters.....	54
4.1: Laboratory Frost Heave Test Schedule.....	73
4.2: Results.....	73
B.1: Laboratory Frost Heave Testing Schedule.....	122
B.2: Results to the Laboratory Frost Heave Testing Schedule	122

LIST OF FIGURES

Figure	Page
1.1: Distribution of temperature and pressure during ice lens formation (Konrad and Morgenstern, 1981).....	4
1.2: Schematic cross-section of roadway during spring thaw (modified from Konrad and Roy, 2000).....	7
2.1: Temperature conditions associated with ice lens formation (Konrad and Morgenstern, 1980).....	13
2.2: The mechanism of ice lens formation (Konrad and Morgenstern, 1980).....	15
2.3: Equations for the one-dimensional frost heave model (Konrad and Morgenstern, 1980).....	20
2.4: Calculated SP values using volume and DCDT measurement methods (Konrad, 1987).....	28
3.1: Excavation of field frost heave test facility.....	33
3.2: Fiberglass trough in bottom of excavation.....	33
3.3: Dual tank water supply system.....	34
3.4: Float switch mounted in stock water tank.....	35
3.5: All-weather insulated shelter.....	36
3.6: Construction of the telltale and reference beams during the backfilling of the soil mass.....	37

LIST OF FIGURES - CONTINUED

Figure	Page
3.7: Sand cone density tests being performed throughout the backfilling of the soil mass	37
3.8: Plan and profile views of the instrumentation and telltale construction at the field frost heave test facility	38
3.9: Photographs of the operational frost heave test facility during the winter of 2004	39
3.10: Schematic illustrating the completed field frost heave test facility	40
3.11: Schematic illustrating the laboratory frost heave testing device	43
3.12: Schematic illustrating the Mariotte tube and interaction with the water reservoir	44
3.13: Temperature profile illustrating a laboratory freeze test without the use of the warm-end boundary control	45
3.14: Temperature profile illustrating a laboratory freeze test with the use of the warm-end boundary control.....	45
3.15: Photograph of laboratory testing device connected to the circuit bridge	46
3.16: Photograph of insulated laboratory testing cylinder placed on the warm plate inside of the cold chamber	46

LIST OF FIGURES - CONTINUED

Figure	Page
3.17: Photograph of steel cover plate and the linear variable displacement transducer (LVDT).....	47
3.18: Graphical illustration showing the effectiveness of fiberglass insulation on the sidewall of the testing cylinder.....	48
3.19: Graphical illustration of modified proctor compaction curve for the S80K20 composition.....	52
3.20: Graphical illustration of the thermal conductivity of the S80K20 composition.....	53
3.21: Graphical illustration of modified proctor compaction curve for the Post Farm clay.....	55
3.22: Graphical illustration of the thermal conductivity for the Post Farm clay.....	56
4.1: Graphical illustration of piezometer readings taken at the field facility.....	59
4.2: Graphical illustration of water content profiles for the Post Farm lean clay.....	59
4.3: Graphical illustration of cumulative water uptake at the field facility during 2003 – 2004 winter season.....	61
4.4: Graphical illustration of temperature profiles for various instrument embedment depths at the field facility.....	61

LIST OF FIGURES - CONTINUED

Figure	Page
4.5: Graphical illustration of the location of the frost front at the field facility	62
4.6: Graphical illustration of maximum and minimum air temperatures compared to ground surface temperatures at the field facility.....	62
4.7: Graphical illustration of telltale readings for various embedment depths at the field facility.....	63
4.8: Graphical illustration of temperature distributions during freezing Test #1.....	67
4.9: Graphical illustration of the frost front location throughout freezing Test #1.....	68
4.10: Graphical illustration of water uptake and volumetric heave measurements for freezing Test #1	70
4.11: Graphical illustration of overall temperature gradient throughout soil column during freezing Test #1	70
4.12: Graphical illustration of calculated SP values for freezing Test #1	71
5.1: Graphical illustration of temperature distributions throughout the soil column during freezing Test #4	88
5.2: Graphical illustration of overall temperature gradient throughout the soil column during freezing Test #4	89

LIST OF FIGURES - CONTINUED

Figure	Page
5.3: Graphical illustration of overall temperature gradient throughout the soil column during freezing Test #1	90
5.4: Graphical illustration of the frost front location throughout various freezing tests	91
5.5: Graphical illustration of heave and water uptake measurements during freezing Test #2	92
5.6: Graphical illustration of calculated thermal conductivity values for freezing Test #4.....	94
5.7: Graphical illustration of calculated SP values for various freezing tests	94
5.8: Tabulated illustration of soil temperature profiles of the field facility.....	96
5.9: Tabulated illustration of calculated incremental heave rates using a predictive numeric model	97
5.10: Tabulated illustration of calculated magnitudes of heave using a predictive numeric model	98
5.11: Graphical illustration of heave and settlement behavior observed at the field facility during 2003-2004 freeze/thaw season.....	99
5.12: Graphical illustration of calculated heave and settlement activity using a predictive numeric model.....	100

LIST OF FIGURES - CONTINUED

Figure	Page
A.1: Schematic illustrating the completed field frost heave test facility	115
A.2: Plan and profile views of the instrumentation and telltale construction at the field frost heave test facility	116
A.3: Graphical illustration of piezometer readings taken at the field facility	117
A.4: Graphical illustration of water content profiles for the Post Farm lean clay	117
A.5: Graphical illustration of cumulative water uptake at the field facility during 2003 – 2004 winter season	118
A.6: Graphical illustration of temperature profiles for various instrument embedment depths at the field facility	118
A.7: Graphical illustration of the location of the frost front at the field facility	119
A.8: Graphical illustration of maximum and minimum air temperatures compared to ground surface temperatures at the field facility.....	119
A.9: Graphical illustration of telltale readings for various embedment depths at the field facility.....	120
A.10: Graphical illustration of in-place moist density results of the backfilled soil mass at the field facility	120

LIST OF FIGURES - CONTINUED

Figure	Page
B.1: Schematic illustrating the laboratory frost heave testing device.....	123
B.2: Graphical illustration of temperature distributions throughout freezing Test #1.....	124
B.3: Graphical illustration of overall temperature gradient throughout freezing Test #1.....	124
B.4: Graphical illustration of the frost front location throughout freezing Test #1.....	125
B.5: Graphical illustration of volumetric heave and water uptake measurements throughout freezing Test #1	125
B.6: Graphical illustration of calculated thermal conductivity values for freezing Test #1.....	126
B.7: Graphical illustration of calculated SP values for freezing Test #1	126
B.8: Graphical illustration of temperature distributions throughout freezing Test #2.....	127
B.9: Graphical illustration of overall temperature gradient throughout freezing Test #2.....	127
B.10: Graphical illustration of the frost front location throughout freezing Test #2.....	128

LIST OF FIGURES - CONTINUED

Figure	Page
B.11: Graphical illustration of volumetric heave and water uptake measurements throughout freezing Test #2	128
B.12: Graphical illustration of calculated SP values for freezing Test #2.....	129
B.13: Graphical illustration of temperature distributions throughout freezing Test #3.....	129
B.14: Graphical illustration of overall temperature gradient throughout freezing Test #3.....	130
B.15: Graphical illustration of the frost front location throughout freezing Test #3.....	130
B.16: Graphical illustration of volumetric heave and water uptake measurements throughout freezing Test #3	131
B.17: Graphical illustration of calculated SP values for freezing Test #3.....	131
B.18: Graphical illustration of temperature distributions throughout freezing Test #4.....	132
B.19: Graphical illustration of overall temperature gradient throughout freezing Test #4.....	132
B.20: Graphical illustration of the frost front location throughout freezing Test #4.....	133

LIST OF FIGURES - CONTINUED

Figure	Page
B.21: Graphical illustration of calculated thermal conductivity values for freezing Test #4.....	133
B.22: Graphical illustration of temperature distributions throughout freezing Test #5.....	134
B.23: Graphical illustration of overall temperature gradient throughout freezing Test #5.....	134
B.24: Graphical illustration of the frost front location throughout freezing Test #5.....	135
B.25: Graphical illustration of volumetric heave and water uptake measurements throughout freezing Test #5	135
B.26: Graphical illustration of calculated thermal conductivity values for freezing Test #5.....	136
B.27: Graphical illustration of calculated SP values for freezing Test #5.....	136
B.28: Graphical illustration of temperature distributions throughout freezing Test #6.....	137
B.29: Graphical illustration of overall temperature gradient throughout freezing Test #6.....	137
B.30: Graphical illustration of calculated thermal conductivity values for freezing Test #6.....	138

LIST OF FIGURES - CONTINUED

Figure	Page
B.31: Graphical illustration of volumetric heave measurements throughout freezing Test #6.....	138
B.32: Graphical illustration of temperature distributions throughout freezing Test #7.....	139
B.33: Graphical illustration of overall temperature gradient throughout freezing Test #7.....	139
B.34: Graphical illustration of the frost front location throughout freezing Test #7.....	140
B.35: Graphical illustration of volumetric heave and water uptake measurements throughout freezing Test #7	140
B.36: Graphical illustration of calculated thermal conductivity values for freezing Test #7.....	141
B.37: Graphical illustration of calculated SP values for freezing Test #7	141

LIST OF SYMBOLS

C	Volumetric heat capacity
CL	USCS classification for lean (low-plasticity) clay
d	Thickness of the frozen fringe
dh/dt , or dh_s/dt	Segregational/incremental frost heave rate
dz/dt , or \dot{X}	Frost penetration rate
e_{\min}	Minimum void ratio
e_{\max}	Minimum void ratio
ε	Proportional constant accounting for unfrozen water in soil pores (dimensionless)
G_s	Specific gravity of solids
$\text{grad}T$, $\text{grad}T_f$, or $\delta T/\delta y$	Thermal gradient across the frozen fringe
$\text{grad}T_+$	Thermal gradient across unfrozen soil region
$\text{grad}T_-$	Thermal gradient across frozen soil region
$h_s(t)$	Magnitude of segregational heave
k	Saturated hydraulic conductivity (permeability) of soil
k_f	Overall hydraulic conductivity (permeability) of the frozen fringe
k_u	Overall hydraulic conductivity (permeability) of the unfrozen soil region
k_t , k_T , or λ	Thermal conductivity
l_u	Length of unfrozen soil region
L_f	Latent heat of fusion of pure water
LL	Liquid Limit

LIST OF SYMBOLS - CONTINUED

ML	USCS classification for low-plasticity sil
n	Soil porosity
P_i	Pressure in the ice lens
P_u	Suction pressure at the frost front (frozen-unfrozen interface)
P_w	Suction pressure at the ice lens (average suction across the frozen fringe)
P.F.	Post Farm
PI	Plasticity Index, LL - PL
PL	Plastic Limit
q/A	Heat flux, where A is the sample area
Q	Internal heat generation term
R_{fz}	Total thermal resistance of the frozen layers
ρ_d	Dry density of soil
ρ_{dmax}	Modified Proctor maximum dry density
S	Saturation level
S80K20	80% silt, 20% kaolinite clay composition (by weight)
SP	Segregation Potential
T_c	Cold-end boundary temperature (ambient)
T_f , or T_i	Freezing temperature of the soil at the frost front (warmest temperature ice can grow within soil pores)
\dot{T}_f	Rate of cooling across the frozen fringe
T_o	Freezing temperature of pure water
T_p	Ground surface temperature

LIST OF SYMBOLS - CONTINUED

T_s	Segregation freezing temperature at the ice lens
T_w	Warm-end boundary temperature (geothermal gradient)
USCS	Unified Soil Classification System
$v_u, v(t)$	Water intake velocity (water migration rate)
V_f	Specific volume of water
V_i	Specific volume of ice
w	Soil water content
w_{opt}	Modified Proctor optimum water content
X	Thickness of frozen soil region
z_i	Thickness of the frozen layer
z^*	Weighted value of depth to frost penetration
Δz_0	Increase in frost penetration rate

ABSTRACT

Damages to engineering structures attributed to frost action of subgrade soils amounts to millions of dollars annually. Theoretical research has been conducted to examine the details of the frost action phenomenon since the 1940's. However, a reliable and practical approach for evaluating the frost susceptibility of soils is nonetheless a goal that has eluded engineers and scientists alike. The research presented herein focuses on the procedures necessary to obtain a numerical model capable of predicting the thermal response of frost susceptible soils.

A field facility was designed and constructed with the purpose of measuring and comparing in-situ frost heave characteristics with laboratory-scale test results. A laboratory-testing device was also designed, constructed, and instrumented in order to measure the thermal response of various soil types in a controlled freezing environment. Geotechnical index testing was conducted on the soil types used in the freezing experiments to fully characterize the soils and examine potential correlations between common soil index properties and frost action behavior.

The results of the first season of experimentation provided the framework for a testing protocol necessary for the development of a predictive numerical model. The data obtained from the laboratory tests was used to calculate a new engineering parameter called the segregation potential (SP), which was used as an input into the numerical model developed throughout this research. The model simulated the freezing and thawing characteristics of the soil type found at the field facility. The simulated results were then compared to the in-situ frost action behavior observed at the facility.

An improved testing protocol is necessary to obtain more accurate and consistent results. As this research progresses and laboratory testing proceeds, a more extensive database will be acquired and used to build empirical correlations between the thermal and geotechnical index properties of frost susceptible soils. Furthermore, continued research will allow for the advancement of a predictive numerical model that design engineers could use to simulate and predict the freezing and thawing effects of frost susceptible soils incorporated into common engineering structures.

CHAPTER 1

INTRODUCTION

Background

Damage to highways and structures supported on shallow foundations within the northern regions of the United States and Canada has become economically more significant as traffic frequency and cost of infrastructure continue to rise. The phenomenon known as frost action occurring below these structures is responsible for significant long-term maintenance problems within regions in which seasonal and perennial freezing occurs.

Since the 1940's, theoretical research ranging from experimental investigation to the development of complex thermodynamic models has been conducted in order to examine the details of the frost action phenomenon. The research herein indicates that despite the abundant history of quality research, a reliable and practical approach for evaluating the frost susceptibility of soils is nonetheless an elusive goal. Furthermore, the ability to effectively predict the magnitude of strength reduction, heave, and compressibility (settlement) of soils exposed to frost action has eluded scientists and engineers alike. The shortcomings in these design methodologies can be attributed to the physical and geomorphologic mechanisms that occur when a heterogeneous mass of soil and water is exposed to repeated cycles of freezing and thawing (Mokwa, 2002).

Frost Action

Perennially and seasonally frozen ground is widely distributed and covers approximately 50% of the earth's landmass, and approximately 30% of the United States (Williams and Smith, 1989). The entire state of Montana can be categorized as a cold climate region subject to continual freeze-thaw cycles.

Catastrophic failures of engineering structures such as buildings, bridges, embankments, and roadways are fortunately quite rare. However, damage to these structures attributed to frost action is readily apparent in many parts of North America. For example, maintenance costs on highways in the United States and Canada alone is estimated to amount to millions of dollars annually (Holtz and Kovacs, 1981).

Early studies by Casagrande (1932), and others focused on identifying conditions in which frost action may occur, and characterizing soils that may be frost susceptible. The results of their research suggest the following three basic guidelines for identifying conditions susceptible to frost action:

- 1) Temperatures below freezing.
- 2) Source of groundwater close enough to allow for capillary action.
- 3) Frost susceptible soil based on grain size distribution.

Frost Heave

Frost formation occurs in soils as temperatures drop below 0 °C. Water within the soil mass experiences a 9% volumetric increase as a result of the water-to-ice phase transformation (Konrad, 1987). Lenses of frozen water forming above the water table

draw additional moisture upward via capillary forces to the frost front, in turn freezing and expanding the migrating water supply. The displacement of the heterogeneous soil and water mass is a process known as *frost heave*. The depth of frost penetration and magnitude of heave are dependent on factors such as soil type, soil permeability and thermal conductivity, water content, and climatic conditions. In and around Bozeman, Montana, the maximum depth of frost ranges from approximately 0.6 to 1.0 m.

Total frost heave occurring within a soil mass is the combination of two processes. First is the heave associated solely with expansion of freezing pore water in the soil voids. The additional displacement is attributed to a phenomenon known as *ice segregation*, which describes the basic mechanism that occurs as in-situ pore water is drawn from unfrozen soil to the freezing front where ice lenses are formed (Konrad and Morgenstern, 1981). The heave resulting from ice segregation is considerably greater than that of pore water expansion.

As frost susceptible soil freezes, ice lenses form as the advancing frost front migrates downward. These ice lenses are typically lenticular in shape and are oriented roughly parallel to the isothermal freezing surface (Farouki, 1981). The heave rate is a function of heat loss, water flow rate to the growing ice lens, and the compressibility characteristics of the unfrozen soil. This coupled process between heat and moisture flow is further complicated because the thermal and hydraulic properties of water, ice, and soil minerals are dependent functions of temperature, degree of saturation, and effective stress (Mokwa et al, 2004).

Introduction to the Segregation Potential Concept

Various models have been developed in an attempt to couple the heat and mass flow processes that are attributed to one-dimensional frost heave and compressibility theory. This research involved the investigation of several models, however, ultimately focusing on one in particular known as the *segregation potential* (SP) theory, proposed by Konrad and Morgenstern (1981). The SP theory is conceptually summarized in Figure 1.1.

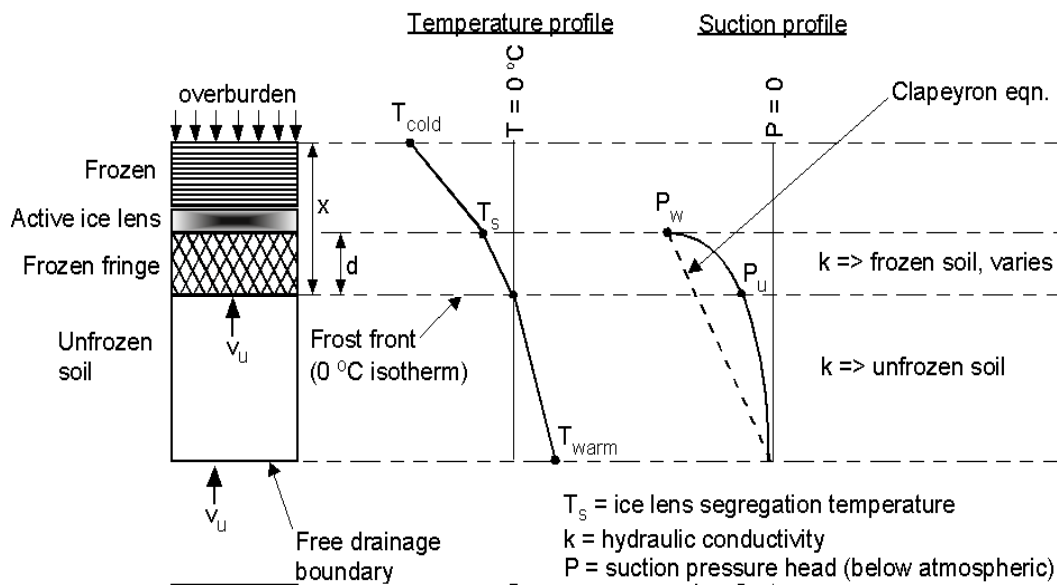


Figure 1.1: Distribution of temperature and pressure during ice lens formation (Konrad and Morgenstern, 1981)

The segregation potential (SP) is an engineering parameter proposed by Konrad and Morgenstern (1980) which encompasses common thermal and hydraulic properties of a specific soil type and matrix in an attempt to generally correlate its frost susceptibility with more commonly known geotechnical index parameters. Past research has shown

that frost susceptible soils generally include fine-grained materials such as silts and clays. Though frost susceptibility can be qualitatively described, quantitative description has deemed extremely difficult. For this reason, the SP parameter was introduced to compare easily measurable characteristics that specific soil types demonstrate under freezing and thawing conditions to their respective and well-defined index properties. These properties include liquid limit, plasticity index, specific gravity, permeability, etc. Konrad and Morgenstern (1980, 1981, and 1987) define SP as the ratio of water intake velocity ($v(t)$) to the temperature gradient across the frozen fringe ($gradT$). It can also be mathematically expressed as:

$$v(t) = \frac{P_w(t) - P_u(t)}{d(t)} k_f(t) = \left(\frac{P_w(t) - P_u(t)}{T_s} k_f(t) \right) gradT = SP * gradT \quad (\text{Eq 1.1})$$

Therefore,

$$SP = \frac{v(t)}{gradT} \quad (\text{Eq 1.2})$$

where P_w is the suction pressure at the ice lens, P_u is the suction at the frost front, k_f is the overall hydraulic conductivity within the frozen fringe, d is the thickness of the frozen fringe, T_s is the segregation freezing temperature, and t is time.

The SP can then be used to calculate the segregational (incremental) frost heave rate (dh/dt) as:

$$\frac{dh}{dt} = \frac{1.09SP(T_f - T_p)}{z_i} \quad (\text{Eq 1.3})$$

where z_i is the depth to the frost front, T_f is the freezing temperature of soil at z_i , and T_p is the surface temperature. The coefficient 1.09 accounts for the 9% volumetric increase as water is transformed into the ice phase. The total heave can be found by integrating the incremental heave rate over the entire depth of the frost zone.

The primary benefit of the segregation potential theory is that the SP parameter is dependent upon values easily obtained in a laboratory environment. Furthermore, the overall characteristics in the frozen fringe can be determined without detailed measurements of thermodynamic and hydraulic properties. The segregation potential theory will be further discussed in Chapters 2 and 5.

Compressibility

Compressibility characteristics of soils are an important engineering consideration for the design of roadway pavement sections, slabs, and foundations. Engineers often use elasticity methods for estimating the compression of cohesionless soils, and Terzaghi's consolidation theory for estimating time rate settlements of cohesive soils (Mokwa, 2002). However, the mechanical properties of subgrade soils can be greatly affected by seasonal fluctuations in soil temperature and moisture content, further exacerbating the difficulties in estimating an appropriate compressibility modulus for a given design application.

As temperatures increase in the springtime, thawing commences from above and below the frozen layer of a frost susceptible soil. Take for example the typical roadway section illustrated in Figure 1.2. The snow that collects on either side of the roadway

embankment acts as an insulating layer, reducing the rate of thaw directly beneath. The water that is released from its frozen state within the thaw zone may not effectively drain because the surrounding frozen ground is relatively impermeable. As the water becomes trapped, the subgrade soil is temporarily saturated, ultimately reducing the bearing capacity (strength) of the soil for supporting traffic loads. This process is commonly referred to as *thaw weakening*. During spring thaw, paved roadways over frost susceptible soils may experience a loss of 50% or more of the normal bearing capacity, while gravel-surfaced roads may experience losses in excess of 70% (C-SHRP, 2000).

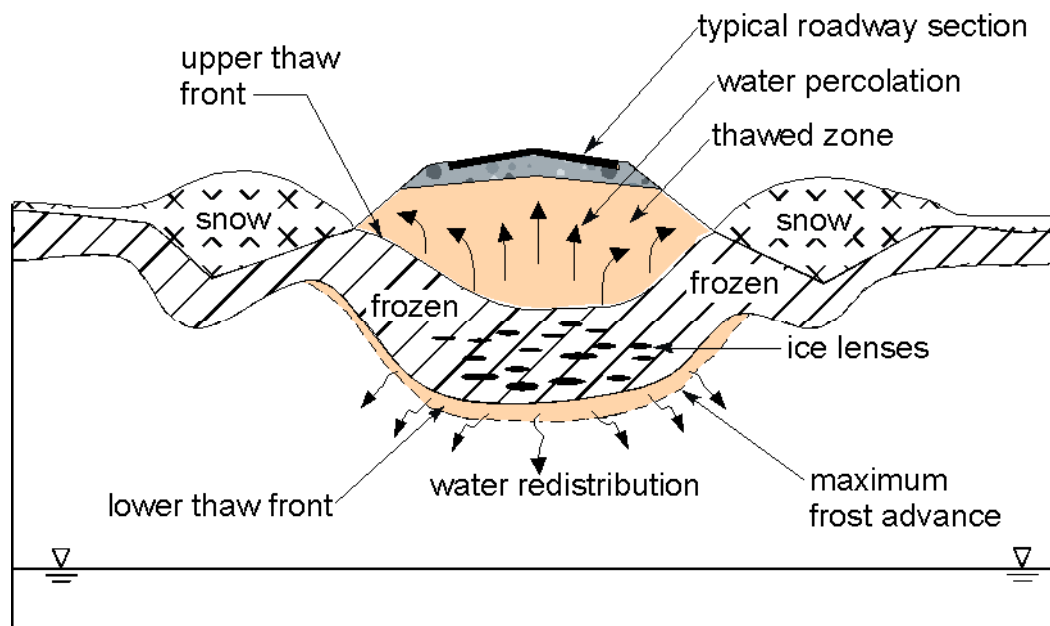


Figure 1.2: Schematic cross-section of roadway during spring thaw (modified from Konrad and Roy, 2000).

Scope of Work

Objectives

The primary objectives of this research are to evaluate heave and thaw-weakening characteristics of regional soils subjected to freezing conditions, and to develop improved methods towards the development of a practical model to predict the effects of heave and settlement in frost susceptible soils.

Experimentation

This thesis focuses on the experimental research that is currently underway at Montana State University to better quantify frost action characteristics of frost susceptible soils common to the state of Montana and similar cold climate regions of the United States. The research includes the construction of a fully instrumented field frost heave test facility, which will allow for the continual collection of seasonal data pertinent to the development of a sufficient database for future research. Furthermore, a laboratory device was designed, constructed, and modified in order to conduct numerous freezing tests on various soils in an environmental chamber at Montana State University's cold regions experimental facility.

Geotechnical index testing was conducted on the various soils exposed to the laboratory freezing experiment in order to examine the correlations between frost susceptibility and common geotechnical properties of soils.

Analytical Study

Following the data collection process from the field frost heave test facility, the laboratory experimentation, and the geotechnical index testing, an analytical study was conducted by applying parameters developed using the segregation potential concept proposed by Konrad and Morgenstern (1981). Ultimately, the objective of this study was to establish the framework towards a model that could predict and quantify the magnitude of heave and settlement in frost susceptible soils.

CHAPTER 2

LITERATURE REVIEW

Introduction

The first section in this chapter discusses the fundamental mechanisms behind the frost heave theory and the difficulties associated with applying a theoretical model to practical engineering problems associated with frost heave behavior. The second section discusses the development of a new engineering parameter called the segregation potential (SP), which may have applications in a potentially reliable and practical method of relating the thermal aspects of a frost susceptible soil to its respective geotechnical index parameters. The final section summarizes some of the other literature reviewed throughout this research.

Mechanics of Frost Heave

Introduction

It is common knowledge that the susceptibility for heave of a soil under freezing conditions is affected by characteristics such as grain size distribution, accessibility to a water source, freezing rate, and magnitude of applied loads. A practical theory of frost heave would allow engineers and scientists to predict both the magnitude and rate of heave for different soil types. This theory would be based on common geotechnical index properties, knowledge of the soil profile (based on the moisture content

distribution), the thermal conductivity, and the boundary conditions - which are largely responsible for the rate at which the frost front advances into the soil.

Past research on frost heave of soils has generally fallen into one of the following three categories:

- 1) Index tests to establish degree of frost susceptibility of soils
- 2) Fundamental thermodynamic analyses
- 3) Empirical studies attempting to quantitatively relate laboratory investigations to field performance (Konrad & Morgenstern, 1980).

Recent literature has reported attempts to combine heat and mass flux in a coupled process; however, predictive results from these studies have not proven to be convincing. The inability to obtain highly accurate measurements of temperature, unfrozen water content, and permeability of frozen soil has steered designers away from a coupled mechanistic theory. One goal of this study is to demonstrate that unique frost heave characteristics of certain soil types can be predicted from controlled laboratory experiments, and that these characteristics constitute input parameters that would be used in a generalized predictive model for solving frost heave problems.

General Observations

A considerable amount of research has been devoted to the process of frost heave over the last sixty years. However, obtaining a practical and reliable theory of this phenomenon is yet an elusive goal. In turn, the ability to complete a rational design on structures such as buried pipelines and highway road embankments in regions where heave predictions are required has proved to be less than consistent. Nevertheless,

common knowledge of the subject matter encompasses three basic requirements that increase the likelihood of frost heave in subgrade soils:

- 1) Rate of freezing
- 2) Source of water
- 3) Frost susceptibility of soil based on grain size distribution

As freezing temperatures are applied to the surface of a soil sample, an unsteady heat flux is initiated. The frost front progresses downward into the soil and ice crystals begin to grow in the direction of heat loss. As the ice crystals continue to form, they develop into ice lenses, which apply pressure to all restraining boundaries. This pressure is relieved in the form of heave in the direction of least resistance (Konrad and Morgenstern, 1980).

Heave resulting from the freezing of in situ water contributes to only a small percentage of the total heave in a frost susceptible soil sample. Past research has shown that liquid water exists as a film on the surfaces of soil particles that are in equilibrium with the ice lenses at temperatures below freezing. Furthermore, thermodynamic principles ascertain that the thermodynamic potential energy of the unfrozen water films decreases as temperatures become more negative. Suction (negative) pressures develop in the frozen zone as a consequence of the temperature gradient, and water migrates from the unfrozen soil into the frozen zone where it freezes behind the frost front (Konrad and Morgenstern, 1980).

The area of soil between the growing ice lens and the unfrozen soil layer has been referred to as the *frozen fringe*. This is illustrated (along with the associated temperature

conditions) in Figure 2.1. The temperature at the base of the ice lens has been designated as T_s , the *segregation freezing temperature*. The in situ freezing temperature, T_i , is the warmest temperature at which ice can grow within the soil pores. Experimental data provided in a study by Konrad and Morgenstern (1980) conclude that the flow of water through the frozen fringe is continuous as it migrates towards the ice lens. Furthermore, the ice lens acts as an impervious barrier, trapping water at the base of the frozen fringe, thus continuing the advancement of the ice lens as in situ water freezes.

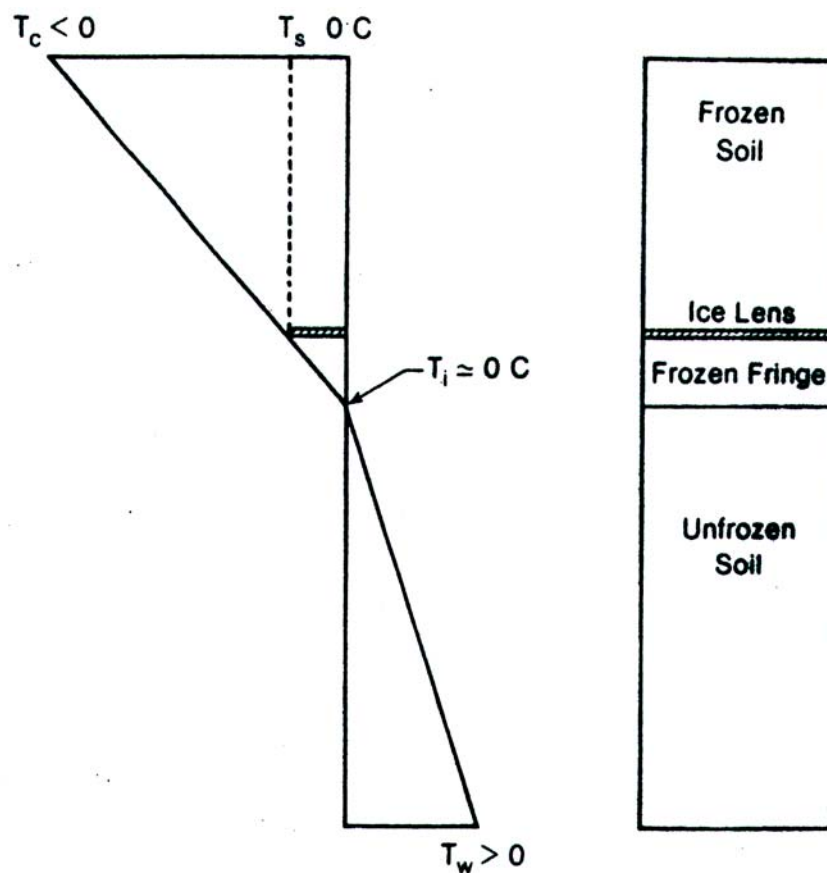


Figure 2.1: Temperature conditions associated with ice lens formation (Konrad & Morgenstern, 1980).

The entire freezing system can be separated into a passive and active system, with regard to mass transfer. The passive system is defined as the zone of frozen soil between the ground surface and the ice lens. Consequently, the active system is made up of the frozen fringe and unfrozen soil layer. As a result of very low frozen soil permeabilities, water migration throughout the passive system is considerably less than that in the active zone. Therefore, the contribution of the passive zone to the total heave has been observed to be negligible in both laboratory and field conditions (Konrad and Morgenstern, 1980).

Ice Lens Formation

Konrad and Morgenstern (1980 and 1981) proposed that the frost front advances continuously during unsteady heat flow throughout the soil – liquid – ice composition, and properties such as suction and permeability vary with temperature changes throughout the profile.

At the onset of freezing conditions, the rate at which the frost front advances downward is relatively high. Water migrating upwards through the soil profile is drawn into an *accumulation zone*, and consequently thickens the layer of unfrozen water surrounding the soil particles. The thickness of the unfrozen water films within the accumulation zone remains constant for a given temperature as some of the incoming water is frozen, thus achieving equilibrium within the system. The rate at which the frost front progresses is high enough that water cannot accumulate fast enough at a given level to produce a continuous ice lens. Therefore, assuming that accumulation of water occurs only above the frozen fringe, a nonlinear suction profile is developed within the fringe

due to the decreasing permeability of the frozen soil as the temperature decreases. This relationship is illustrated in Figure 2.2. In the presence of a discontinuous ice lens, freezing occurs in a segregated pattern at the top of the soil column in response to the zone of least resistance. In turn, heave occurs locally in a nonhomogeneous manner, causing the ice matrix to strain at the top of the frozen fringe. It is assumed that high strains are developed in the ice lens only in the zone near the top of the fringe, and that the rest of the ice is essentially unaffected. Under these conditions (during the initial

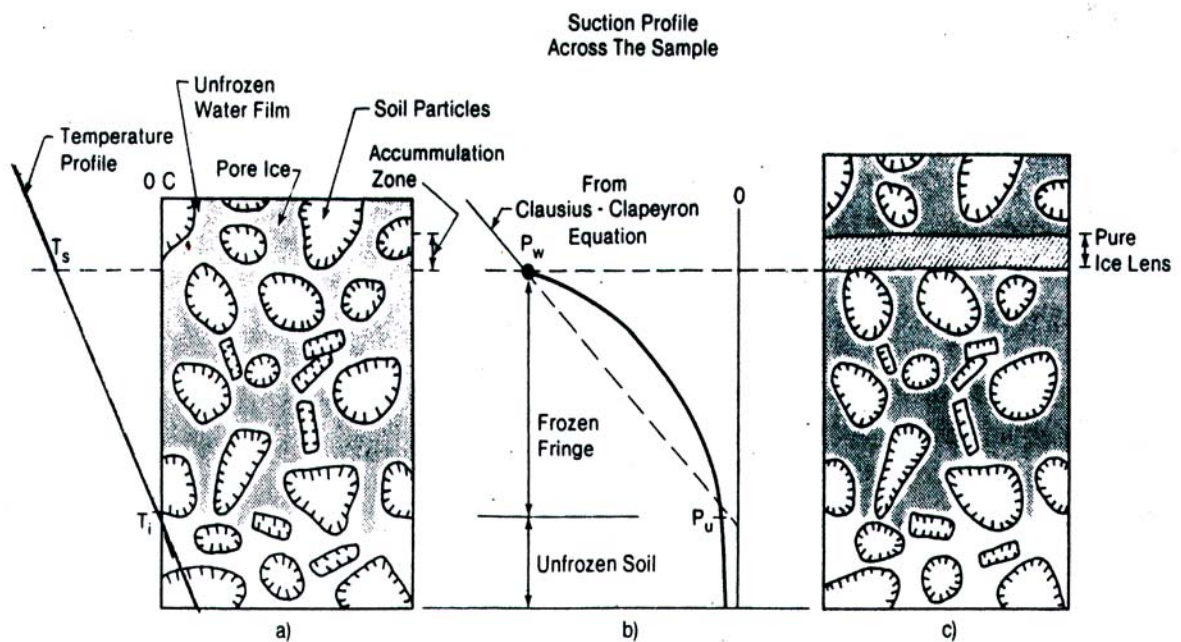


Figure 2.2: The mechanism of ice lens formation (Konrad & Morgenstern, 1980).

As the rate of frost penetration decreases, the rate of temperature change across the profile also decreases, allowing water to accumulate longer at a specific depth. This leads to the formation of a continuous ice layer in the zone above the frozen fringe, as illustrated in Figure 2.2. For the case of zero overburden pressure, it is assumed that the

pressure within the discrete ice lens is atmospheric, and the state of thermodynamic equilibrium can be described using the Clausius-Clapeyron equation (Konrad and Morgenstern, 1980).

Mass Transfer

Most researchers in the frost heave field agree that a unified engineering theory is necessary in order to predict both the magnitude and rate of heave as a function of specific soil properties, characteristics of the freezing system, and the boundary conditions involved. This theory, it is agreed, would require the coupling of heat flow and mass transfer. In the case of one-dimensional freezing of an incompressible soil, the classical conduction equation may be used to model heat flow, while Darcy's Law governs the flow of water (Konrad and Morgenstern, 1981).

In the following section, equations are given in a detailed manner in order to analytically represent the frost heave theory proposed by Konrad and Morgenstern in 1980. The fundamental conditions within the freezing system that are assumed in validating these equations include zero overburden pressure, a fully saturated soil profile, and an incompressible soil skeleton (Konrad and Morgenstern, 1980).

The Clausius-Clapeyron equation can be used to relate the suction pressure at the ice lens to temperature based on thermodynamic equilibrium between the ice-water interface:

$$P_w = \frac{L_f}{V_w T_o} \Delta T + \frac{V_i}{V_w} P_i \quad (\text{Eq 2.1})$$

where:

L_f = the latent heat of fusion of pure water,

P_w = the total suction potential in the frozen fringe,

P_i = the pressure in the ice lens,

T_o = the temperature of the freezing point of pure water in Kelvin,

ΔT = the actual temperature at the ice lens, $^{\circ}\text{C}$ (that is, $\Delta T = T_s -$ the segregation freezing temperature), and

V_i, V_f = the specific volumes of ice and water, respectively.

This equation is valid only for solute-free water at the ice lens. Furthermore, the mechanics behind the frost heave theory rely strongly on the problem of inhibited drainage at the ice lens. It is assumed that all of the water migrating through the frozen fringe freezes at the ice lens. Consequently, Darcy's Law can be used to calculate v , the water intake velocity:

$$v(t) = \frac{P_w(t) - P_u(t)}{d(t)} k_f(t) \quad (\text{Eq 2.2})$$

where:

P_u = the suction potential at the frozen-unfrozen interface,

d = the thickness of the frozen fringe,

k_f = the overall hydraulic conductivity of the fringe, and

t = denotes time.

Finally, the segregational heave, $h_s(t)$, can be calculated by integrating the segregational heave rate over the duration of the freezing cycle as follows (Konrad and Morgenstern, 1980):

$$h_s(t) = 1.09 \int_0^t v(t) dt \quad (\text{Eq 2.3})$$

where the 1.09 accounts for the 9% volume increase during the phase change of liquid water to ice.

Heat Transfer

Fourier's general conduction equation can be used to express the conditions that govern the unsteady heat flux across boundaries. For one-dimensional heat flow, the equation reduces to (Konrad and Morgenstern, 1980):

$$\frac{\partial}{\partial z} \left(\lambda \frac{\partial T}{\partial z} \right) + Q = C \frac{\partial T}{\partial t} \quad (\text{Eq 2.4})$$

where:

C = the volumetric heat capacity,

λ = the thermal conductivity, and

Q = an internal heat generation term (per unit area and per unit time).

Konrad and Morgenstern (1981) proposed that the internal heat is given off at two different locations: at the base of the growing ice lens, where the temperature is equal to the segregation freezing temperature, T_s ; and at the interface between the frozen fringe

and the unfrozen soil region (frost front), where the temperature is equal to the in situ freezing temperature, T_i .

At T_s :

$$Q = v(t)L \quad (\text{Eq 2.5})$$

At T_i :

$$Q = \varepsilon n L \frac{dz}{dt} \quad (\text{Eq 2.6})$$

where:

$L =$ the latent heat of fusion of water,

$\varepsilon =$ a dimensionless factor taking into account the proportion of unfrozen water remaining in the sample,

$n =$ the porosity of the soil, and

$\frac{dz}{dt} =$ the rate of advance of the frost front.

In order to complete the analyses, both initial conditions and boundary conditions must be established. A cold room temperature, T_c , is applied to the top of the sample, while the bottom (*warm-plate*) temperature, T_w , is held constant. The system between the warm and cold end boundary conditions can be divided into three different sections in which independent heat conduction equations hold true: (1) the region of frozen soil, (2) the frozen fringe, and (3) the underlying unfrozen soil region.

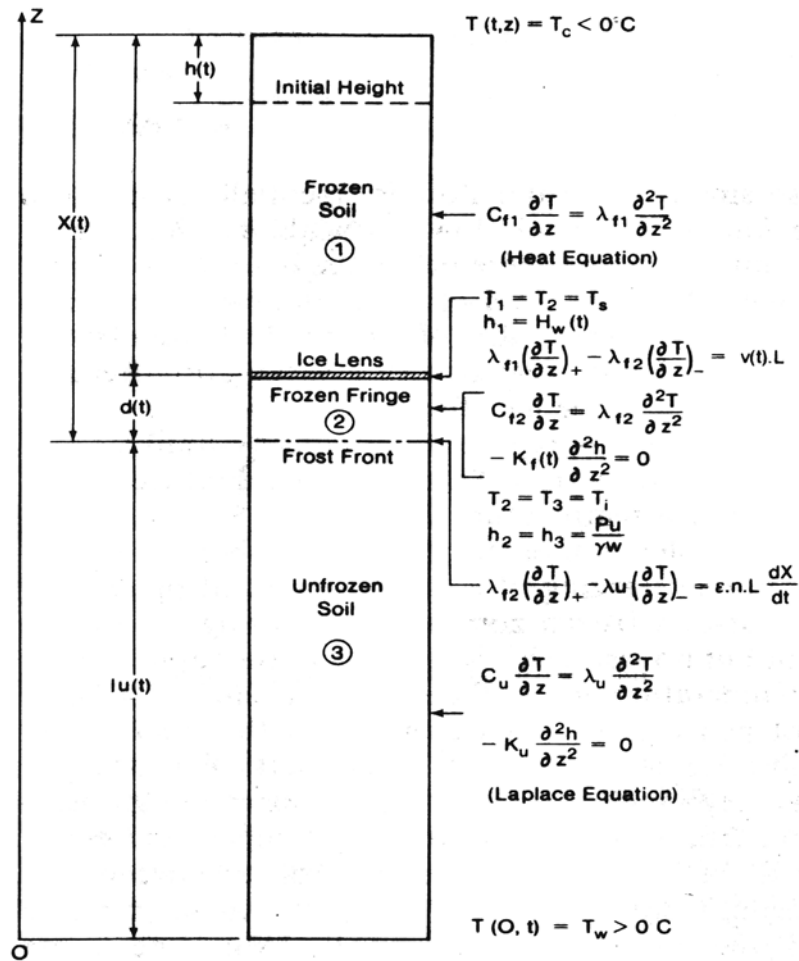


Figure 2.3: Equations for the one-dimensional frost heave model (Konrad & Morgenstern, 1980).

The system of equations shown in Figure 2.3 is valid for one-dimensional frost heave with no externally applied load. Water flow within the frozen fringe (2) and the unfrozen soil (3) is governed by the Laplace equation, while heat transfer within each region is governed by Fourier's conduction equation. Note that while the water pressure is continuous across the frost front, the suction profile at the interface between ice lens and the frozen fringe is represented by the Clausius-Clapeyron relationship.

The system of equations may be solved using finite difference techniques, assuming the necessary soil parameters can be defined. Note that in addition to the conventional geotechnical and thermal parameters, the characteristics within the frozen fringe must also be defined. This is accomplished by defining two parameters: (1) the segregation freezing temperature, T_s , and (2) the overall permeability throughout the frozen fringe, k_f (Konrad and Morgenstern, 1980).

It has been discovered in past research that determination of these parameters (at the laboratory scale) with any significant amount of accuracy is a tedious and unrealistic task. In response, Konrad and Morgenstern (1981 and 1987) conducted additional work on the one-dimensional frost heave model in an attempt to simplify the analytical work by introducing a new engineering parameter referred to as the Segregation Potential (SP). This parameter and its application are discussed in depth in the following section.

Segregation Potential Concept

Introduction

Researchers have tried for years to relate frost heave to soil index properties. Though empirical relationships have proven effective for some seasonal freezing situations, the ability to extend these criteria to prolonged freezing conditions has proved to be inadequate. Other problems related to the frost heave theory include lack of uniformity of testing equipment (i.e. freezing cell) among researchers, discrepancies in testing procedures, and the subsequent methods used to interpret the results. These

problems have resulted in incongruence of experimental data and confusion with regard to achieving a common, accurate and practical approach.

Background

The basis of frost heave theory requires coupling the fundamentals of heat transfer and mass flow. With this relationship between both thermal and physical parameters, the theoretical approach leaves ample room for incorrect assumptions, incongruent boundary conditions, and ultimately misinterpretation of experimental results.

Both theoretical and experimental results reported by Konrad and Morgenstern (1980) indicate that the theory behind the frost heave phenomenon is primarily dependant on the average suction and the rate of cooling within the *frozen fringe* (Konrad, 1987). Furthermore, their study showed that it is difficult to determine the average suction (P_w) due to the fact that the pressure profile throughout the frozen fringe is non-linear. This is a direct result of varying hydraulic conductivity (permeability, k_f) with varying temperatures (T_f) (i.e. k_f decreases with colder temperatures). However, it has been argued that the suction potential at the frozen-unfrozen interface (P_u) gives a relatively good estimate of the average suction (P_w) in the frozen fringe. The suction potential (P_u) is easily determined if Darcy's law is applied to the unfrozen soil layer. Once the permeability of the unfrozen soil (k_u) is determined and the water migration rate (v) measured, P_u can be calculated as follows:

$$P_u = \frac{vl_u}{k_u} \quad (\text{Eq 2.7})$$

where:

$v =$ water migration rate,

$l_u =$ length of unfrozen soil, and

$k_u =$ permeability(hydraulic conductivity) of unfrozen soil region.

This relationship holds true with the assumption that the unfrozen soil is incompressible and fully saturated, which is realistic for laboratory conditions.

The other parameter of primary concern is the rate of cooling within the frozen fringe (\dot{T}_f), which is defined as the change in average temperature in the frozen fringe per unit of time:

$$\dot{T}_f = \text{grad}(T_f)\dot{X} \quad (\text{Eq 2.8})$$

where:

$\dot{X} =$ the rate of frost advancement,

$\text{grad}(T_f) = \Delta T$ per unit length.

Closer examination of this equation reveals that T_f is a function of the temperature at the base of the growing ice lens (segregation freezing temperature, T_s) and the temperature at the frozen-unfrozen interface (T_i).

Therefore, the estimation of the suction potential and the rate of cooling within the frozen fringe require tedious extra steps and robust assumptions prior to further one-dimensional frost heave analysis. For example, estimating an overall value of the soil's unfrozen hydraulic conductivity (k_f) and subsequently approximating an average suction

throughout the frozen fringe (regardless of changing temperatures) seems to be a loose approach to solving a theory notorious for its small tolerance for error. That is why Konrad and Morgenstern have proposed a new engineering parameter called the *Segregation Potential* (SP) in an attempt to easily characterize a soil under freezing conditions (Konrad and Morgenstern, 1987).

The *segregation potential* (SP) is the engineering parameter that couples heat flow and mass transfer. Theoretical considerations have shown that SP is a function of both the segregation freezing temperature (T_s), and the overall permeability of the frozen fringe (k_f). However, it has been discussed that soil permeability varies with changing temperatures, thus making the approximation of its value another audacious task. The experimental determination of the segregation potential is relatively simple in a controlled freezing test, considering SP is the ratio of two measurable quantities. Konrad and Morgenstern (1981) define SP as the ratio of water migration rate to the temperature gradient across the active system (unfrozen soil and frozen fringe):

$$SP = \frac{v(t)}{\text{grad}(T_f)} \quad (\text{Eq 2.9})$$

where:

$v(t)$ = volume of H_2O uptake per unit time,

$\text{grad}(T_f) = \Delta T/l_u$ and

l_u = length of soil column.

This relationship assumes constant temperature boundary conditions (warm and cold end). One of the primary advantages to this approach is the fact that no assumptions

regarding the thermodynamic properties of the system are necessary to solve the set of equations illustrated in Figure 2.3.

Fundamental Characteristics of a Freezing Soil

The thermal boundary conditions on either end of a freezing soil are fundamentally important. Konrad and Morgenstern (1980) have conjectured through experimental processes that the warm-end temperature (T_w) is primarily responsible for affects on the suction potential at the frost front for a uniform soil layer. They found that variations in the cold-end temperature have negligible impact on the SP of a freezing soil. Furthermore, T_w affects the temperature gradient through the frozen fringe, which, in turn, changes the length of unfrozen soil remaining after the active system reaches steady state conditions. Therefore, for a given warm-end temperature, the suction profile throughout the frozen fringe, and, particularly, the suction potential are unique to a given soil type. Fluctuations with suction potential directly affect the water migration rate through the frozen fringe to the ice lens, and ultimately affect the SP.

Experimental results by Konrad and Morgenstern (1980) support conceptual claims that the SP of a uniform soil is directly linked to the temperature gradient and water migration rate, and are unique and constant for a given suction potential. Recall that the suction potential (p_u) is the value of the negative pore water pressure at the frost front. Experimental data demonstrates that the SP is highest when the suction potential is near atmospheric. Furthermore, SP decreases with increasing suction (decreasing pore water pressure) – Konrad and Morgenstern (1981). It is therefore possible to characterize a frost susceptible soil at steady state conditions (formation of the final ice lens) by

illustrating the relationship between the SP and its corresponding suction potential.

Another remarkable characteristic here is that the water migration rate (intake flux) is dependent upon the freezing path. That is, for a given soil and a given temperature gradient through the frozen fringe, it is possible to achieve different water intake velocities providing that the suction potential (p_u) varies for the same soil.

The relationship between the segregation potential and its corresponding suction potential offers a unique method to characterize a given soil under one-dimensional freezing conditions.

Calculation of SP

The analysis of frost heave data in terms of the segregation potential applies for transient freezing conditions only. Analysis of a stationary frost front is dictated by the overall heat removal rate at the ice lens, and has been shown to be independent of soil type. Konrad and Morgenstern (1987) discuss the different methods used during their experimentation process to calculate the segregation potential during a freeze test. The first method proposed involves directly measuring the segregational heave rate with a direct current displacement transducer (DCDT). From here, the water intake velocity can be calculated using the following equation based on the central difference method:

$$v(t) = \frac{[h(t + \Delta t) - h(t - \Delta t)][1 + 0.09n\varepsilon] - 0.09n\varepsilon[X(t + \Delta t) - X(t - \Delta t)]}{2.18\Delta t}$$

(Eq 2.10)

where:

h = total heave from DCDT,

X = the thickness of frozen soil,

n = the porosity of unfrozen soil, and

ε = proportional constant accounting for unfrozen water remaining in the frozen specimen.

Once the water migration rate (*v(t)*) has been calculated, and the temperature gradient determined, Equation 2.9 can be employed to calculate SP. However, it is a tedious process to back-calculate a parameter that can be easily measured in the laboratory, which leads to the other proposed method.

Konrad and Morgenstern also proposed the calculation of SP by direct measurement of the water intake velocity. However, this requires the use of very sensitive force or pressure transducers that measure the change in water height within a buret (Konrad & Morgenstern, 1987). Their output, which is calibrated to capture the change in water height (pressure head), is usually very sensitive to noise. In other words, large fluctuations are graphically observed when calculating the SP value using the volume of water intake rate by pressure transducer (as shown in Figure 2.4a).

Note the “spike” in SP value observed in the early part of the test before stabilizing to an overall value. This is due to the high rate of cooling commonly detected during the onset of freezing, as illustrated in Figure 2.4b.

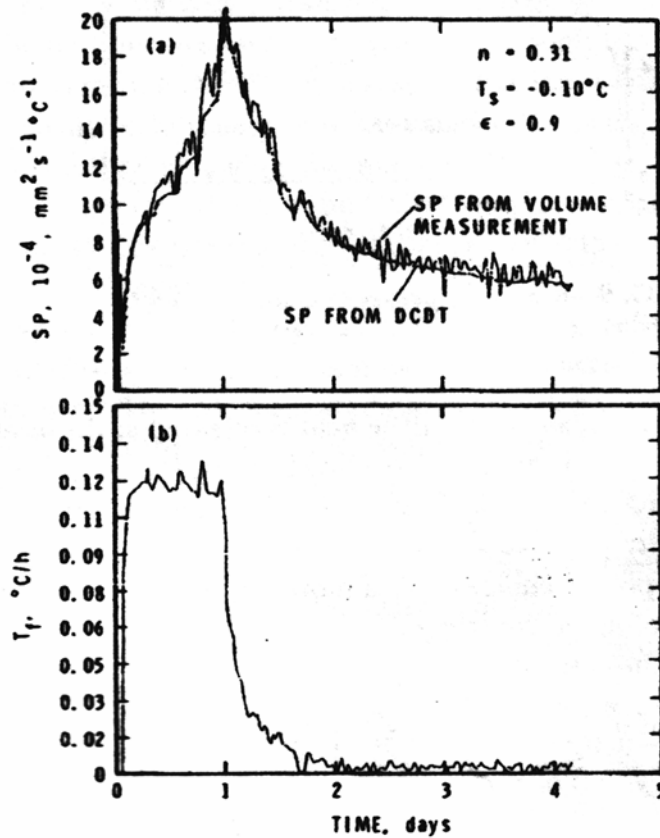


Figure 2.4: Calculated SP values using volume and DCBT measurement methods (Konrad, 1987).

Both methods of SP calculation proposed by Konrad and Morgenstern offer reasons for seeking and achieving a more direct and accurate method for measuring the water intake velocity. The laboratory freezing tests, which are further discussed in Chapter 3, were configured to measure and record the changes in water volume manually.

The results will illustrate that this methodology offers an accurate, though tedious, means of ultimately obtaining SP values throughout a laboratory-scale freezing test.

Conclusions

Researchers have tried for years to achieve a reliable and practical approach to coupling the fundamental principles of frost heave theory: heat transfer and mass flow. Until recently, the theoretical approaches used have offered too much room for experimental mistakes, assumptions, and misinterpretation of results. It is because of the diligent research conducted by Konrad and Morgenstern that a new methodology towards this goal is becoming widely adopted.

Experimental results have proved that the basis of the frost heave theory is primarily dependent on the average suction (p_u) and the cooling rate within the frozen fringe. Furthermore, the average suction is a function of the overall permeability within the frozen fringe, which, it has been suggested, to approximate with value of the permeability of unfrozen soil. Fortunately, Konrad and Morgenstern have introduced a method to combine the fundamental principles of the theory into a single engineering parameter known as the segregation potential (SP).

The segregation potential (SP) is the engineering parameter proposed by these researchers in an attempt to relate frost action behavior of soils to the more common geotechnical index parameters. It is defined as the ratio of water intake velocity to the overall temperature gradient within the active system of a freezing soil.

Calculation of segregational and total heave in terms of SP applies only to a transient (dynamic) freezing front. Different methods of the calculation of water intake

velocity (migration rate) have been proposed. However, for the purpose of the research conducted by the author it was determined that manual observation of water volume change be employed until an automated method be better developed in an attempt to eliminate “noisy” data.

Overall, the segregation potential concept offers a unique advantage to combining the fundamental characteristics of frost heave behavior (both physical and thermodynamic) to common geotechnical index parameters in an attempt to achieve a predictive model to better aid in engineering design of civil engineering subsurface structures.

Summary of Literature

Though much of the material reviewed throughout this study was based on the work done by Konrad and Morgenstern (1980, 1981, 1987, and 1994), other studies that were conducted were referenced in an attempt to gain an overall understanding of the theory of frost heave in soils.

Farouki (1981) conducted an in-depth study on the thermal properties of soils and the effects that water migration has on these properties. This paper thoroughly discussed different methods of measuring and calculating the thermal conductivity of soil, which benefited our research.

Boutonnet et al (2003) discussed several numerical models that have been developed to analyze the thermal behavior of frost susceptible soils. One model in

particular (SSR model) spawned the development of a predictive numerical model applied to this research (further discussed in Chapter 5).

Saarelainen (1992) examined the theoretical background of the heat balance equation at the freezing front and further discussed the development of the SSR model. The SSR model provides a means to calculate the incremental rate and magnitude of heave, and relies heavily on the segregation potential (SP) parameter. This model was used as a guideline for developing a method to numerically calculate and predict the thermal behavior of soils subjected to freezing conditions.

Ho (1969) introduced some of the early studies conducted on frost action in which the mathematical theory of heat conduction (Fourier equation) is examined in the context of one and two-dimensional numerical models.

A large amount of material was reviewed that did not fit into our scope of work. However, this emphasizes the dedication towards, and complexity of, the theory behind frost action in soils. As engineers and scientists have proven thus far, the need to accurately and practically predict the rate and magnitude of heave and thaw weakening is increasingly important.

CHAPTER 3

EXPERIMENTAL METHODS

Introduction

A large field-scale frost heave test facility was designed and constructed with the purpose of measuring and comparing in-situ frost heave characteristics with laboratory scale test results. Furthermore, a laboratory device was also designed, constructed, and instrumented in order to measure the thermal response of various soil types in a controlled freezing environment. Laboratory testing was conducted on two types of fine-grained soils (a silt-clayey mixture, and the Post Farm lean clay). Laboratory index tests were conducted to fully characterize the soils and to examine correlations between standard soil properties and frost action behavior. This chapter describes in detail the field facility and laboratory testing apparatus.

Field Frost Heave Test Facility

Facility Location

Construction of the facility occurred from June to October 2003. The site is located within a fenced area adjacent to a NOAA weather station at the Montana State University (MSU) Arthur Post Agricultural Research Farm (Post Farm), which is located approximately 8 km west of the MSU Bozeman campus. The facility is essentially a large-scale, long-term experiment that will enhance the current state of knowledge concerning frost heave and thermal behavior of soils subjected to sub-freezing

temperatures. Furthermore, it will provide valuable data for comparison with laboratory-scale testing and for the development of a practical and reliable numerical approach for predicting frost action behavior.

Construction of Facility

The first stage of construction required the excavation of a 7.6 m long, 2.4 m wide, by 1.5 m deep trench, as shown in Figure 3.1. A 5 m³ fiberglass trough was placed in the bottom, west side of the trench as shown in Figure 3.2. The trough functioned as an impermeable base for the water infiltration system beneath the backfill test soil.



Figure 3.1: Excavation of field frost heave test facility.



Figure 3.2: Fiberglass trough in bottom of excavation.

A dual tank water supply system was designed and implemented to simulate a groundwater source that would be available for uptake by the soil mass, which was backfilled into the fiberglass trough (Figure 3.3). The water is gravity fed from the supply tanks to the bottom of the soil through a system of one-inch diameter PVC pipes that are embedded in a four-inch layer of sand at the bottom of the trough. The pipes are

four meters long, and perforated with 1/8-inch diameter holes at twelve inches on center along the length of pipe. The layer of sand and the small perforations provide for even distribution of the water throughout the soil mass. The pipes were then wrapped in geotextile fabric to prevent sand and soil from entering and clogging the waterway.

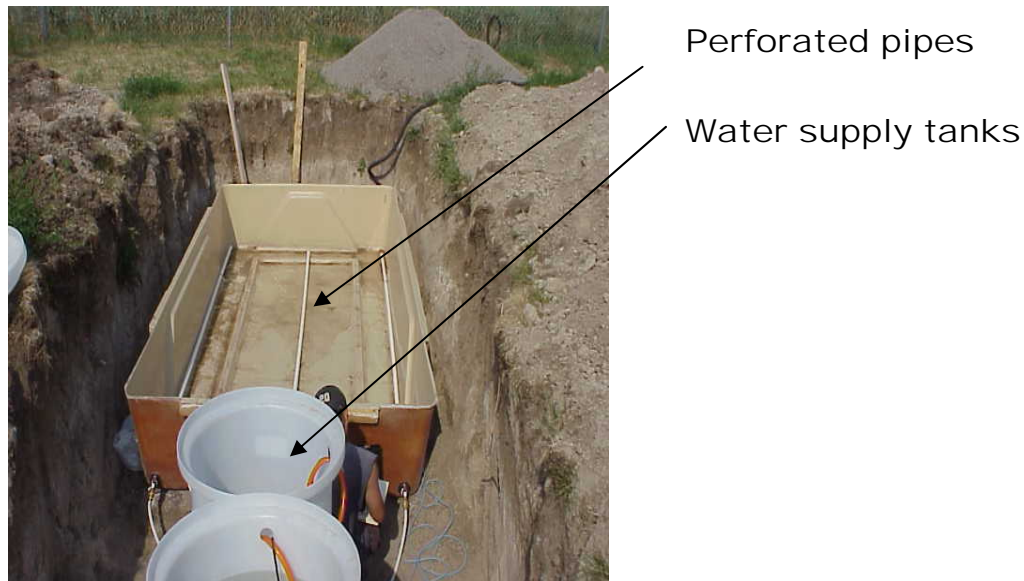


Figure 3.3: Dual tank water supply system.

One of the design considerations for the supply system included maintaining a constant water level within the test soil. This was accomplished by the use of a float switch, which was placed in the tank nearest the trough, as illustrated in Figure 3.4. The float switch controls the pump in the first supply tank by turning the pump on once the switch falls to a pre-determined level in the second tank. This pre-determined level corresponds to the static water level in the soil mass. The pump supplies the second tank with water until the height of the switch reaches the “off” position. The water from the

second tank drains into the soil mass area until the level drops enough to turn the pump on again, thus continuing the cycle.



Figure 3.4: Float switch mounted in stock water tank.

A tape measure was installed in the first supply tank (pump tank) in order to monitor and record the drop in water level. The pump tank requires manual refilling approximately once a week. Piezometers were also installed on both east and west sides of the soil mass area for the purpose of monitoring fluctuations in the groundwater level throughout the freeze-thaw cycle. This artificial groundwater system provides a means to measure the quantity and rate of upward water migration from the base of the soil mass to the frost front. Figure 3.5 illustrates the simulated groundwater system within the all-weather insulated shelter.



Figure 3.5: All-weather insulated shelter.

Before beginning the backfilling process, a vapor barrier was placed around the trough area in order to minimize water migration through the sidewalls of the soil mass. Four-by-four wooden posts were driven into the ground and fastened to the sides of the trough in order to support the reference beams that would be used to observe heave and settlement behavior. The excavated soil was then mixed and used to backfill the tank up to ground level. The backfill was placed in 15-cm thick layers and compacted using a 25-pound hand tamper. After each compacted lift, sand-cone density tests were conducted to measure the in-situ densities throughout the soil profile (see Figures 3.6 and 3.7).

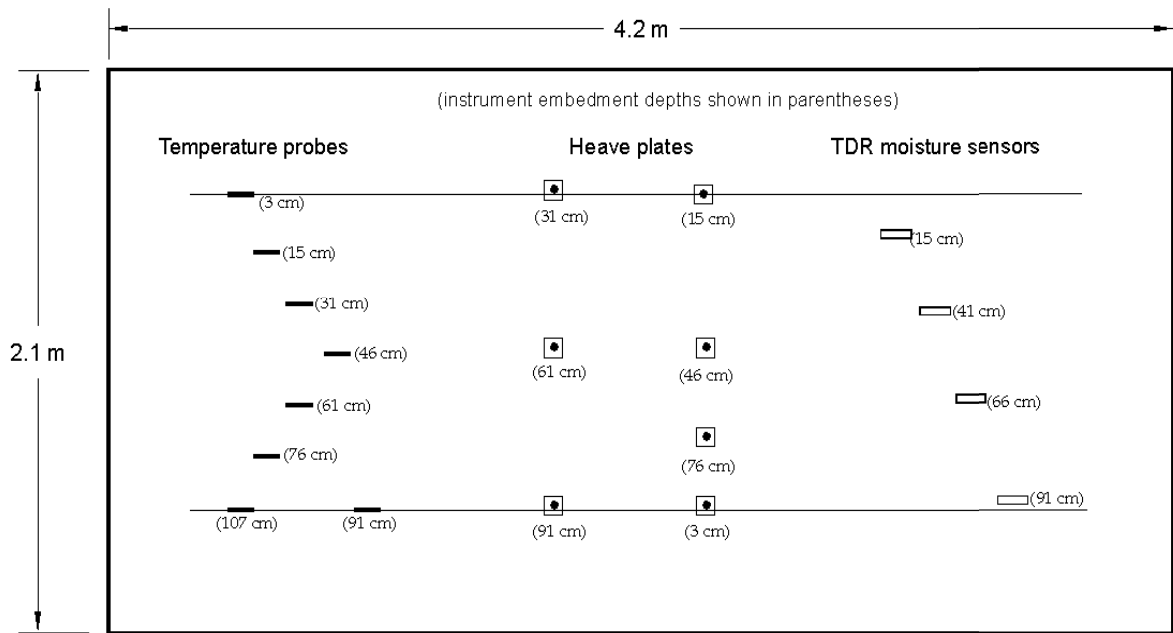


Figure 3.6: Construction of the telltale and reference beams during the backfilling of the soil mass.

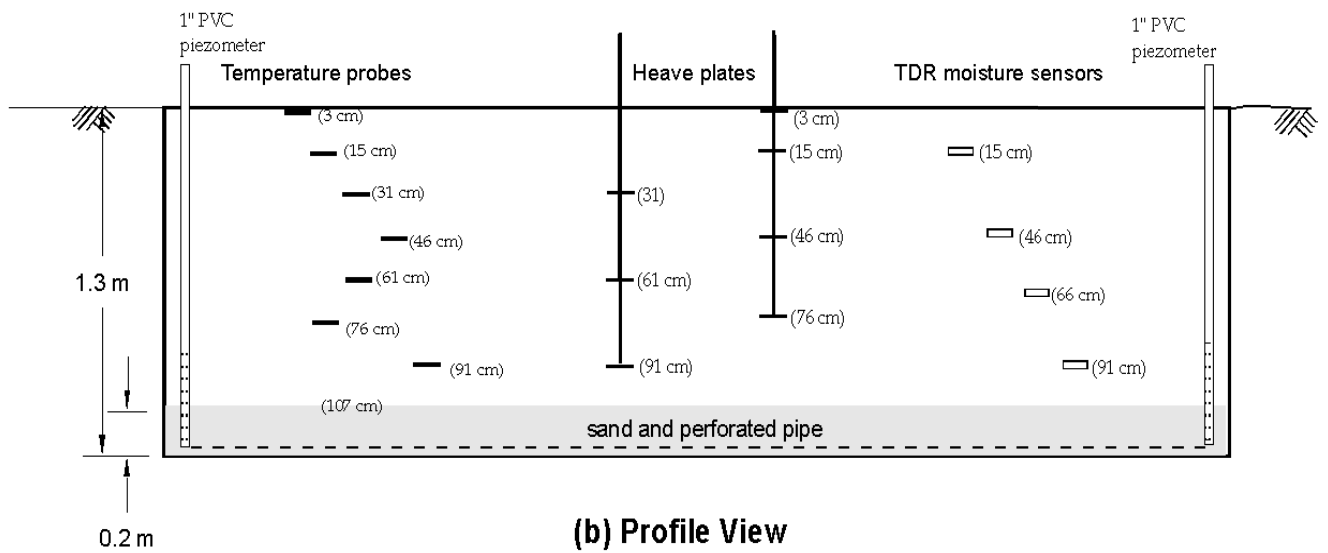
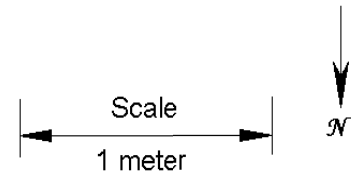


Figure 3.7: Sand cone density tests being performed throughout the backfilling of the soil mass.

Instrumentation was installed within the soil throughout the backfilling process at predetermined depths according to the schematic shown in Figure 3.8. This included thermocouples, time domain reflectometry (TDR) moisture sensors, heave/settlement telltales, and piezometers to measure temperature gradients, changes in soil moisture content, heave, and groundwater fluctuations during the freezing process respectively.



(a) Plan View



(b) Profile View

Figure 3.8: Plan and profile views of the instrumentation and telltale construction at the field frost heave test facility.

Construction of the facility was completed in early October 2003. Photos of the operational site are shown in Figure 3.9.



Figure 3.9: Photographs of the operational frost heave test facility during the winter of 2004.

A schematic of the completed facility, which better illustrates the water supply system, can be seen in Figure 3.10.

Data Collection

HOBO® Micro and Weather Station data loggers were used to collect and store the temperature and moisture content data throughout the freeze/thaw season. Aluminum reference beams were installed over the heave/settlement telltales, which served as benchmarks for taking readings throughout the freeze/thaw season. An electronic caliper with an accuracy of ± 0.01 mm was used to measure the changes in height between the telltales and the reference beams. The changes in water level in the supply tanks and piezometers were manually measured using a tape measure. Data collection took place at intervals of approximately one week.

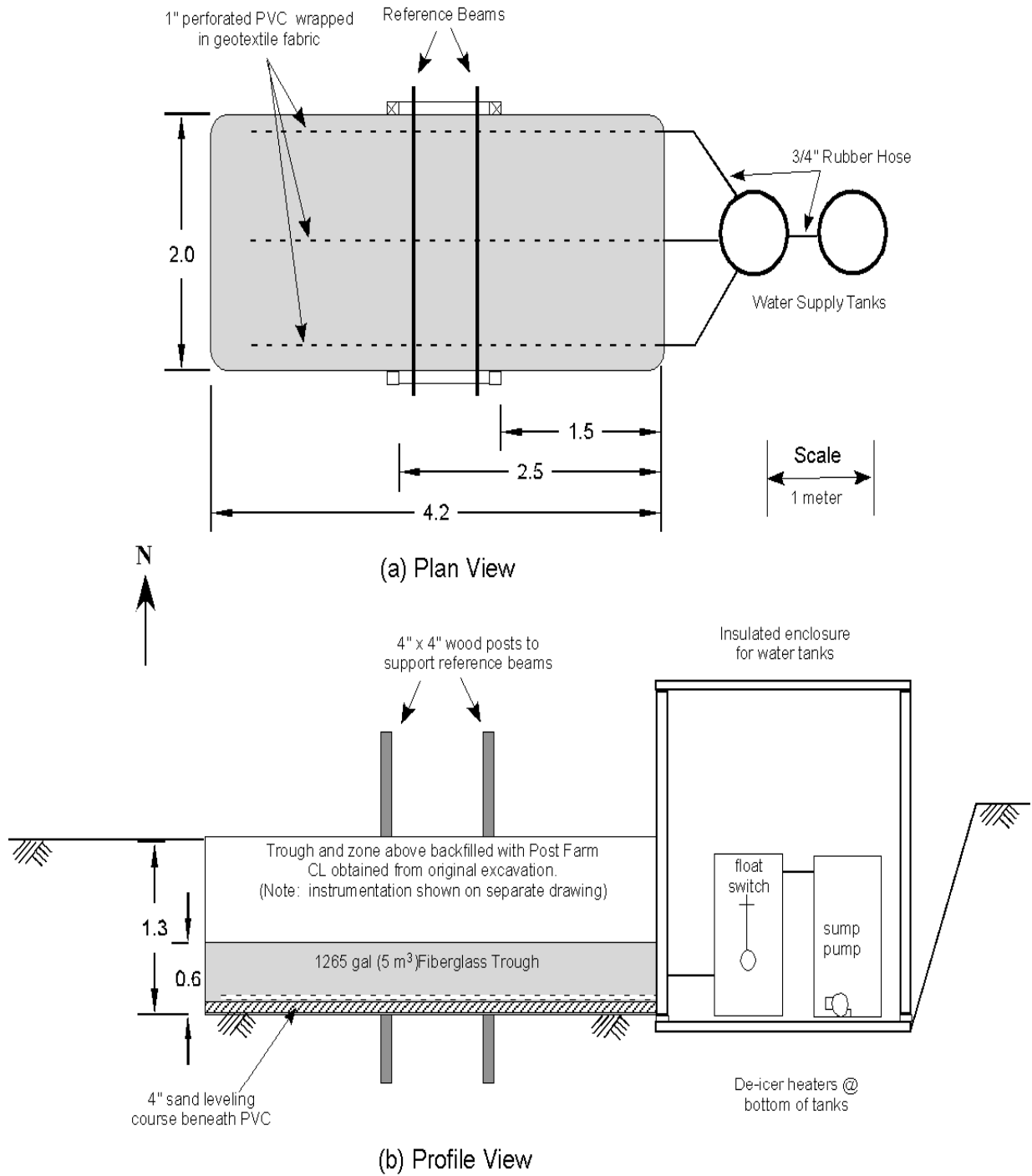


Figure 3.10: Schematic illustrating the completed field frost heave test facility.

Readings for the fall and winter season of 2003-04 were used for preliminary numerical and analytical analyses and will continually be collected over the upcoming seasons to develop a sufficient database for further research. The results are illustrated and discussed in Chapter 4.

Laboratory Freeze-Thaw Tests

Experimental Setup

A laboratory-testing device was designed, constructed, and instrumented for the purpose of measuring the thermal response of soil in a controlled freezing environment. A controlled freezing environment was achieved by placing the testing apparatus containing the soil sample within a cold chamber room located in the MSU snow mechanics lab. The device evolved through numerous cycles of testing and modification in order to obtain a reliable and efficient tool for measuring and collecting frost heave data and soil thermal properties at a laboratory scale.

Equipment Description

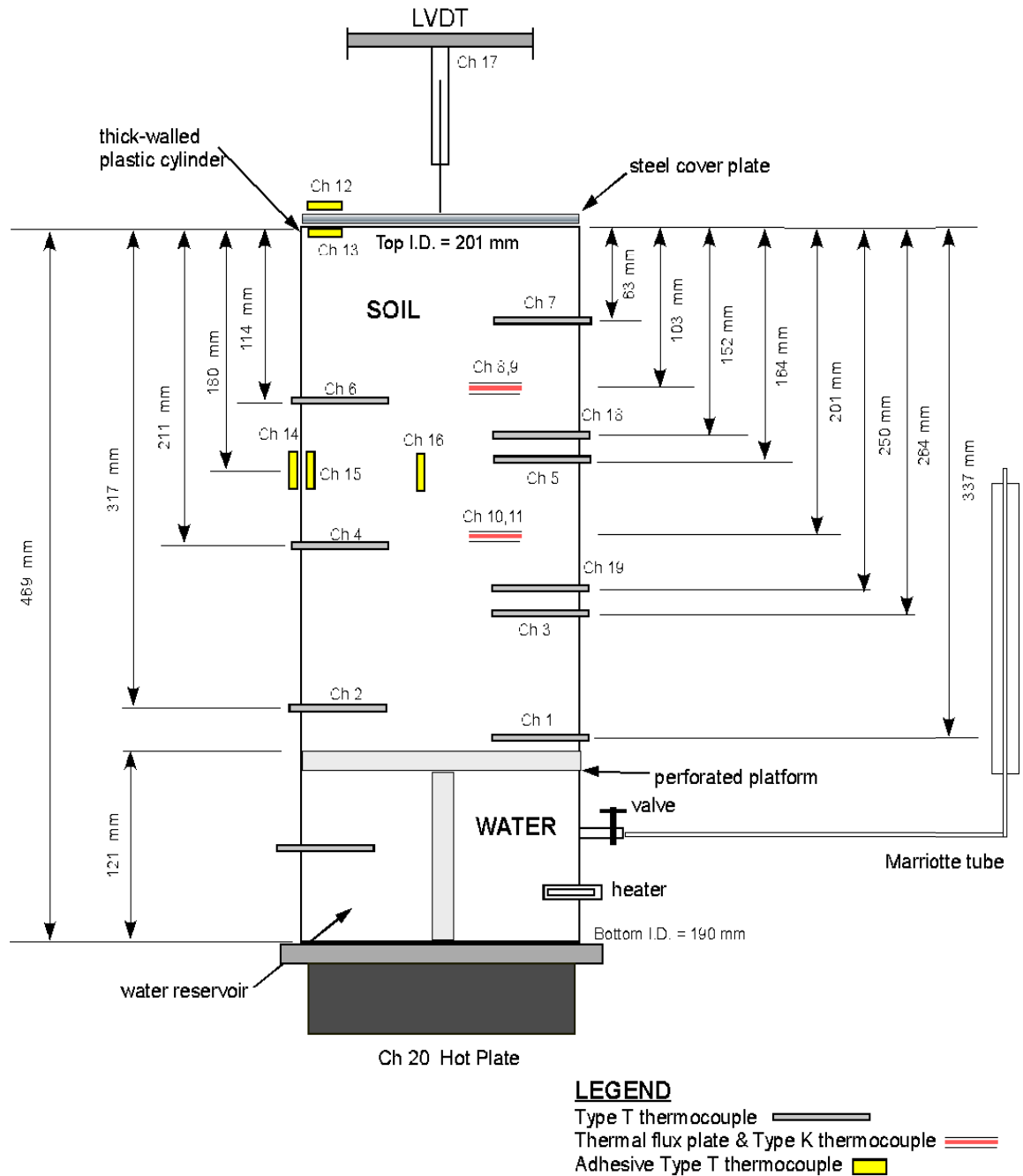
Soil Test Cylinder. The soil test cylinder consists of a 470 mm tall thick-walled PVC cylinder with a nominal inside diameter of 200 mm. The inner walls are tapered outward at an angle of 1.2° (starting 250 mm below the top of the cylinder) in order to reduce friction between the advancing soil and the sidewalls. The bottom 100 mm section of the cylinder serves as a water supply reservoir, which supplies a source of unfrozen water to the overlying soil mass. The reservoir and soil mass are separated by a

removable perforated platform, which serves as a filter screen. Water advances upward into the soil column by capillarity forces, which are enhanced by suction pressures that develop at the freezing front. A schematic of the laboratory-testing device is shown in Figure 3.11.

Mariotte Tube. The water level in the soil test cylinder is maintained at a constant height using a Mariotte tube, which is a dual tube device that provides a means of supplying water to the soil mass while maintaining a constant outlet pressure. The height of the bottom of the inner air tube with respect to a datum corresponds to the water level in the soil cylinder with respect to a common datum (in this case, the floor of the cold regions lab) as shown in Figure 3.12. As water is taken up into the soil mass by capillary forces, the water level drops and the gravitational head is decreased in the reservoir. In turn, the water-filled Mariotte tube supplies the reservoir with enough water until the system returns to a state of equilibrium. The Mariotte tube also contains a built-in measuring tape accurate to 1 mm to provide a means for measuring the quantity of water that migrates into the soil column.

Boundary Conditions

Control of the boundary conditions and accurate measurements of water uptake, temperature gradients, and thermal flux constitute the crucial aspects of the experimental setup. The boundary conditions specific to the laboratory frost heave device are the temperatures at the top and bottom of the soil cylinder, which affect the rate of heat transfer.



Notes:

- (1) Inside diameter taper begins 250 mm from top (taper not shown).
- (2) Cylinder encapsulated with insulation and placed inside of environmental cold chamber.
- (3) Agilent technologies data acquisition system used to record data.
- (4) Data acquisition channel indicated on drawing as Ch X, where X = channel number.

Figure 3.11: Schematic illustrating the laboratory frost heave testing device.

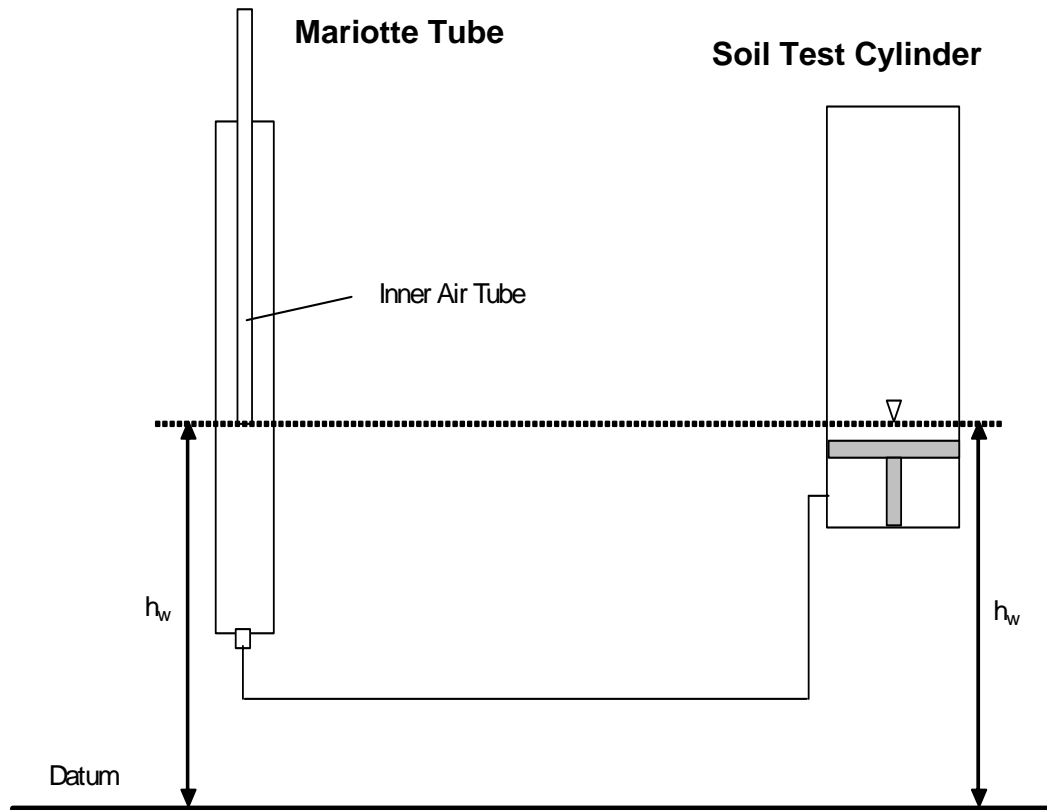


Figure 3.12: Schematic illustrating the Mariotte tube and interaction with the water reservoir.

Initially, a small immersion heater was used as the sole means of keeping the water temperature at the bottom (warm) end above freezing. However, this method proved insufficient, as the heater was not powerful enough to keep the water in the reservoir from freezing after several days of testing. The latest prototype includes a warm plate, which was designed and constructed to simulate a radiant heat floor system in order to assist in maintaining a constant temperature in the water reservoir. The plate consists of thin aluminum strips overlaying coiled sections of copper pipe. A heated liquid (ethanol glycol) is pumped through a looped tubing system in and out of the cold

room in order to heat the copper pipe and ultimately supply a warm end boundary condition. This setup has proved to increase the efficiency in keeping a constant boundary temperature at the warm end of the cylinder. Figures 3.13 and 3.14 illustrate the difference in temperature profiles when using a warm plate during the freeze test.

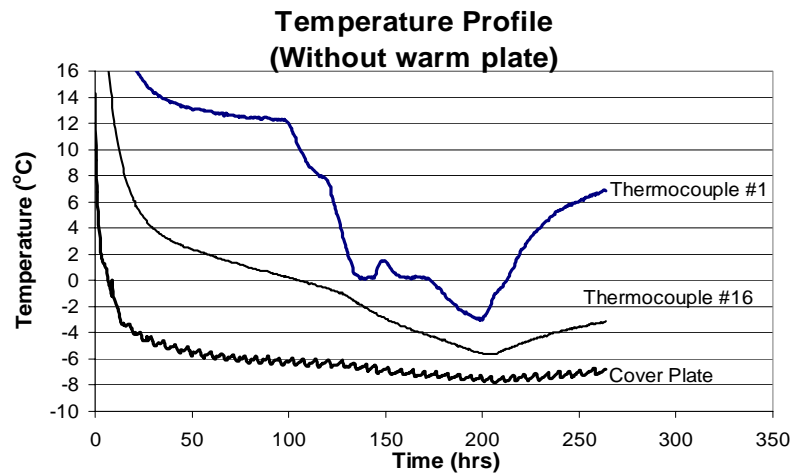


Figure 3.13: Temperature profile illustrating a laboratory freeze test without the use of the warm-end boundary control.

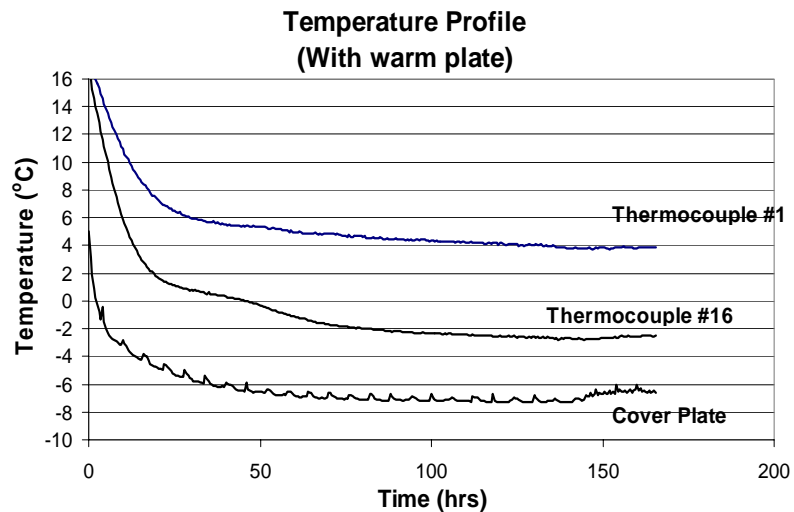


Figure 3.14: Temperature profile illustrating a laboratory freeze test with the use of the warm-end boundary control.

A thin steel cover plate placed on top of the soil mass serves as means to keep a constant temperature boundary condition at the cold end of the cylinder. The thermal properties of steel minimize fluctuations in ambient temperatures within the cold chamber. The plate, while providing 850 Pascals of vertical confinement pressure, also serves as a datum for measuring the vertical movement (heave) of the soil throughout the freezing process. Figures 3.15 - 3.17 show the test cylinder inside of the cold room.

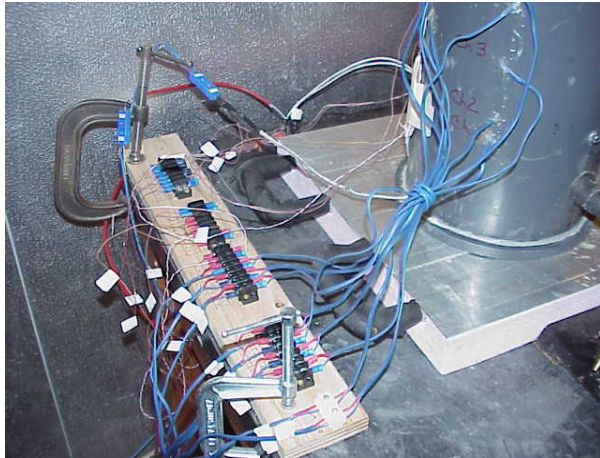


Figure 3.15: Photograph of laboratory testing device connected to the circuit bridge.



Figure 3.16: Photograph of insulated laboratory testing cylinder placed on the warm plate inside of the cold chamber.



Figure 3.17: Photograph of steel cover plate and the linear variable displacement transducer (LVDT).

The soil cylinder is wrapped in fiberglass insulation to minimize heat transfer through the sidewalls. The combination of the custom made warm plate, the steel cover plate, and the insulation serve as an efficient means in maintaining constant boundary conditions within the soil sample. These constant boundary conditions are important in achieving consistent temperature gradient and advancement of the frost front throughout the soil profile.

Figure 3.18 graphically illustrates the effectiveness of the fiberglass insulation. Thermocouples 14, 15, and 16 are placed at equal depths within the soil column, varying only in horizontal position (see Figure 3.11). Thermocouple 16 is located in the center of the soil mass, while 14 is placed on the outer sidewall of the plastic cylinder. The data shows that only the slightest temperature change occurs from the center of the cylinder to the sidewall.

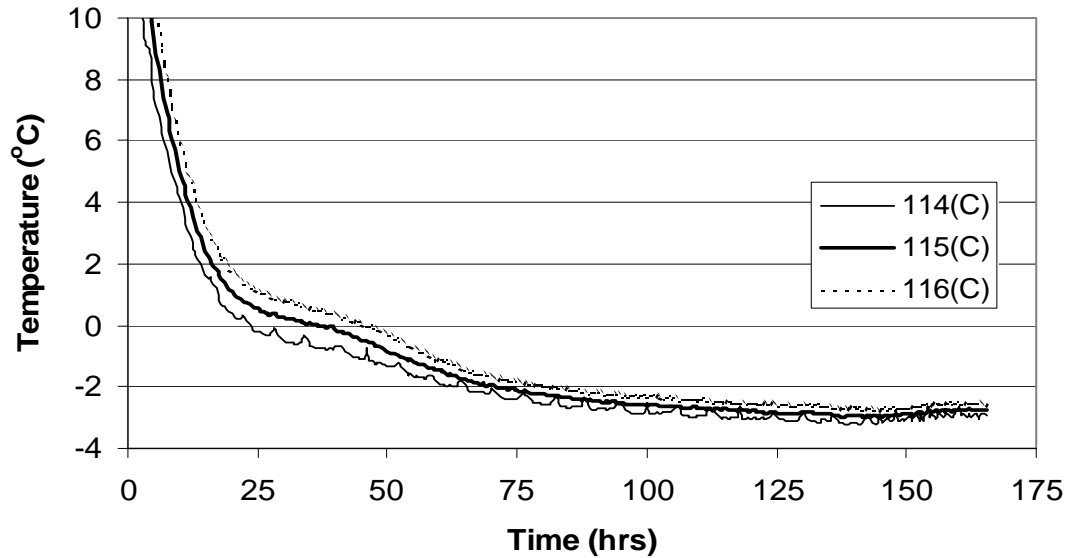


Figure 3.18: Graphical illustration showing the effectiveness of fiberglass insulation on the sidewall of the testing cylinder.

Instrumentation and System Controls

Frost heave at the top of the cylinder is measured using a LD600 series linear variable displacement transducer (LVDT) manufactured by Omega Engineering, Inc. The LVDT is positioned vertically and makes contact with the surface of the steel heave plate as shown in Figure 3.18.

Type T and K thermocouples and two thin-film heat flux sensors (Omega Engineering, Inc.) are placed at fixed locations throughout the soil profile, as shown in Figure 3.11. Using Fourier's law, the thermal conductivity of the soil (k_t) can be determined from measured values of heat flux and thermal gradient using Eq. 3.1.

$$q = -k_t A \frac{\delta T}{\delta y} \quad (\text{Eq 3.1})$$

where

$q = \text{heat flux,}$

$k_t = \text{thermal conductivity,}$

$A = \text{sample area,}$

$T = \text{temperature, and}$

$y = \text{depth.}$

Thermal conductivity is not a unique property, but depends on water content, temperature, and stress state (Ho, Harr, and Leonards 1970; Farouki 1981). For example, the thermal conductivity of frozen soil is greater than the thermal conductivity of the same soil in an unfrozen state because k_t of ice is approximately 4 times greater than k_t of water (Andersland and Ladanyi, 2004).

The displacement transducer, thermocouples, and flux plates are wired with quick-connects to a circuit bridge that interfaces with an Agilent Technology 34970A data acquisition system, as shown in Figure 3.15.

The small immersion heaters placed inside the water reservoir and the tank supplying warm ethanol glycol to the hotplate are wired to separate Omega I-series temperature process controllers, which regulate the temperature of the fluids and ultimately minimize fluctuations in the warm-end boundary conditions.

Sample Preparation

Before placing the soil sample into the testing cylinder, the water reservoir was filled to the top surface of the perforated platform and the cylinder mass was recorded as a tare value. Filter paper was placed over the platform to keep soil from entering into the

reservoir. The test soil was then added to the cylinder in three equal lifts. For each lift, the moisture content and mass of the cylinder were measured in order to develop moisture content, saturation, and unit weight profiles before and after the freezing process. Each lift was compacted with a modified proctor compaction hammer, while attempting to maintain consistent compaction effort throughout the soil profile. Finally, the cylinder was placed in the cold chamber, wired to the circuit bridge, wrapped in fiberglass insulation, and connected to the water supply line leading from the Mariotte tube (see Figures 3.11-3.17).

In total, seven tests were conducted that produced valuable data, although several others were attempted throughout the design modification process. The first two tests were performed on an 80% silt and 20% kaolinite clay composition by weight. The next five tests were conducted on soil collected at the Post Farm frost heave test facility, which was determined to be a lean clay (USCS classification, CL).

Data Collection

Heat flux, temperature, and displacement data were collected at 30-minute intervals using Agilent Benchlink software compatible with the Agilent 34970A data acquisition system. Water uptake readings were manually recorded by observing the change in water level in the Mariotte tube. The immersion heater process controllers were closely monitored in order to observe any drastic fluctuations in the warm-end boundary conditions. The freeze test continued until it was observed that the frost front had reached the second thermocouple from the bottom, or the thermal interface between the frozen and unfrozen soil layers was no longer showing signs of transient freezing.

Thaw Process

At the completion of the freezing test, the apparatus was removed from the cold chamber, and the soil sample was recovered from the cylinder as it thawed. During this process, water content samples were obtained in order to compare to the initial values.

Laboratory Index Testing

Geotechnical laboratory index tests were conducted on both the manufactured silt-clay composite and the natural lean clay collected from the Post Farm site. Geotechnical index property tests were conducted in accordance with the American Society of Testing Materials (ASTM) standard methods. Test results are summarized in Tables 3.1 and 3.2.

Silt-Clay Composition

Table 3.1 80% Silt - 20% Clay Geotechnical Parameters

USCS classification ASTM D2487	ML
Liquid limit, LL ASTM D4318	20
Plastic limit, PL ASTM D4318	20
Plasticity index, PI ASTM D4318	0
% finer than #200 sieve ASTM D422	56
% finer than 0.02 mm ASTM D422	15
Specific gravity of solids, G_s ASTM D854	2.72
Saturated permeability, k	0.1246 cm/hr
Maximum void ratio, e_{max} ASTM D4253	1.18
Minimum void ratio, e_{min} ASTM D4254	0.94
Modified Proctor max. dry density, ρ_{dmax} ASTM D1557	19.5 kN/m ³
Modified Proctor optimum water content, w_{opt} ASTM D1557	11.0%
Thermal conductivity (unfrozen), k_{tu}	1.4 W/m°C
Thermal conductivity (frozen), k_{tf}	1.82 W/m°C

Discussion. Table 3.1 summarizes the geotechnical index properties for tests conducted on the 80% silt and 20% clay composition (by mass). The silt was obtained from the asphalt processing plant at the JTL quarry in Belgrade, Montana. The clay used in the mix is a white China clay, also known as kaolinite. This soil composition is referred to as S80K20 throughout the remainder of this report.

According to the Unified Soil Classification System (USCS), S80K20 is classified as a low-plasticity silt (ML) with a $LL = 20$, and a $PI = 0$. It had 56% passing the #200 sieve with a specific gravity of 2.72. The saturated permeability (k) was found to be 0.125 cm/hr. The Modified Proctor dry density was 19.5 kN/m^3 at an optimum water content (w_{opt}) of 11%. The compaction curve is shown in Figure 3.19. The maximum and minimum void ratios were 1.18 and 0.94, respectively, in accordance with ASTM D4253 and D4254.

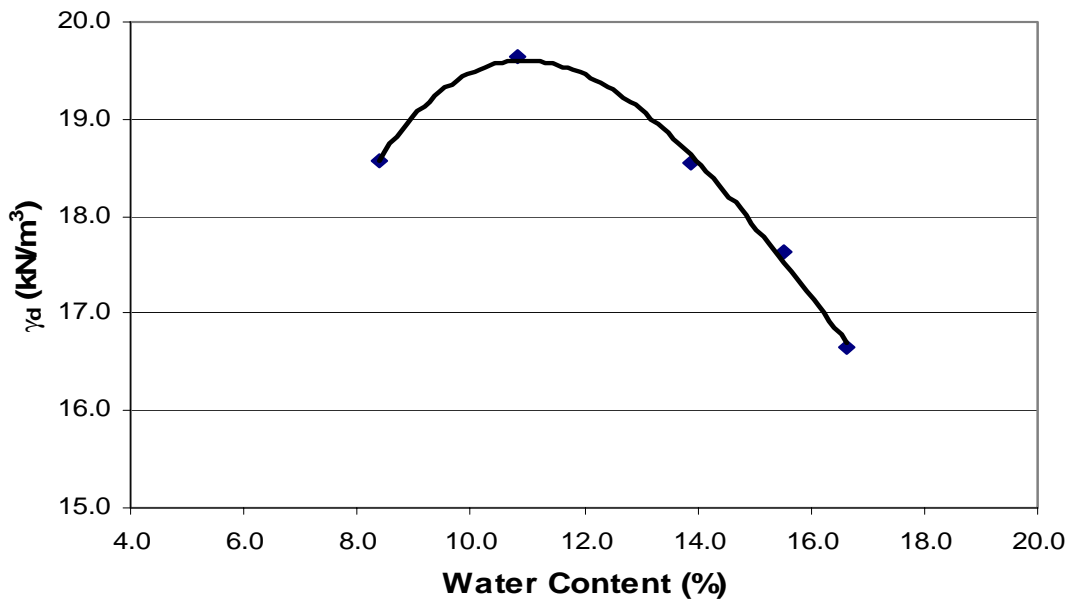


Figure 3.19: Graphical illustration of modified proctor compaction curve for the S80K20 composition.

Figure 3.20 illustrates the thermal conductivity of S80K20. The heat flux plates used were responsible for measuring the flux term (q/A) in Equation 3.1. After the temperature gradient was determined, the graph representing the value of thermal conductivity was developed by back calculating for k_t . According to Andersland and Ladanyi (2004), the thermal conductivity of ice is greater than that of liquid water. This follows the trend for the laboratory freeze test conducted on S80K20, as depicted in Figure 3.20. It can be seen that once the frost front advances past the heat flux plate positioned within the soil column, the thermal conductivity of the soil increases. Average values for the unfrozen and frozen conductivities were taken during the relevant time periods throughout the freezing test. It was reported that the unfrozen and frozen conductivities for S80K20 were 1.4 and 1.82 $W/m^{\circ}C$, respectively.

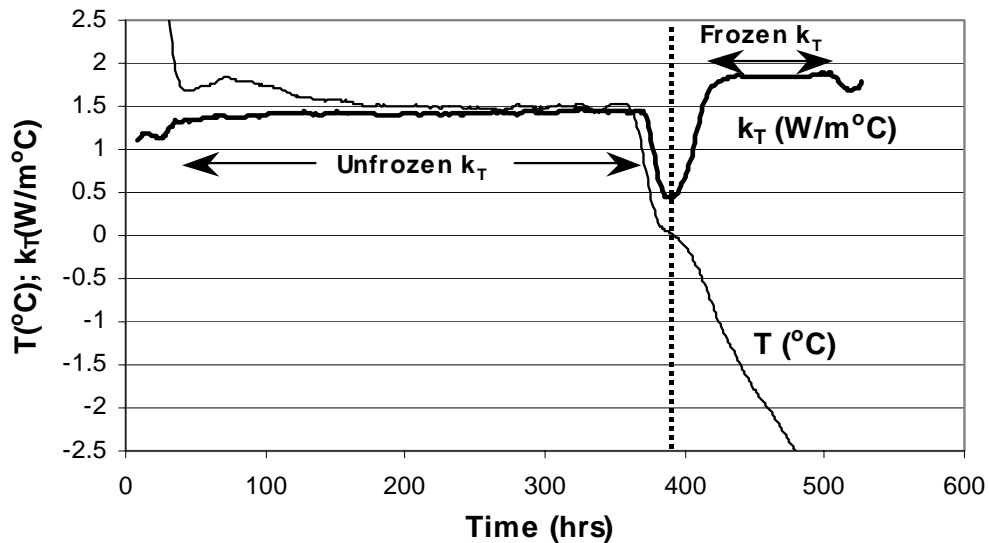


Figure 3.20: Graphical illustration of the thermal conductivity of the S80K20 composition.

Post Farm Lean Clay**Table 3.2 Post Farm Clay Geotechnical Parameters**

USCS classification ASTM D2487	CL
Liquid limit, LL ASTM D4318	36
Plastic limit, PL ASTM D4318	24
Plasticity index, PI ASTM D4318	12
% finer than #200 sieve ASTM D422	70
% finer than 0.02 mm ASTM D422	37
Specific gravity of solids, G_s ASTM D854	2.85
Saturated permeability, k	0.094 cm/hr
Maximum void ratio, e_{max} ASTM D4253	1.42
Minimum void ratio, e_{min} ASTM D4254	1.24
Modified Proctor max. dry density, ρ_{dmax} ASTM D1557	18.0 kN/m ³
Modified Proctor optimum water content, w_{opt} ASTM D1557	15.5%
Thermal conductivity (unfrozen), k_{tu}	0.25 W/m ^o C
Thermal conductivity (frozen), k_{tf}	0.46 W/m ^o C

Discussion. Table 3.2 summarizes the geotechnical index properties for tests conducted on the Post Farm clay. According to the Unified Soil Classification System (USCS), the Post Farm clay is classified as lean clay (CL) with a LL = 36, and a PI = 12. It had 70% passing the #200 sieve with a specific gravity of 2.85. The saturated permeability (k) was 0.09 cm/hr. The Modified Proctor dry density was 18 kN/m³ at an optimum water content (w_{opt}) of 15.5%. The compaction curve is shown in Figure 3.21. The maximum and minimum void ratios were 1.42 and 1.24, in accordance with ASTM D4253 and D4254, respectively.

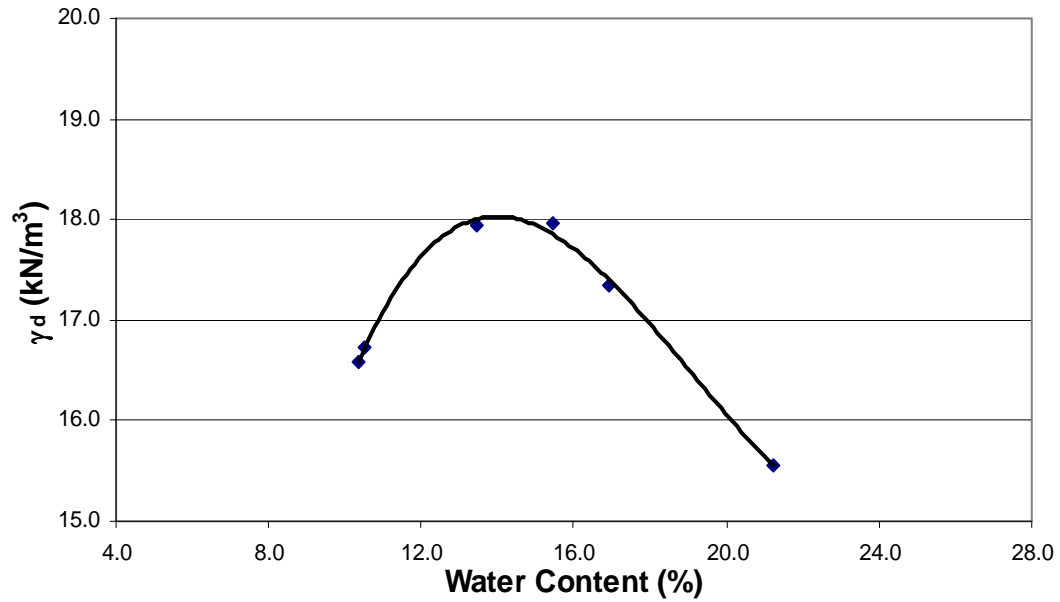


Figure 3.21: Graphical illustration of modified proctor compaction curve for the Post Farm clay.

Figure 3.22 shows the results of the thermal conductivity measurements during one of the laboratory freezing tests conducted on the Post Farm CL. Average values of conductivity were taken for time intervals before and after the frost front reached the depth of the heat flux plate. Note the “jump” in conductivity values after the soil temperature drops below freezing (0°C). The unfrozen and frozen thermal conductivities of the Post Farm lean clay are 0.25 and 0.46 $\text{W}/\text{m}^{\circ}\text{C}$, respectively.

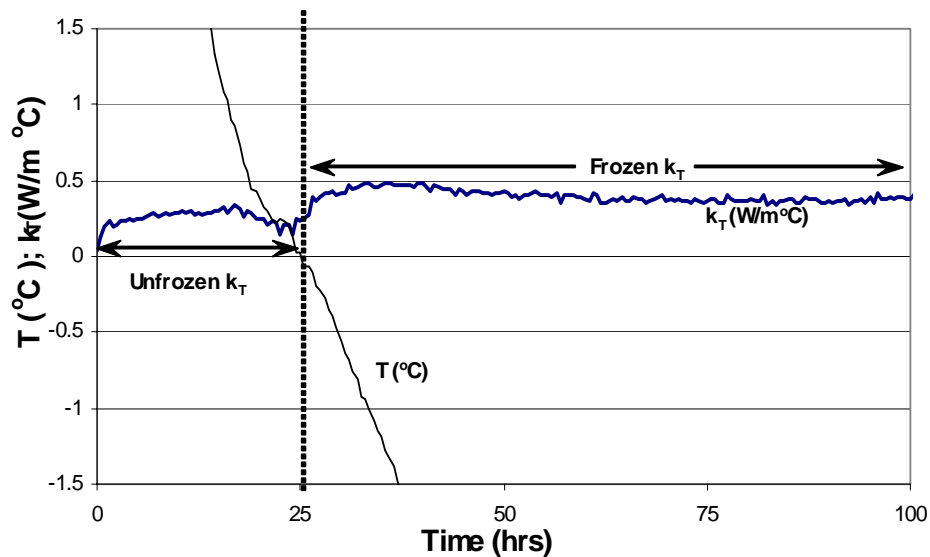


Figure 3.22: Graphical illustration of the thermal conductivity for the Post Farm clay.

Summary

This chapter discussed the main aspects of the development of a field frost heave test facility to monitor the current and long-term thermal behavior of soils exposed to cyclical freezing and thawing temperatures. The facility will continue to be used to measure and collect data that can be used in numerical analyses and will be supplemental with laboratory tests. At the completion of construction and instrument installation, as-built drawings were developed, which accurately document the placement of all instruments in the soil mass, as well as the dimensions of the all-weather insulated shelter and stock tank water supply system (see Figures 3.8 and 3.10).

At the end of the 2003 – 04 season, the facility proved to function well. It was encouraging to know that the water supply system worked efficiently, which was a key component of the system.

The development of a laboratory-testing device was also discussed. The device endured numerous cycles of testing and modification in the attempt to obtain an efficient and reliable tool for measuring and collecting frost heave data and soil thermal properties. Seven tests were conducted between the S80K20 mix and the Post Farm lean clay (CL). Results from these tests are presented in Chapter 4.

Overall, the process of research and development with regard to experimental heave testing has proven to be beneficial for the future growth of achieving a practical and reproducible testing protocol in the MSU civil engineering department. With the framework laid for further development, continued research and testing is possible using the resources developed in this study.

CHAPTER 4

EXPERIMENTAL RESULTS

Introduction

The experimental test results of the frost heave test facility and the laboratory frost heave experiment are described herein. Overall, the results prove to be encouraging in an attempt to develop an observation site where seasonal measurements can be compared to those at the laboratory scale while working to achieve a practical and predictive frost heave model.

Experimental Test Results

Field Frost Heave Test Facility

Construction of the field frost heave test facility located at the Montana State University (MSU) Post Farm was completed (and data collection commenced) on October 3, 2003. Piezometer readings taken at the east and west end of the soil mass indicate that the saturation level reached a high of 33 cm from the bottom of the trough (1 m deep). Average values taken for the elevation heads within both standpipe piezometers are illustrated in Figure 4.1.

Moisture content and temperature readings were measured and recorded for specific depths (as shown in Figure 3.8) using buried TDR probes and temperature sensors. Water content profiles for this first winter of monitoring (2003 – 2004) are illustrated in Figure 4.2. The data supports the concept that the soil at the greatest depth

has the highest moisture content due to the fact that the water supply line fed the water from the bottom of the trough upwards.

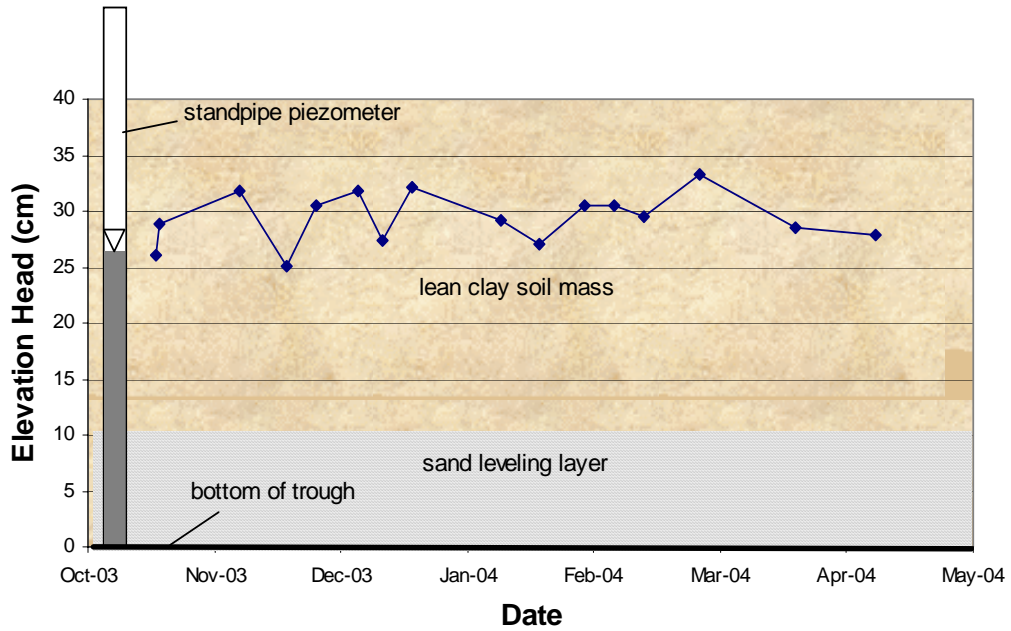


Figure 4.1: Graphical illustration of piezometer readings taken at the field facility.

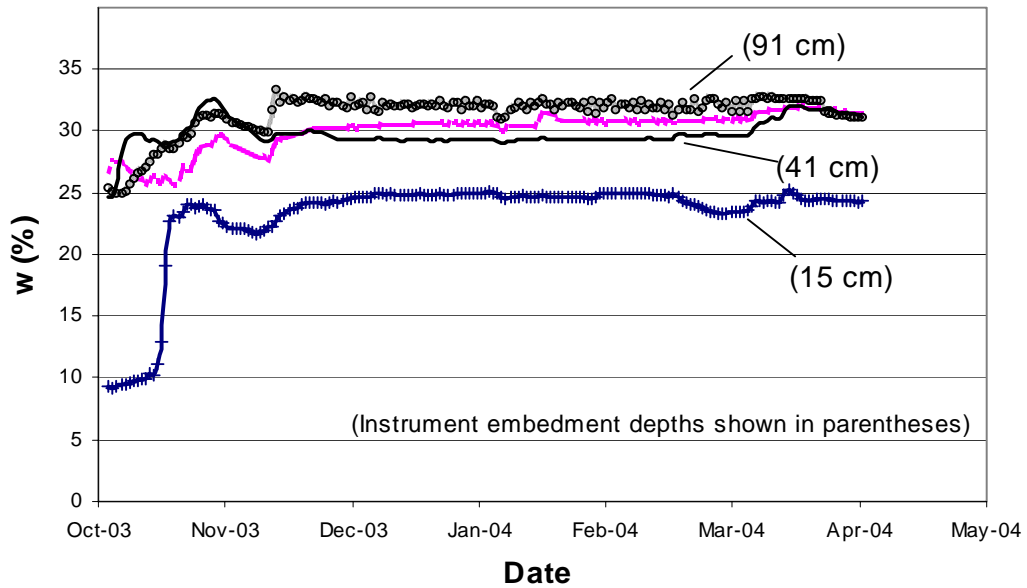


Figure 4.2: Graphical illustration of water content profiles for the Post Farm lean clay.

In addition to the water being added to the soil mass via the water supply tanks and perforated pipes at the bottom of the trough, a portable sprinkler provided moisture at the surface in an attempt to increase the water content, which was low as a result of disturbing and stockpiling the soil during the hot, dry summer months. The sprinkler was active for 2 to 3 hours at a time during the initial ten days of data collection, which explains the spike in surface moisture content. Subsequently, only the supply tanks were employed. The water level in the first supply tank was manually measured and recorded at approximately one-week intervals in order to determine the amount of water uptake throughout the freeze/thaw cycle. Additional water was supplied to the tank by means of an onsite hand pump and hose following each measurement session. Monthly and cumulative water uptake quantities are illustrated in Figure 4.3. Measurements indicate that the soil mass accumulated the highest volume of water at the onset of the freezing season, while the quantity of uptake generally decreased as the system reached equilibrium.

Temperature profiles for different instrument embedment depths within the soil mass are illustrated in Figure 4.4. Data from the temperature sensors indicate the maximum depth of frost front advancement was 46 cm. This corroborates the data illustrated in Figure 4.5, which is a diagram portraying the location of the 0 °C isotherm. Both graphs indicate the maximum advancement depth was reached on approximately February 20, lasting only a few days before thawing commenced.

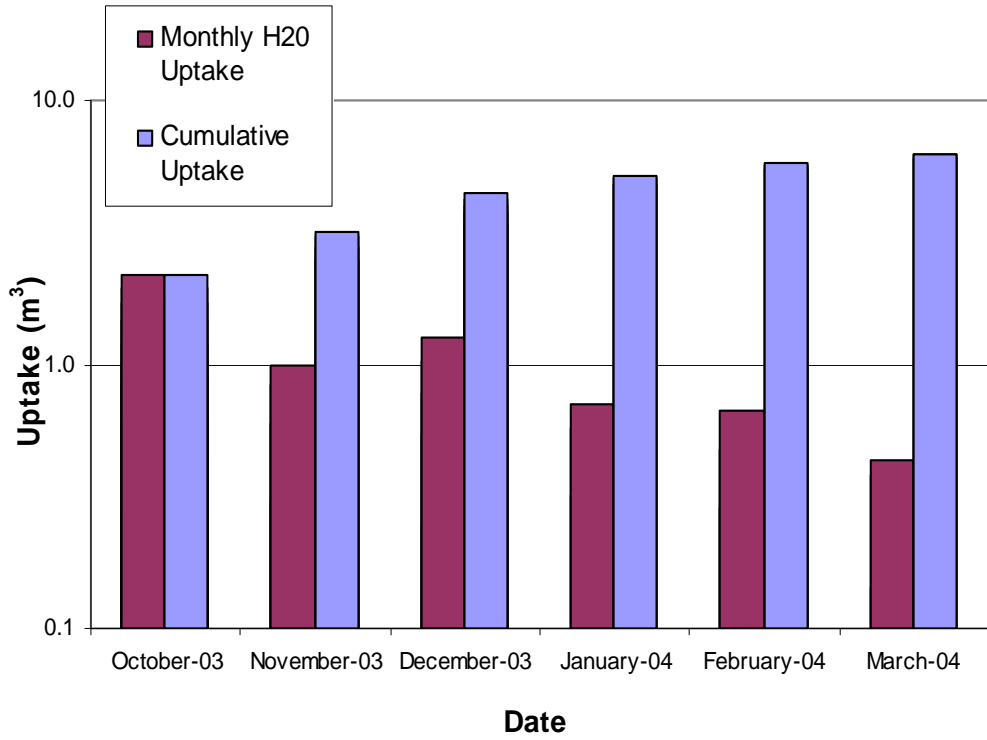


Figure 4.3: Graphical illustration of cumulative water uptake at the field facility during 2003 – 2004 winter season.

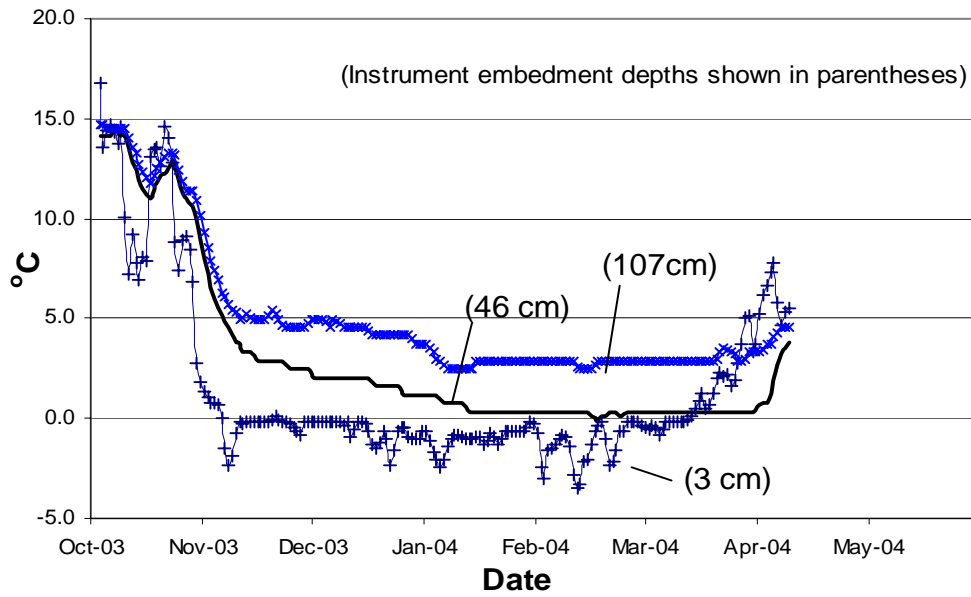


Figure 4.4: Graphical illustration of temperature profiles for various instrument embedment depths at the field facility.

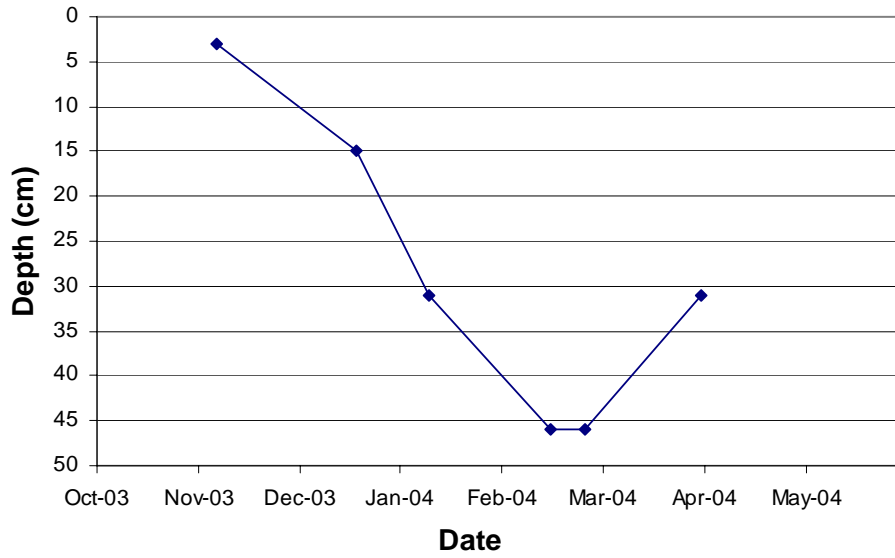


Figure 4.5: Graphical illustration of the location of the frost front at the field facility.

Figure 4.6 illustrates the average daily ground surface and ambient temperatures at the field frost heave test facility, demonstrating relatively significant air temperature fluctuations and the corresponding effect on surface temperatures.

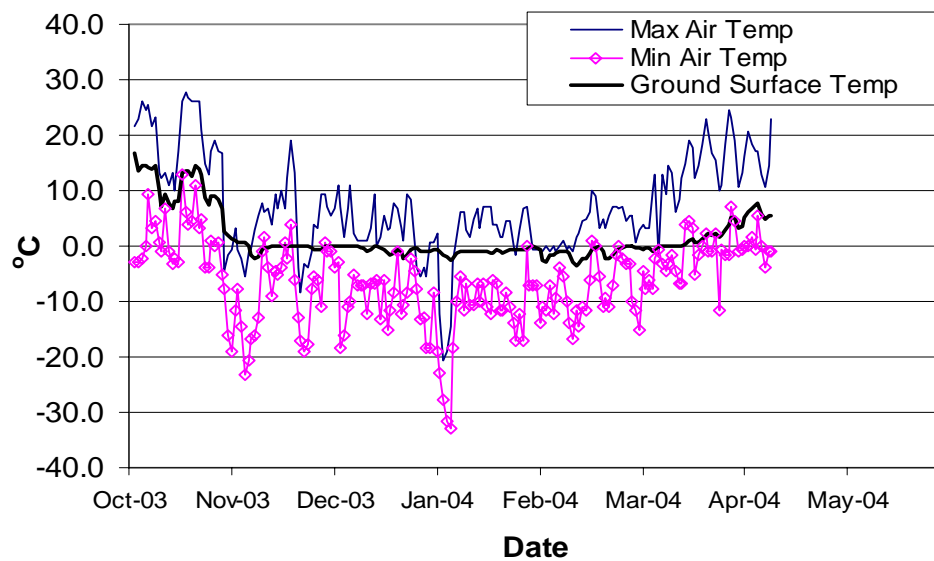


Figure 4.6: Graphical illustration of maximum and minimum air temperatures compared to ground surface temperatures at the field facility.

The results of the telltale readings, which were taken simultaneously with the water uptake measurements, are illustrated in Figure 4.7. Each telltale consisted of a ¼ - inch diameter rod of varying length, a ½ - inch diameter PVC sleeve (which loosely fit around each rod to minimize skin friction) an aluminum top plate measuring 2 cm x 2 cm, and an 8 cm x 8 cm base plate. The purpose of the telltales was to monitor the ground movement at different depths within the soil mass. The PVC sleeves were employed in order to reduce skin friction between the soil mass and the ¼ - inch diameter rods while ground movement (heave or settlement) was taking place. Thus, the movement of the top plates relative to the reference beams would be indicative of the amount of movement at the specified depths within the soil mass. Measurements were made using an electronic caliper by recording the distance between the aluminum reference beams and the top of each of the seven telltales. An illustration showing the layout of the telltales and their corresponding depth can be found in Chapter 3 (Figure 3.8.)

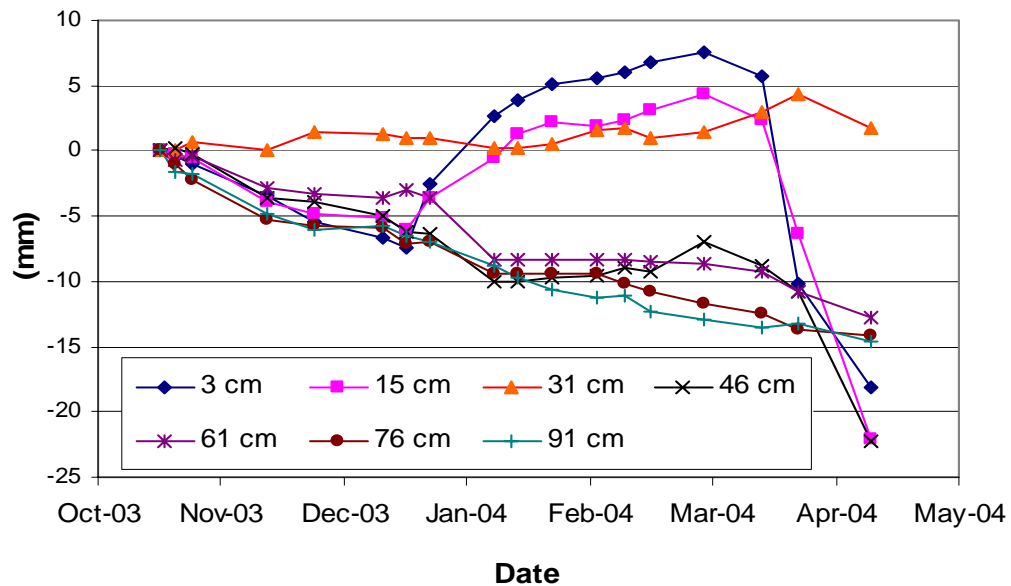


Figure 4.7: Graphical illustration of telltale readings for various embedment depths at the field facility.

The results indicate that the soil mass initially demonstrated settlement behavior, until freezing commenced, at which point an upward heave was measured as the frost front dropped below the telltale base plate elevation. The data indicates that heave initially occurred at the shallowest depth (3 cm) on December 15, 2003. The frost front slowly advanced to a maximum depth of 46 cm, which is illustrated by the upward heave beginning on February 15. The telltale measurements indicate that the soil mass settled during the thaw season.

The general procession of frost front advancement and subsequent heave indicates the soil type (lean clay) is at least moderately susceptible to frost action. Obscurities in the measured data, such as heave out of chronological order or heave at depths greater than frost front advancement, are attributed to telltale measurement error.

Discussion. Overall, the results of the field frost heave test facility over the 2003-04 freeze/thaw season proved to be encouraging. It was demonstrated that the water supply system worked smoothly and efficiently. All instruments embedded within the soil mass indicated that valid data was being recorded. The facility structure proved its integrity and weathering capabilities, specifically after the January 2004 snowstorm, in which the Bozeman area received over 20 inches of snow.

It should be noted that the backfilling of the test soil into the trough area probably had some effect on the outcome of the heave, settlement, and water uptake during the first season of measurements. In addition, it is probable that compaction efforts between lifts during the backfilling process were not consistent, regardless of the concern taken in the field to minimize inconsistencies between layers. For this reason, the author

concluded that typical results were not absolutely achievable during the first year of testing due to the natural settlement and pore water redistribution that would be experienced with a newly placed fill.

In order to increase the accuracy of heave measurements in the future, it is suggested that a more accurate method of telltale measurement be employed in order to minimize human error. One possible resolution towards alleviating any telltale measurement errors would be the implementation of an electronic survey transit system, in which elevation changes between the telltale top plates and reference beams could be more accurately monitored. After establishing an onsite elevation benchmark, the necessary readings could be easily taken and stored within the transit system data logger.

Laboratory Freeze-Thaw Tests

Preliminary laboratory testing began in May 2003, in which two experiments were conducted on the S80K20 mix. These first two tests served as groundbreaking exercises with the purpose of developing a generalized and consistent testing protocol. Modifications, including the addition of a custom-made hot plate and heat flux sensors, were made on the laboratory-testing device in order to polish the experimentation process and increase the efficiency of the laboratory testing components. Data collected from the earlier tests were used to refine the testing apparatus and protocol; consequently the data collected from these tests are not presented significantly in this report.

Seven laboratory-freezing tests were conducted on a combination of the S80K20 mix and the Post Farm lean clay (CL). The following section uses Test #1 as an example

to illustrate the procedures used for sample preparation and how certain variables may be affected depending on these setup procedures.

Example. Test #1 was conducted on the S80K20 mix beginning on June 17, 2003 and ending on July 8, 2003. Careful preparations were made in placing the test soil into the laboratory frost heave device prior to placement into the cold regions environmental chamber. The first step required the water reservoir to be filled to a level just below the top surface of the perforated platform such that when the device was connected to the Mariotte tube, all of the water leaving the Mariotte during the test could be attributed directly to water uptake. The test soil was then placed in three separate loose lifts. After each lift was placed, the soil received approximately 25 blows from a modified proctor compaction hammer in an attempt to compact each lift into three equal layers within the testing cylinder. Soil was added or removed respectively in order to achieve this. Extreme caution was taken during compaction in order not to disturb any thermocouples or heat flux plates, which is why it was decided not to add and compact all of the test soil at one time.

Water contents were taken for each lift to determine an average value for the entire soil profile. This value was used to develop a phase diagram of the test soil and calculate the initial saturation level (S) and dry density (ρ_d) prior to the test. For test #1, the S80K20 mix had an initial water content (w) of 13.4% with a corresponding saturation level of 46.3% and dry density of 1524 kg/m^3 .

A predetermined duration of testing was not established. Instead, it was decided to keep the laboratory test device in the cold chamber until positive movement of the

frozen soil (heave) ceased. Test #1 lasted 528 hours with only moderate adjustments being made to the setup throughout including adjustments to the thermal environment. While monitoring the data throughout the test, it was determined that the warm end temperature was too high, inhibiting frost front advancement and ultimately prohibiting further heave. At approximately the 360th hour, the heater temperature in the water reservoir was lowered from 18 °C to 10 °C. The temperature of the hot plate was also lowered from 20 °C to 8 °C, and the ambient temperature in the cold chamber room was lowered from -6.7 °C to -12 °C. Figure 4.8 illustrates the effect of this adjustment.

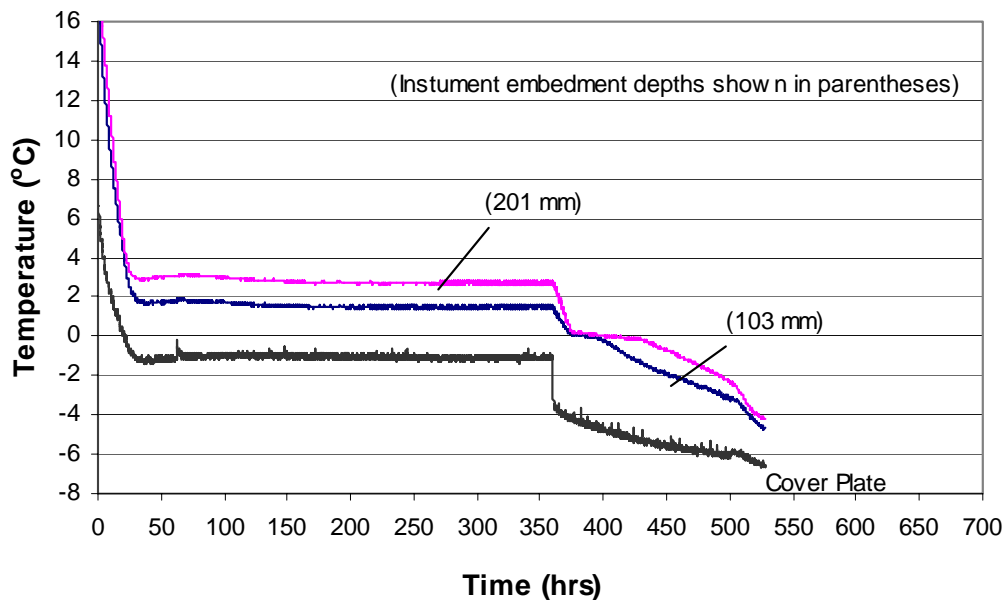


Figure 4.8: Graphical illustration of temperature distributions during freezing Test #1.

The rapid decrease in temperature at the top of the soil column is represented by the temperature taken by the thermocouple adhered to the underside of the steel cover plate (Refer to Figure 3.11). The data illustrates the significant impact that changes in

ambient conditions can have on ground surface temperatures. Furthermore, the rapid temperature change at a depth of 201 mm suggests that the warm end temperature control also has a significant impact on soil temperatures near the lower boundary condition. The data at the midpoint between these two depths (103 mm) shows a slower decline in temperature, suggesting that as the distance from the warm end boundary increases (while still at a significant depth from the surface) the impact on temperature change decreases.

Figure 4.8 does not show a temperature distribution nearer the bottom of the soil column due to complications that were experienced with some of the temperature measurement devices. This is explained in detail within the discussion section of the laboratory freeze thaw tests.

Figure 4.9 shows the location of the 0 °C isotherm and gives the rate of frost front advancement.

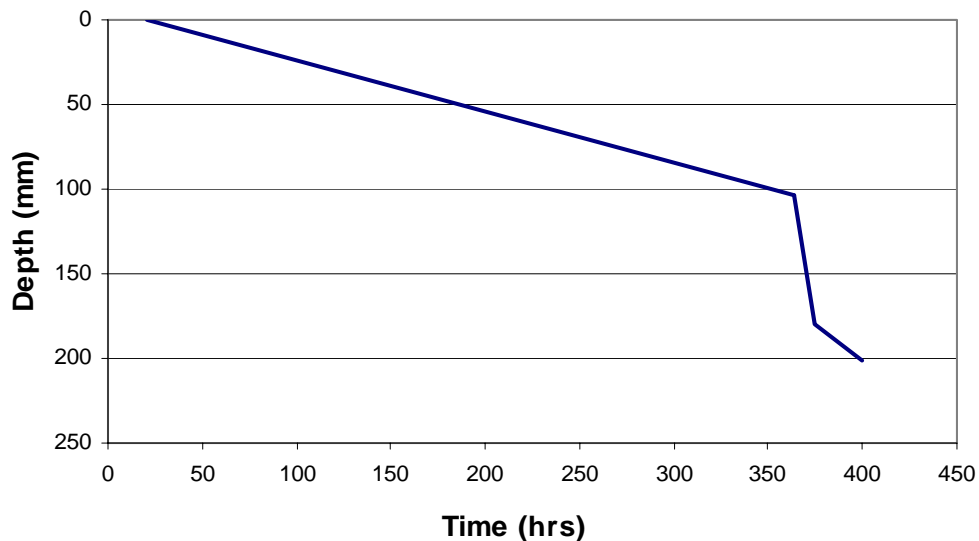


Figure 4.9: Graphical illustration of the frost front location throughout freezing Test #1.

The temperature reductions applied to the laboratory testing set up significantly impacted the rate at which the frost front advanced through the soil column. Recall from Chapter 2 that at the onset of a newly initiated cold side temperature, the rate of frost front advancement is relatively high. Temperature changes eventually decrease with time, causing the rate of advancement to slow down, as can be seen near the end of the laboratory test.

The location of the frost front could not be accurately defined due to the instrument malfunctions at depths greater than 201 mm. Therefore, Figure 4.9 does not show data for the entire duration of test #1. However, it can be logically predicted that the frost front did advance to greater depths for at least part of the remaining 128 hours of data collection, until system equilibrium was attained.

Figure 4.10 illustrates the water uptake measurements, as well as the volumetric heave experienced by the test soil. Recall that a linear variable displacement transducer (LVDT) was set up to capture the movement of the steel cover plate. The instrument measured only vertical motion. From here, a simple calculation was made using the known surface area of the test cylinder to determine the volumetric heave (cm^3).

The total volumetric heave experienced during heave Test #1 was 582 cm^3 . The amount of water migrating into the soil column throughout the freezing process was 350 cm^3 . Note the asymptotic behavior of water uptake near the end of testing. This may suggest the time at which the in-situ water level reached the final ice lens, prohibiting further water migration due to an impermeable interface.

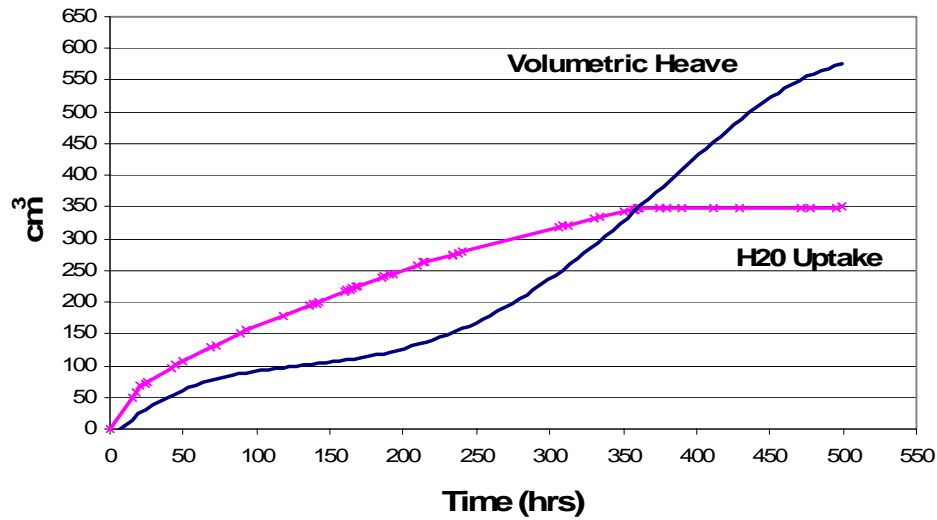


Figure 4.10: Graphical illustration of water uptake and volumetric heave measurements for freezing Test #1.

Figure 4.11 represents the overall temperature gradient throughout the soil column. The temperature gradient is a measure of the change in temperature (ΔT) per unit length. In this case, temperature data used in the calculation was taken from the thermocouple adhered to the underside of the cover plate and the thermocouple located at a depth of 201 mm (channel 11, Figure 3.11).

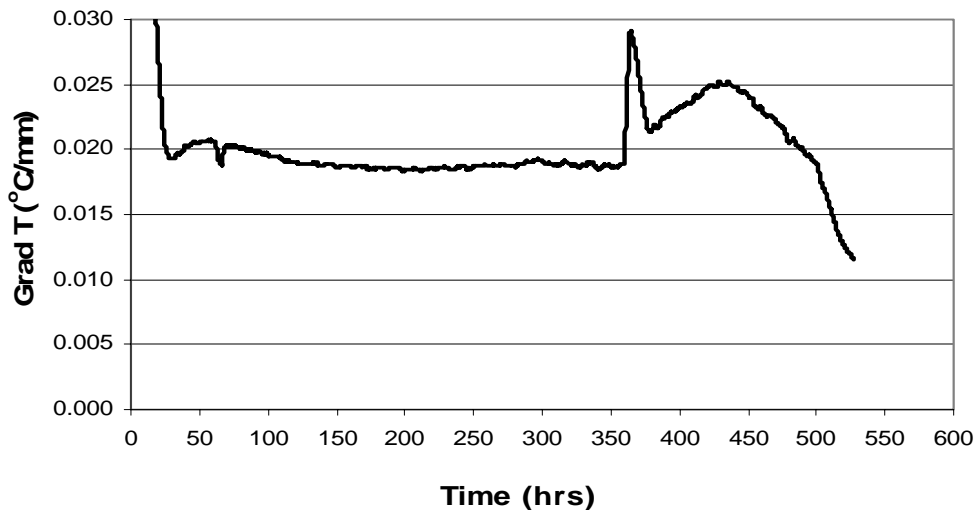


Figure 4.11: Graphical illustration of overall temperature gradient throughout soil column during freezing Test #1.

Examination of Figure 4.11 leads to the conclusion that the temperature gradient throughout a soil profile under freezing conditions should eventually become constant. The disturbance that is apparent beginning at the 360th hour is due to the adjustments made to the boundary temperatures, as previously mentioned. More specifically, the jump in temperature gradient is due in part to the fact that the ambient conditions changed very quickly, while the temperature at 201 mm remained unaffected for some time after. Theoretically, the gradient should begin to approach a constant value. However, the gradient continues to decrease through the remainder of the test due to heat loss of unequal rates at each of the boundary conditions.

Figure 4.12 illustrates the calculated value of segregation potential (SP), employing Equation 2.9. The SP is defined as the ratio of water uptake to temperature gradient in the frozen fringe.

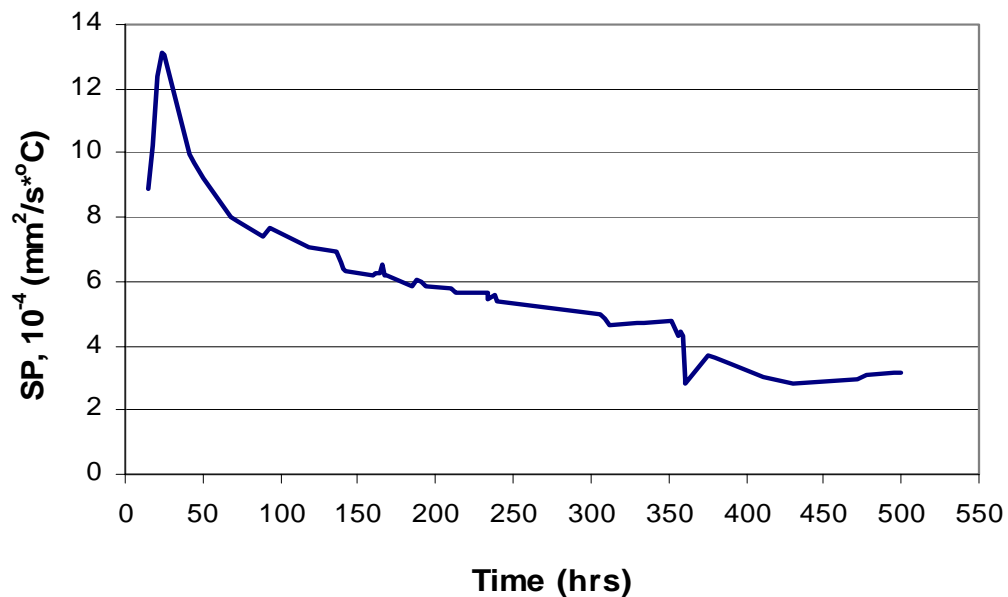


Figure 4.12: Graphical illustration of calculated SP values for freezing Test #1.

Recall that the amount of water migrating into the soil column was regulated by a device called a Mariotte tube, as discussed in Chapter 3. Initially, a pressure transducer was used in an attempt to electronically record changes in the water level within the Mariotte tube. However, calibrating the transducer was not possible for this test setup. The transducer proved to be extremely sensitive to pressure changes, which resulted in significant disturbance (noise) throughout data collection. This made determining an accurate measurement of water uptake with time virtually impossible. Therefore, readings of water level changes in the Mariotte tube were manually taken throughout the test. This was a practical solution that provided useful data. Results of the water migration rate yielded graphical representations of the segregation potential (SP) value similar to those presented by Konrad and Morgenstern (1987).

Discussion concerning the changing values for segregation potential is limited among papers by Konrad and Morgenstern. It is, however, logical to assume that the value of SP should approach a constant value as water migration rates and temperatures reach steady-state conditions. Therefore, the overall value of SP that should be applied to calculation of segregational and total heave is the value nearest the end of the test (in this case $3.0 \times 10^{-4} \text{ mm}^2/\text{s}^\circ\text{C}$).

Results. The remainder of the laboratory frost heave testing program continued through April of 2004. In all, seven tests were conducted: two using the S80K20 mix, and five with the Post Farm lean clay (CL). Table 4.1 summarizes the testing schedule and initial conditions of the test soil following sample preparations (i.e. prior to placement into the cold chamber). Table 4.2 summarizes the results of each of the seven

freezing tests. It should be noted that graphical illustrations were developed for all of the tests, similar to that of Test #1 described in this section (see Appendix B).

Table 4.1- Laboratory Frost Heave Test Schedule

Test No.	Date	Soil	Initial w(%)	Initial S(%)	Initial ρ_d (kg/m ³)
1	6/17-7/8/03	S80K20	13.4	46.3	1524
2	11/20-12/9/03	S80K20	11.5	42.7	1568
3	12/24 -1/4/04	P.F. CL	17.7	37	1205
4	2/25 - 3/3/04	P.F. CL No H ₂ O Uptake	16	36	1255
5	3/5 - 3/17/04	P.F. CL w/ H ₂ O Uptake	16	36	1255
6	3/24 - 4/1/04	P.F. CL; S=100% No H ₂ O Uptake	44.6	100	1255
7	4/5 - 4/12/04	P.F. CL; S=100% w/ H ₂ O Uptake	44.6	100	1255

Table 4.2 - Results

Test No.	Length of Test (hrs)	Total Heave (mm)	Total Vol. Heave (cm ³)	Total H ₂ O Uptake (cm ³)	Avg. Temp. Gradient (°C/mm)	Avg. Frozen Thermal Conductivity (W/m°C)	SP 10 ⁻⁴ (mm ² /s°C)
1	528	17.4	582	350	0.019	1.82	3.054
2	462	12.4	394	1003	0.024	N/A	7.919
3	263.5	8.4	266.5	830.5	0.03	N/A	9.197
4	165	0	0	N/A	0.033	0.4	N/A
5	285.5	0	0	1199	0.03	0.46	12.255
6	191	4.4	138.7	N/A	0.025	0.44	N/A
7	163	1.77	56.2	86.3	0.031	0.3	1.495

Discussion. For the first laboratory-freezing test, both thermistors and thermocouples were used to measure temperature within the soil specimen. The thermistors were installed throughout the soil profile at depths indicated by Channels 1 through 7 in Figure 3.11. All other instruments were used as indicated in the same diagram. However, at the conclusion of Test #1 it was determined that the thermistors had not been correctly calibrated, which resulted in discrepancies in temperature data. Further examination led to the conclusion that data measured using the thermocouples were the only valid quantities that could be used for analysis. For the remaining tests, it was decided that only thermocouples would be used for temperature measurement for the sake of accuracy and uniformity throughout the soil profile. For laboratory tests 2 through 7, the set-up used was exactly as indicated in Figure 3.11. Simply put, Type T thermocouples replaced the thermistors at the locations shown.

Frost heave Test #2 had similar initial boundary conditions to those of the first test on the S80K20 mix. However, it was discovered at the completion of the test that the heat flux plates had been damaged following Test #1. Therefore, any data recorded was deemed insignificant and the calculation of thermal conductivity values proved to be invalid. Furthermore, the water uptake and heave results proved to be quite different. The total water uptake was almost three times that of Test #1, while the duration of the test was shorter by 66 hours. This resulted in a higher water migration rate and, ultimately, a significantly higher SP value. The results of the temperature data illustrated a uniform profile indicating relatively small amounts of disturbance to the thermal conditions throughout the test. Furthermore, the temperature gradient approached an

overall value of approximately 0.2 C/mm, which was consistent with the overall value of Test #1. This was encouraging considering the adjustments made to the temperature reading instruments.

Test #3 was conducted on samples of the Post Farm lean clay (CL) obtained from the field test site. Again the heat flux plates were incapacitated, and the test was conducted without the use of them. Overall the freezing test showed a significant amount of total heave. However, it was discovered during the testing that the warm plate being used malfunctioned, which resulted in an unstable temperature profile. At the completion of the test, a new and improved warm plate was fabricated and used throughout the final four experiments. Furthermore, a new heat flux plate was ordered and installed to be used throughout the final laboratory freezing tests. The flux plate was reinforced by placing the thin foil within an aluminum and Plexiglas housing, ensuring the instrument would not be damaged during preparatory procedures, or removal of the test specimen.

Tests 4 through 7 were conducted on the Post Farm CL as a parametric study. A fresh sample was prepared before Test #4 with the initial conditions shown in Table 4.1. A freezing test was then performed without the availability of water to the system. As the results indicate in Table 4.2, there was no observable total heave by the end of the test. However, the uniform temperature distributions and consistent temperature gradient indicate that the new warm plate worked efficiently, maintaining a relatively constant warm-end boundary condition. Furthermore, the heat flux device installed within its new protective casing performed very effectively measuring significant data to be used in the calculation of the unfrozen and frozen thermal conductivity of the soil specimen.

Following the conclusion of laboratory freeze Test #4, the frost heave device was removed from the cold room to thaw. Plastic was wrapped around the column to avoid moisture loss. After it was determined that the entire soil profile had reached room temperature again, the device was placed back into the cold chamber to begin the next test in the parametric study of the Post Farm CL.

Test #5 assumed the same initial conditions of #4, but added the availability of water to the system. At the onset of freezing Test #5, it was discovered that the immersion heater which controlled the temperature of the ethanol glycol being pumped through the warm plate system was reaching extremely hot temperatures. Throughout the freezing test, adjustments were made to the warm plate system in an attempt to achieve a lower and more consistent fluid temperature. These adjustments led to the instability in temperature distribution and gradient throughout the freeze cycle, as illustrated in Figure B.21 and B.22 respectively. On the other hand, the heat flux sensor casing once again proved its durability and reliability as it measured flux values which were very consistent with those measured in Test #4, resulting in an overall frozen thermal conductivity of $0.46 \text{ W/m } ^\circ\text{C}$

The amount of water from the Mariotte tube being taken up by the soil column proved to be rather significant, as the water supply system had to be refilled twice during the test. However the system again experienced zero total heave. Prior to the third test in the parametric study (Test #6) of the Post Farm lean clay, the testing device was again removed and allowed to thaw.

Before Test #6 was conducted, the device was connected to the Mariotte tube outside of the cold chamber in an attempt to saturate the soil sample. It was during this phase that it was discovered that the testing apparatus contained leak points in the PVC column. After hours of repair work, the device eventually began to hold water, and the sample was nearly saturated. The device was then placed in the cold chamber to freeze under saturated conditions, but without the availability of water uptake from the Mariotte tube.

Other complications included the loss of power to the data acquisition system for the initial 86 hours of the experiment. As a result, the graph illustrations included in Appendix B for Test #6 demonstrate only the latter half of the freeze cycle. For this reason, the temperature gradient that was interpreted from the available data was significantly less than that observed for the Post Farm CL in Tests 3 – 5.

It should be noted that the temperature data corresponding with the calculated thermal conductivity values cannot be seen on the graph (Figure B.29) as the soil temperature at the depth of the heat flux sensor had already dropped well below 0 °C. Also, the location of the frost front could not be accurately traced and is therefore not included in the illustrations. As the data indicates however, some total heave was measured, though significantly less than Test #3.

Test #7 began after the sample was removed from the cold room and thawed. The testing device was connected to the Mariotte tube prior to freezing in attempt to again achieve saturation levels. A relatively small amount of water was taken up by the

system, indicating that the sample was not completely saturated in Test #6. Furthermore, the water was available to the soil column for uptake during the freezing test.

Test #7 resulted in a lesser amount of total heave than that observed in #6, which led the author to the conclusion that the methods of test preparation and the testing device itself needed to be even further modified in order to produce consistent, reliable results. The heat flux sensor appeared to be measuring unstable heat flow rates at the onset of the freezing cycle, as illustrated in Figure B.34. However, the soil mass eventually achieved more stable conditions as the frost front progressed throughout the depth of the flux sensor.

The adjustments and repairs that were made to the laboratory freeze test setup seemed natural for this initial phase of testing. Regardless, some important conclusions can still be drawn from results of these first seven tests. Aside from the complications that arose due to calibration error and application of different temperature instruments, the author suspects that the adjustment of the warm end boundary condition has a significant impact on the test soil at depths closer to the boundary. The same can be said for the impact that fluctuations in ambient conditions can have on the soil at depths closer to the surface, as was demonstrated in Test #1. The reasoning and answers to the behavioral characteristics of the soil “in between” the warm and cold end boundaries as a reaction to these changes lies within the fundamental principles of the frost heave theory. The purpose of the development of a laboratory frost heave testing device was to ultimately answer the questions: How much do the fluctuations in ambient and warm end conditions affect the test results, and where does the greatest impact occur?

Furthermore, the location of the 0 °C isotherm (frost front) is a crucial aspect behind the mechanics of frost heave theory. Recall that as soil temperatures approach 0 °C, the in-situ pore water begins to freeze causing ice crystals to grow between soil particles. As the phase change from a liquid to solid occurs, a 1.09% volumetric increase is experienced causing the expansion (heave) of the soil. However, as indicated in the test results, there exists the possibility that freezing of pore water and segregational heave are not the only variables contributing to the total heave of the system. It is the author's presumption that in the case of Tests # 4 and 5, the amount of in situ pore water was not significant enough to result in a positive total heave of the soil column. Furthermore, as observed in Test #5, sample preparation appears to significantly affect the outcome of the test.

Among the many steps involved in preparing a soil sample for a freeze test, the method of placement and compaction seem to be of the most crucial. For example, it is extremely difficult to hypothesize with any degree of accuracy that the compaction efforts applied to each of the three layers during preparation maintained a level of consistency that would or would not affect the amount of segregational and total heave. Even if the layers were consistently compacted, there would still exist density gradients as a result of pressure redistribution throughout the soil column. Therefore, the author suggests that a more viable protocol be implemented in the future towards preparing laboratory test soils into the freezing apparatus.

One approach would be to predetermine a level of consolidation for each soil following placement into the PVC cylinder. In addition, the method of placement could

be modified in order to improve uniform distribution and reduce the disturbance induced upon the instruments. For example, the test soil could be poured over a sieve in an attempt to achieve a “raining” effect into the cylinder, and ultimately facilitate uniform placement. Furthermore, the soil column could then be placed on a vibratory table used for compaction effort instead of using the hand-tamping device to compact the soil. This approach would also minimize damage done to the instruments inside of the cylinder. Theoretically, this modified approach to soil placement would eliminate any voids throughout the soil profile and, ultimately, eliminate the possibility of segregational heave without any observable total heave.

Konrad and Morgenstern (1987, 1981, and 1980) have dedicated an exceptional amount of time in the laboratory to identifying the quintessential characteristics of soil behavior during freezing conditions. Overall, the results of the seven laboratory freezing tests described in this chapter proved to be an encouraging start in the attempt to develop a practical approach to predicting the magnitude of frost heave at the laboratory scale. However, discrepancies among the tests in the parametric study indicate that modifications need to be made to the test sample preparation protocol before further testing commences. Because of the fact that there are so many variables involved with developing a feasible frost heave model, consistent preparation practices are necessary in developing the framework towards examining correlations between common geotechnical index properties, and observable laboratory frost heave behavior.

CHAPTER 5

PREDICTIVE FROST HEAVE MODEL

Introduction

The objectives of this component of the study were to examine the effectiveness of a numerical model based on the segregation potential (SP) concept, and to compare the analytical results to observations made at the field frost heave test facility during the 2003 – 2004 season. The fundamental mechanisms behind the one dimensional frost heave theory, as discussed in this paper, have proven in the past to be far too complex to accurately model using analytical solution methods. This chapter discusses the SSR model (Saarelainen, 1992) which is a numerical (approximation) model developed to calculate the incremental heave rate and total heave of freezing soils under laboratory conditions based on the segregation potential parameter. The model is based on thermal equilibrium at the frost front and relies carefully on the parameters that are specified as input values. The author's approach for developing a predictive model based on the SSR approach is described herein.

The SSR Frost Heave ModelBackground

The SSR model as proposed by Saarelainen (1992) is based on thermal equilibrium at the freezing front, which primarily consists of three components:

- 1) The heat transfer to the frost front from the unfrozen ground,

- 2) The heat flow generated by the freezing of in-situ pore water, and
- 3) The heat flow generated by ice segregation.

It is assumed that these components constitute the total amount of heat transfer through the frozen layer.

Ground surface temperature appears to be a decisive factor driving the rates of frost penetration and thawing (Saarelainen, 1992). Fluctuations in ground temperatures are directly dependent upon thermal variations at the ground surface. The main contributors to ground temperature fluctuations include the loss of heat stored in the ground, the heat transfer between the ground surface and the atmosphere (convection), the radiation balance at the ground surface, and the heat generated in both the ground and atmosphere through conductive processes.

At the onset of freezing, heat is released from the ground as freezing temperatures penetrate the ground surface and begin the cooling process. Heat is either transferred from great depths via the geothermal gradient (approximately $3\text{ }^{\circ}\text{C}/100\text{m}$), or heat stored in the ground from the previous warm period (summer) is lost. The heat transfer from unfrozen ground to the freezing front can be accounted for using numerical techniques. This requires the consideration of thermal conditions at the ground surface at the onset of freezing, the soil profile, and the appropriate thermal properties (Saarelainen, 1992).

In-situ pore water will freeze only if the rate of heat flow through the frozen layer is greater than that of heat flow to the freezing front generated by stored heat or the geothermal gradient. Pore water freezes as temperatures fall below $0\text{ }^{\circ}\text{C}$. However, it is possible for pore water to exist at temperature below $0\text{ }^{\circ}\text{C}$ due in part to impurities found

in the water, and due partly to the lowering of the freezing point caused by suction pressures that develop at the ice lens.

The rate in which heat is lost at the onset of a laboratory-freezing test is relatively rapid. While pore water within the soil matrix begins to freeze, ice grows in the direction of heat loss. As soil temperatures continue to fall below freezing, pore pressures decrease in the unfrozen water films between the growing ice body and the mineral grains causing moisture to migrate from the unfrozen soil region below towards the accumulation zone (ice lens), as depicted in Figure 2.2. The growing ice lens acts as an impermeable moisture barrier. Suction is further induced by the rapid cooling of pore water (Saarelainen, 1992). The process of ice segregation is maintained as long as a continuous flow path exists from a source of water to the frozen fringe and ice lens.

Heat transfer due to the fluctuation of surface temperature takes place primarily in the frozen region. The continuous rate of cooling at the ice lens produces heat exchange which opposes the heat flow from the ground surface. However, this effect is negligible compared with the cumulative heat flux resulting from in-situ pore water freezing, geothermal or preexisting ground heat conditions, and the effects of ice segregation (Saarelainen, 1992).

Heat Balance Equation

The equation that represents the thermal equilibrium at the freezing front – according to the SSR model (Saarelainen, 1992) – can be written as follows:

$$\lambda_f gradT_- = \lambda_t gradT_+ + \frac{L\Delta z_o}{\Delta t} + \frac{L_w(SP)T_p}{z^*} \quad (\text{Eq 5.1})$$

where:

λ_f = thermal conductivity of the frozen soil,

$gradT_-$ = temperature gradient of the frozen soil,

λ_t = thermal conductivity of the unfrozen soil at the frost front,

$gradT_+$ = temperature gradient of the unfrozen soil,

L = volumetric latent heat of the freezing soil at the frost front,

Δz_o = increase in frost penetration with time,

Δt = change in time,

L_w = volumetric latent heat of water,

SP = segregation potential, and

T_p = surface temperature.

Saarelainen further defines $gradT_-$ as $(T_f - T_p)/z^*$, the difference between the surface temperature and the temperature of the freezing soil at the frost front (T_f), divided by (what the author of this paper presumes is) a careful estimation of the average depth to frost penetration. Specifically, the author of this report interprets z^* to be a weighted average value of depth to frost penetration, incorporating the thickness and respective thermal conductivity of individual frozen layers throughout the entire frozen region as a function of time. The SSR model as described by Saarelainen (1992) defines this parameter as follows:

$$z^* = \lambda_{fz} R_{fz} + 0.5\Delta z_o \quad (\text{Eq 5.2})$$

where:

λ_{fz} = thermal conductivity of the frozen layer at the frost front,

R_{fz} = total thermal resistance of the frozen layers – $\Sigma(z_i/\lambda_{fi})$,

z_i = thickness of the frozen layer i ,

λ_{fi} = thermal conductivity of the frozen layer i .

The discussion by Saarelainen goes on to solve Δz_o (net increase of frost penetration) as a function of the above parameters (including the thermal resistance) and time, while introducing a new coefficient (S) which accounts for the intensity of ground heat dependent upon the time of year. This equation becomes iterative as the individual frozen layers change location (depth) with increasing time.

The amount of frost heave can then be calculated by employing the definition of segregation potential (Konrad and Morgenstern, 1980, 1981, and 1987), which incorporates the parameters defined in Equations 5.1 and 5.2 as follows:

$$dh_s = 1.09 * SP grad T_- dt = \frac{1.09 * SP(T_p - T_f) dt}{\lambda_{fz} R_{fz}} \quad (\text{Eq 5.3})$$

Closer examination of the parameters defined in Equations 5.2 and 5.3 reveals that the denominator $\lambda_f R_f$ is equal to the depth to the frost front z_f at the completion of the freeze cycle.

The SSR model incorporated a computer program which was written on the basis of an iterative calculation procedure to solve for incremental frost heave as a function of time. In order to calculate the total heave expected based on carefully determined

thermal and other engineering parameters, a numerical integration method would be used to solve for Equation 5.3.

The SP Model

Objective

The primary purpose of this numerical analysis was to examine the effectiveness of a model that could be used for predicting freezing and thawing behavior of frost susceptible soils. The model, which is based largely on the theory behind the SSR concept, predicts the amount of frost heave or settlement a specific soil type would experience for a given set of input parameters and thermal conditions. The parameters are determined from laboratory freezing tests, and the thermal conditions are intended to be representative of typical freezing and thawing cycles.

Procedure

The following assumptions were made in the development of the predictive numerical frost heave model:

- 1) One-dimensional range of motion (i.e., only vertical heave and compression).
- 2) Solute-free soil-water-void matrix.
- 3) Average overall thermal conductivity value throughout depth of the frozen zone.
- 4) Average overall SP value determined by laboratory freezing tests.

The following procedural steps were employed to analyze laboratory freeze test data and develop input parameters for the numerical analyses:

- 1) Obtain temperature distributions for specified soil depths.
- 2) Calculate temperature gradients throughout soil profile.
- 3) Determine the location of the 0 °C isotherm (frost front).
- 4) Determine the volume of water taken up by the soil mass during the freeze cycle.
- 5) Calculate the volumetric heave experienced by the laboratory test specimen.
- 6) Calculate the thermal conductivity (k_t) of the soil using Equation 3.1.
- 7) Calculate the segregation potential (SP) throughout the duration of the freeze cycle using Equation 2.9.
- 8) Apply the SP value as an input to the numerical model.

Temperature Profiles. The first step in analyzing the data acquired from the laboratory freezing test was the development of temperature distributions throughout the depth of the soil profile. This information graphically illustrates the efficiency and consistency of both the warm and cold-end boundary conditions (Figure 5.1). The “steepness” of the curve at the beginning of the test demonstrates the high rate of frost penetration at the onset of freezing. This information also presents an estimate of the frost penetration depth.

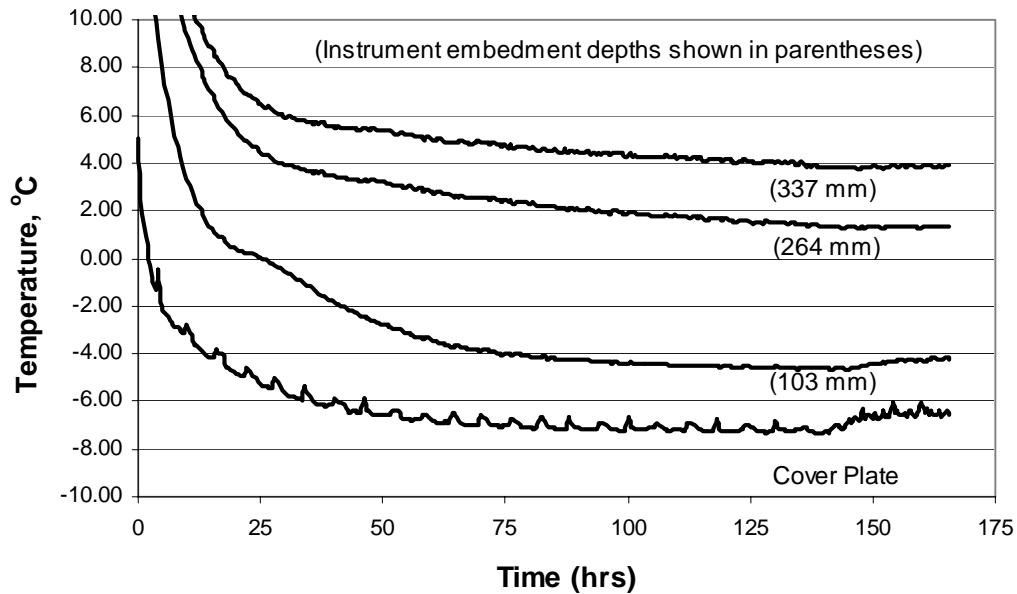


Figure 5.1: Graphical illustration of temperature distributions throughout the soil column during freezing Test #4.

Temperature Gradient. The development of the thermal gradient throughout the soil profile is the second step in the analysis. The model requires the overall gradient in the frozen fringe throughout the duration of the laboratory freezing test. This required the temperature distribution at the soil column surface (cover plate), the thermal distribution at the final frost front, and the depth to frost penetration. The temperature data in Figure 5.1 reveals that fluctuations in ambient conditions (temperature changes in the cold chamber) are more significantly observed by the thermocouple adhered to the underside of the steel cover plate. Regardless, the temperature profiles specific to this depth were consistently used in the calculation in order to emphasize the significance of the cold-end boundary condition. The temperature distribution at the final depth of frost front varied between tests, and was dependent on soil type, initial conditions, and duration of the freezing test.

The author chose to evaluate the thermal gradient of each laboratory freezing test during the period of time that the system demonstrated steady-state conditions (temperature changes with time were approximately equal throughout the soil column). Ideally, this should occur at the end of the test, pending the consistency of the boundary conditions (as illustrated in Figure 5.2). The value of overall temperature gradient that was reported in Table B.2 for Test #4 was calculated as the average value from $t > 25$ hours.

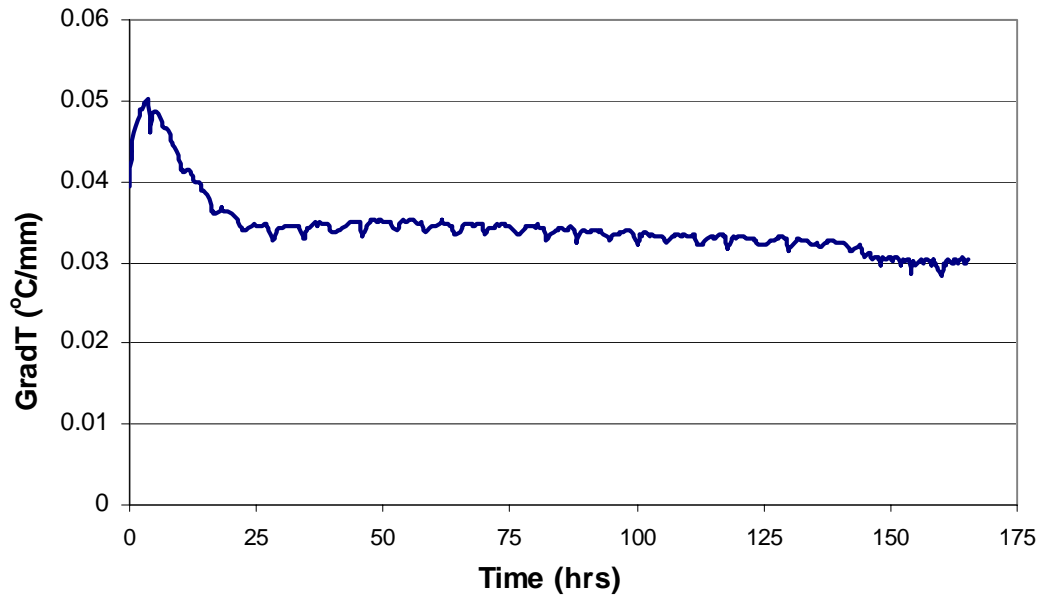


Figure 5.2: Graphical illustration of overall temperature gradient throughout the soil column during freezing Test #4.

However, some of the early laboratory freezing tests experienced significant modifications as part of the natural procedural development (as discussed in Chapter 4). Specifically, the temperature of the warm plate was adjusted in an attempt to increase the frost penetration rate. This resulted in steady-state conditions during the middle of the

test before adjustments were made (see Figure 5.3). The overall thermal gradient reported in Table B.2 was the average value taken from $100 < t < 350$ hours.

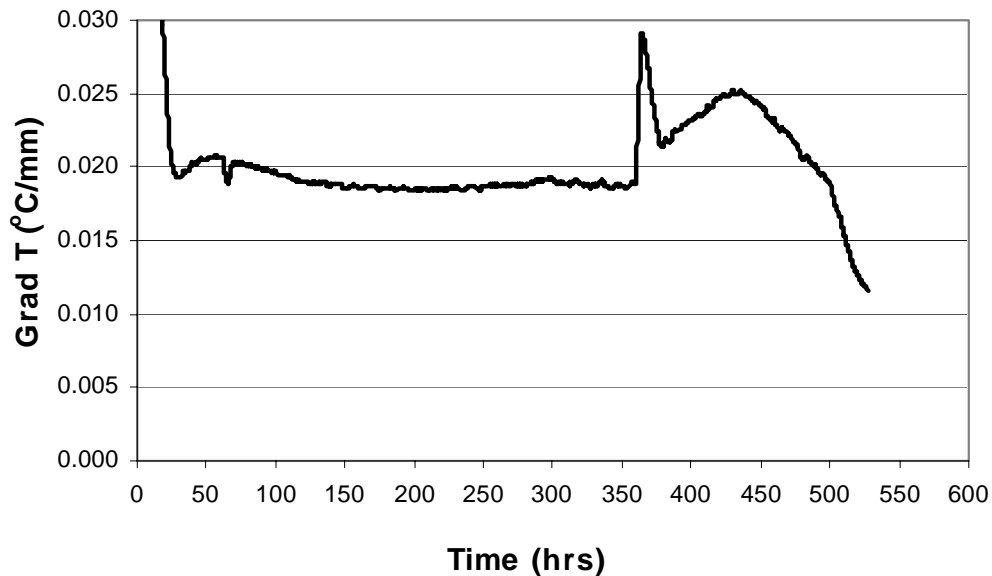


Figure 5.3: Graphical illustration of overall temperature gradient throughout the soil column during freezing Test #1.

It should be noted that the values for thermal gradient reported in Table B.2 are presented for comparative reasons only. The purpose was to examine the similarities and differences in overall thermal gradients between equivalent soil types for different laboratory freezing experiments. The predictive model actually utilizes real-time values in the calculation step to achieve incremental frost heave rates at the corresponding moment in time. This allows the model to incorporate natural fluctuations in ground surface temperatures in the analysis.

Frost Front. By isolating the location of the 0°C isotherm, certain behavioral characteristics of specific soil types under freezing conditions can be observed. For

example, the S80K20 composition can be compared to the Post Farm CL in terms of the frost penetration rate and maximum depth. Figure 5.4 illustrates the frost front profiles for S80K20 and the Post Farm CL during separate laboratory freezing tests.

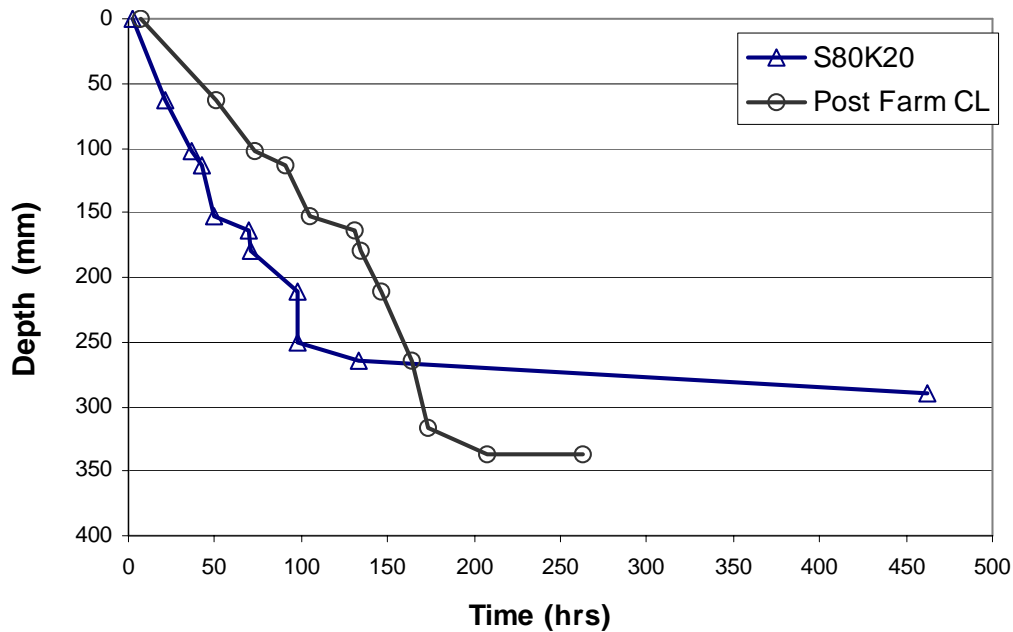


Figure 5.4: Graphical illustration of the frost front location throughout various freezing tests.

The frost penetration profiles illustrated in Figure 5.4 represent a means to characterize different soil types based on thermal behavior. The chart shows that the S80K20 composition demonstrated a higher penetration rate to a depth of 250 mm, but rapidly slowed its progression after that depth. The Post Farm CL demonstrated slower, but more deliberate frost penetration, reaching the maximum depth of 337 mm. Though more empirical data is necessary in order to draw accurate conclusions from these tests, one may presume that lean clays are naturally more susceptible to deeper frost penetration than silty compositions.

Water Uptake. The other parameter of primary concern when evaluating the segregation potential of a frost susceptible soil is the amount of water migrating into the soil mass due to suction pressures developed at the growing ice lens. Water levels within the Mariotte tube were observed and manually recorded. These values were converted into volumetric flow rates and plotted over the duration of the laboratory freezing test with the corresponding volumetric frost heave, as illustrated in Figure 5.5.

Heave. A linear variable displacement transducer (LVDT) was positioned to measure the vertical motion of the surface of the soil column. Vertical displacements were recorded and converted into volumetric heave by multiplying the displacements by the known surface area of the plate.

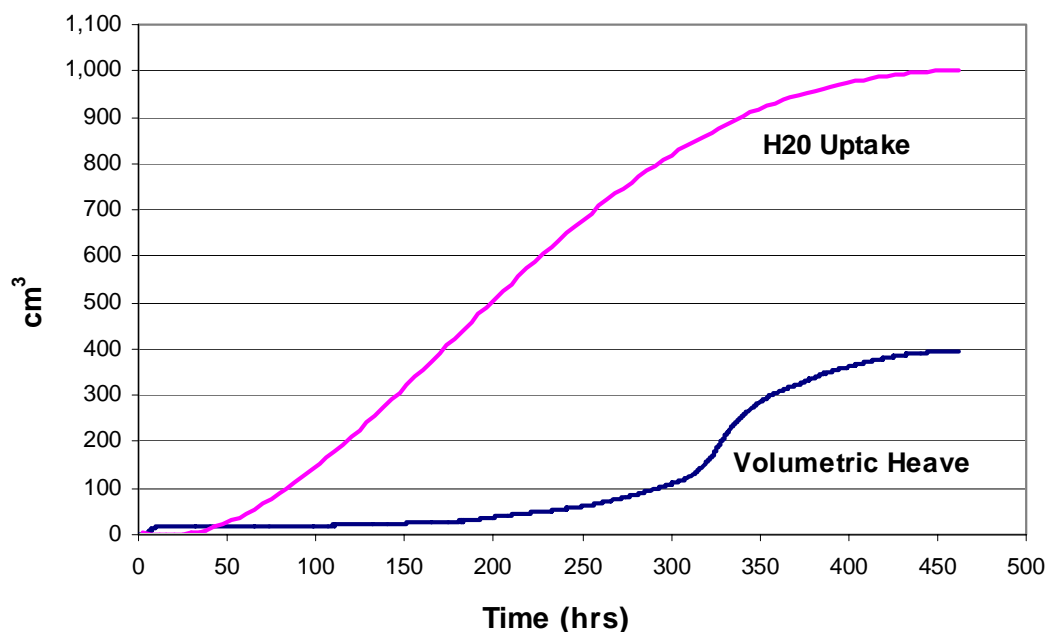


Figure 5.5: Graphical illustration of heave and water uptake measurements during freezing Test #2.

Thermal Conductivity. Evaluation of the thermal conductivity throughout the frozen fringe required the use of sensitive heat flux sensors. These sensors consisted of a thin film coil apparatus, which measured the temperature differential across its surface and converted it into a measure of the heat transfer rate (q/A). This data was then used to calculate the thermal conductivity at specific depths using Equation 3.1, which was dependent upon the heat flux and the thermal gradient. These instruments proved to be extremely delicate, as two were damaged after removing the soil specimen from Test #1. Subsequently, a reinforced casing consisting of aluminum and Plexiglas plates was constructed to house the new flux sensor.

Figure 5.6 illustrates typical behavior of the thermal conductivity of soil during a laboratory freezing test. The rapid increase as the frost front advances past the depth of the flux sensor supports the relationship between the thermal conductivity of pure ice and water. The thermal conductivity of ice has been found to be approximately 4 times that of water (Andersland and Ladanyi, 2004).

Segregation Potential. Once the volumetric flow rate and overall thermal gradient throughout the frozen fringe was determined, the SP was calculated by employing Equation 2.9. According to results presented by Konrad and Morgenstern (1987), the calculation of SP should indicate a “spike” at the beginning of the freezing test, as the maximum thermal gradient occurs at the onset of freezing (see Figure 5.7).

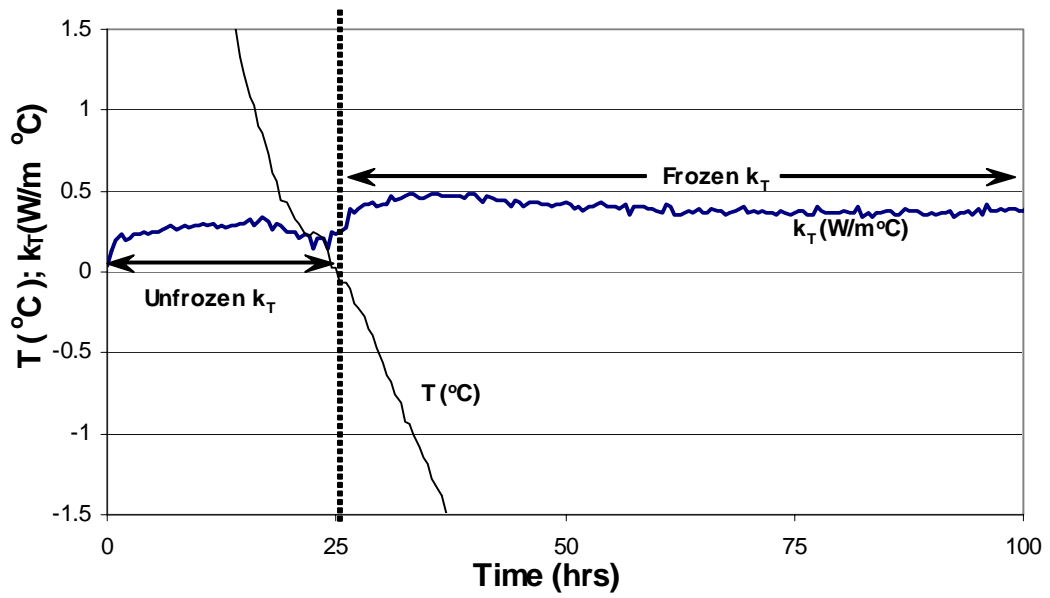


Figure 5.6: Graphical illustration of calculated thermal conductivity values for freezing Test #4.

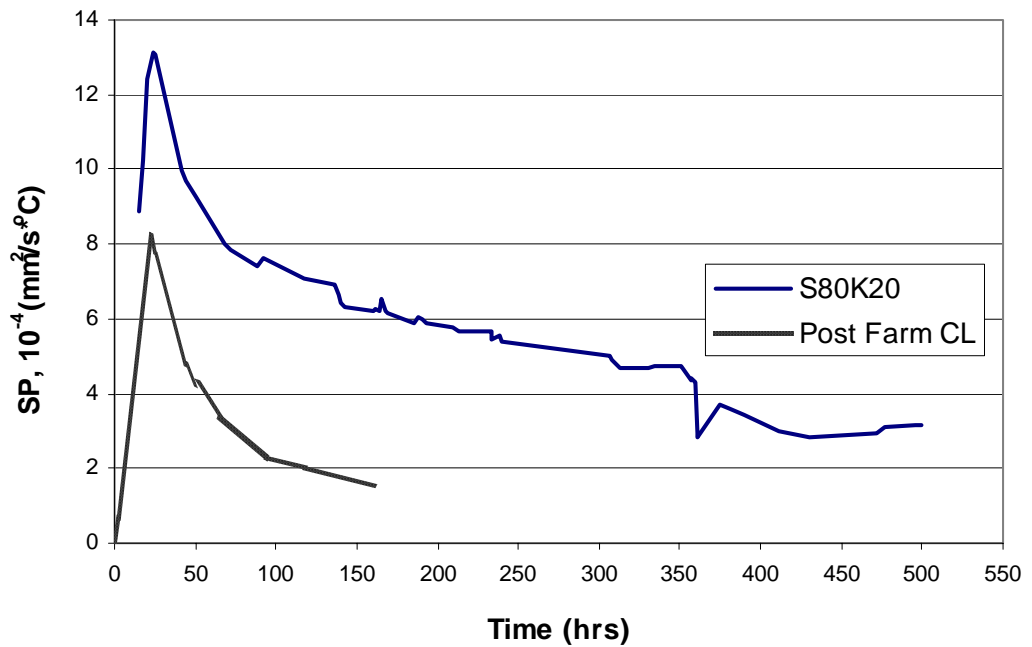


Figure 5.7: Graphical illustration of calculated SP values for various freezing tests.

Numerical Model Application. The overall value of SP was approximated by observing the behavior of the soil as the system approached steady-state conditions (that is the point at which the frost front no longer penetrated the soil depth). This can be seen in Figure 5.7 at the end of the freezing test as the segregation potential asymptotically approached a constant value. During the initial development stages of the predictive numerical model, it was this “constant” value that was used as an input parameter to calculate the incremental heave rates. For example, the SP value to be used in the model to predict heave rate and displacement activity for the S80K20 composition was $3.1 \times 10^{-4} \text{ mm}^2/\text{sec } ^\circ\text{C}$.

Development of a Predictive Model

The theory behind this numerical study was based on the SSR model proposed by Saarelainen (1992). The objective of the model was to compare actual heave and compressibility behavior observed in the field with calculated values (of equal duration) based on an SP value for the same soil type determined from laboratory experimentation. The model was constructed in a spreadsheet format that used temperature distributions at specified soil depths and a constant SP value as input boundary conditions. Incremental heave rates were calculated using Equation 5.3. Because the denominator ($\lambda_f R_f$) is equal to the depth of frost penetration (z_i), the calculation of incremental heave rate simplifies to a function of only SP and gradT, as follows:

$$\frac{dh}{dt} = 1.09 * SP gradT = \frac{1.09 * SP(T_f - T_p)}{z_i} \quad (\text{Eq 5.4})$$

where $\text{grad}T$ equals the temperature differential between the depth of frost penetration and surface temperature, divided by the depth to frost penetration. Therefore, the model (spreadsheet) needed only to include the temperature distributions as function of time, the corresponding depth at which the temperatures were recorded, and the measured input value for SP, which is representative of the soil's overall activity throughout the freezing cycle.

Figure 5.8 illustrates the temperature distributions within the soil mass at the field frost heave test facility for specified depths. Note that these values were taken at arbitrary time intervals, but are representative of the observed temperature activity throughout the duration of the 2003 – 2004 freeze/thaw cycle.

Depth (mm)	150	310	460
T (°C)	1.17	3.31	4.99
	-0.16	1.17	1.60
	-0.16	0.73	1.60
	-1.06	-0.16	0.29
	-1.06	-0.16	0.29
	-1.06	-0.16	0.29
	2.89	-0.16	-0.16
	2.89	-0.16	-0.16
	2.89	-0.16	0.29
	2.89	-0.16	0.29
	2.89	-0.16	0.29
	2.89	-0.16	0.29
	2.89	0.29	0.29

Figure 5.8: Tabulated illustration of soil temperature profiles of the field facility.

Calculated values of incremental frost heave rate using Equation 5.4 are shown in Figure 5.9. The input constants incorporated in this calculation are the SP value and the

depths (z_i) at which the temperatures were recorded. This procedure utilized a logical statement that specified the beginning of calculations based on the location of frost penetration ($0\text{ }^\circ\text{C}$ isotherm). The values correspond chronologically with the temperature data in Figure 5.8 and represent arbitrary snapshots in time of incremental heave rates throughout the entire freeze/thaw cycle.

Input Parameters		Depth (mm)	150	310	460
SP =	9.197E-04 mm ² /s°C	dh/dt	0	0	0
Δt =	1/2 hr	↓	8.83E-06	0	0
	1800 sec	Δt	2.94E-06	0	0
			2.94E-06	4.27E-06	0
			2.94E-06	4.27E-06	0
			2.94E-06	4.27E-06	9.81E-07
			0	-1.4E-05	1.96E-06
			0	-1.2E-05	0
			0	-1.2E-05	0
			0	-1.1E-05	0
			0	-1.1E-05	0
			0	-1.1E-05	0
			0	0	0

Figure 5.9: Calculated values of incremental heave rate based on Equation 5.4.

The model utilizes the temperature data at a depth of 30 mm as an assumed ground surface temperature distribution (T_p) - see Figure A.2. The SP value used in this particular iteration was the reported value in Table B.2 for Test #3 (Post Farm CL). Table B.2 illustrates a large variation between reported SP values. Therefore, the author chose to use the median SP value for Tests 3 – 7 for demonstrative purposes. As the development of the laboratory testing device and procedures progresses, a more determinant value of SP should be applied to the model.

Figure 5.10 illustrates the calculated (predicted) values of displacement activity that correspond in time with the temperature and heave rate values shown in Figures 5.8 and 5.9.

Depth (mm)	150	310	460
Δh	0	0	0
	0.015892	0	0
	0.005297	0	0
	0.005297	0.00769	0
	0.005297	0.00769	0
	0.005297	0.00769	0.000883
	0	-0.023383	0.004413
Δt	0	-0.022215	0
	.	.	.
	.	.	.
	.	.	.
	0	-0.018569	0
	0	0	0
Σ Displacement (mm) =	15.37694	2.744452	0.290551

Figure 5.10: Calculated displacement values (mm) representative of the entire 2003 – 2004 freeze/thaw cycle based on Equation 5.5.

The values shown in Figure 5.10 were calculated using a numerical integration method (Trapezoid Rule) to approximately calculate the heave or settlement activity based on the corresponding heave rate. The following equation was used in the calculations:

$$h(t) = \int h'(t)dt = \Delta t \left(\frac{h'(t)_t + h'(t)_{t+\Delta t}}{2} \right) \tag{Eq 5.3}$$

where

$h(t)$ = displacement (mm) and

$h'(t)$ = dh/dt = heave rate (mm/sec).

The numerical integration method applied here calculates the area under the heave rate versus time curve to obtain the amount of heave or settlement activity experienced at each depth interval. Both positive and negative values are present in Figure 5.10, which correspond with either heave or settlement behavior, respectively. The sum (Σ) displacement is the net vertical displacement experienced at the specified depth interval.

This model represents the predicted (calculated) values of incremental heave rate and heave or settlement behavior at depth intervals that correspond with the telltale positions in the soil mass at the field frost heave test facility. Figure 5.11 illustrates the actual heave and settlement behavior observed throughout the 2003 –2004 freeze/thaw season. This graph was derived from Figure A.9 and illustrates the displacement activity for the tell tale depths corresponding to the temperature distributions used in the model calculations.

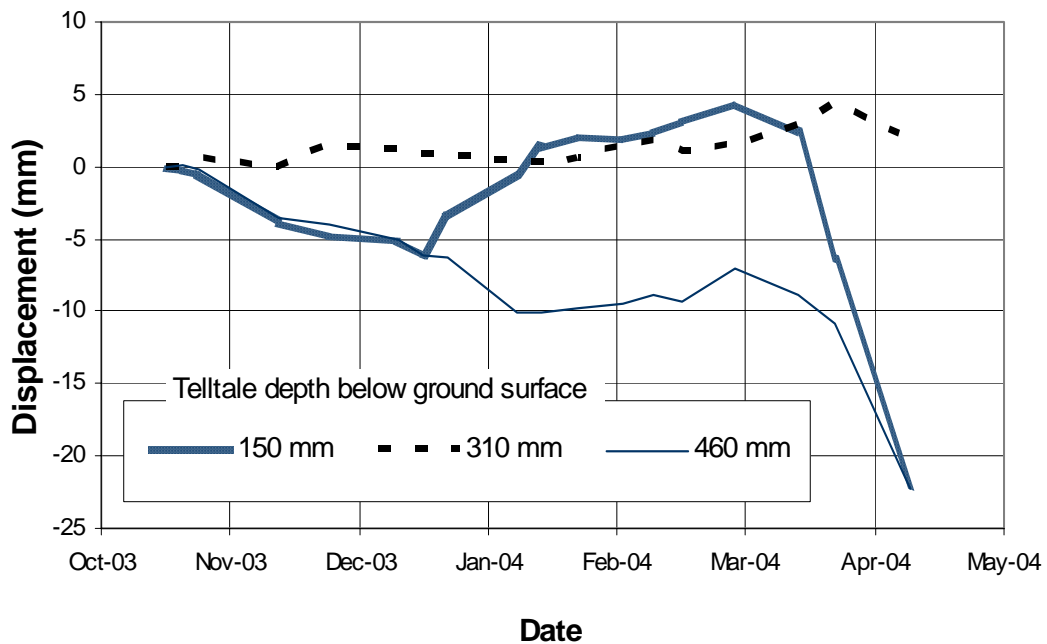


Figure 5.11: Heave and settlement behavior observed at the Post Farm frost heave facility during the 2003 – 2004 freeze/thaw season.

Figure 5.12 illustrates the predicted behavior of the Post Farm lean clay (CL) based on a laboratory measured SP value for the same duration of freezing and thawing. The value of SP (shown in Figure 5.12) was taken from the results of the laboratory freezing tests, as presented in Table B.2, Test #3 of Appendix B. The observed temperature distributions at the field test facility for depths corresponding with the tell tale locations (as in Figure 5.11) were utilized in the model calculation procedure.

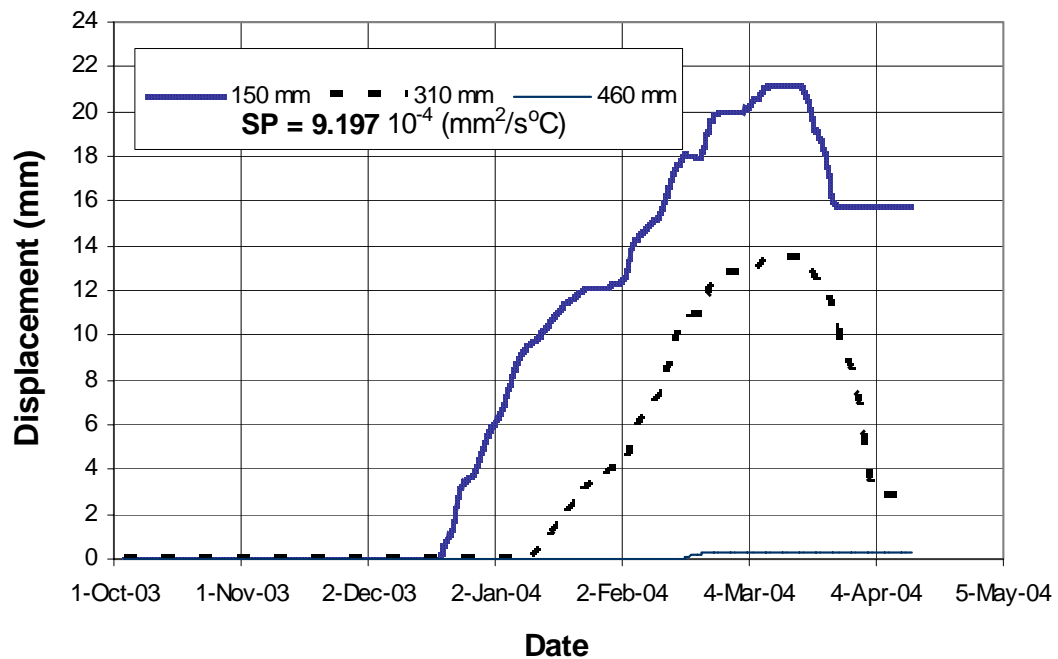


Figure 5.12: Calculated heave and settlement behavior of the Post Farm lean clay (CL) using a predictive numerical model.

Discussion

The objective of the segregation potential concept was to characterize the freezing behavior of a frost susceptible soil based on fundamental geotechnical index properties. Ideally, one would hope to obtain empirical correlations between Atterberg Limits and

SP values for different soil types classified by the USCS (Unified Soil Classification System) or the AASHTO Soil Classification System. Using a single engineering parameter (SP), the development of a predictive model would allow engineers to examine the freezing and thawing behavior of a certain soil type over a range of seasonal applications. For example, an engineer interested in highway pavement design would be able to examine the effects of seasonal variations (temperature fluctuations; length of freezing and thawing cycles) on soil types identified in the geographical area of interest. The model would allow the engineer to determine if the local soil types could be used in constructing pavement subgrade, or if the site required and over-excavation and placement of imported structural fill that would be less inclined to demonstrate frost heave behavior.

The results of the model described in the previous section (Figure 5.12) demonstrate expected heave and settlement behavior during a given freeze/thaw season for a specified soil type and corresponding SP value. For example, displacement activity proved greatest at the shallowest depth (150 mm), while minimal displacement was experienced at the greatest depth of frost penetration (460 mm). The model also illustrates a time lag in displacement activity. The deeper zones of the soil mass experienced disturbances well after the upper zones, as the frost front slowly penetrated with time. This type of behavior indicates that zones of soil nearer the ground surface are more susceptible to greater temperature fluctuations, and therefore experience the maximum amount of displacement activity, as would be expected.

It is unfortunate that the maximum values of heave and settlement calculated by the model do not better agree with that observed in the field. However, the behavior of the soil is consistent between the two, which is of primary concern. This indicates that the model generally works, but additional data is required to better calibrate the model. Furthermore, the results of the observed behavior at the field facility may not accurately represent the behavior of an in-situ soil mass throughout a typical freeze/thaw season because the measurements were obtained during the first season of construction. Settlement as a result of inconsistent compaction efforts and the redistribution of pore pressures of the re-worked soil mass may be partly responsible for the discrepancies between measured and calculated values (as discussed in Chapter 4).

The framework of the predictive model has been constructed. It will remain in the development stage as further research is conducted. Some of the shortcomings may be generally overcome as more representative seasonal data is collected at the field frost heave facility. Furthermore, an examination of future laboratory testing should be made in an attempt to achieve a more accurate measure of the SP parameter to be input into the model.

CHAPTER 6

SUMMARY, CONCLUSIONS, AND RECOMMENDATIONS

Summary

A large field-scale frost heave test facility was designed and constructed at the Montana State University (MSU) Arthur Post Agricultural Research Farm (Post Farm), located approximately 8 km west of the MSU – Bozeman campus. The purpose of the facility was to implement a large-scale, long-term observation site that would enhance the current state of knowledge concerning frost heave and compressibility behavior of soils subjected to continual freezing and thawing cycles. Data collection was initiated in October 2003 to compile thermal, moisture, and displacement activity of a known volume of on-site material (Post Farm CL).

A laboratory-testing device was also designed, constructed, and instrumented in order to measure the thermal response of various soil types in a controlled freezing environment. The freezing tests were environmentally controlled using the cold chamber room located in the MSU snow mechanics laboratory. After several trial runs and numerous modifications, seven freezing tests were conducted and recorded. Two different soil types were used: 1) an 80% silt and 20% kaolinite clay composition (S80K20); and 2) the soil found at the frost heave test facility (Post Farm lean clay, CL). Data collected from the laboratory freezing tests was compiled and applied to the initial

development of a numerical model capable of predicting frost action behavior of different soil types.

Laboratory geotechnical index testing was conducted on the two soil types as an initial step towards developing empirical correlations between common geotechnical index parameters and thermal properties of frost susceptible soil. Results of the geotechnical index tests conducted on the S80K20 sample and the Post Farm CL are presented in Tables 3.1 and 3.2 respectively. Based on the tests conducted in this study, it was determined that a larger data base is necessary to develop reliable empirical correlations.

A numerical model was developed to predict the freezing and thawing behavior of frost susceptible soils. The model is based largely on a relatively new engineering parameter called the segregation potential (SP), which was introduced by Konrad and Morgenstern (1993, 1987, 1981 and 1980). The model calculates the rate and magnitude of heave/compression using numerical analysis techniques. For comparative purposes, the temperature data recorded at the field frost heave facility from October 2003 to April 2004 was used as input into the model, and the results were compared to the field facility heave measurements.

Conclusion

A reliable and practical approach toward predicting the thermal response of frost susceptible soils subjected to seasonal and perennial freezing conditions has eluded engineers and scientists for many years. Most of the research presented thus far has been based on a mechanistic theory that couples two processes: heat and mass transfer

between pre-determined and well-defined boundary conditions. However, the process of heat transfer within a soil mass is complex. In order to fully understand the process, one must carefully examine each constituent separately before studying their overall interactions with each other.

The author's proposed scope of work was presented with the purpose of gaining an understanding of the theoretical background of frost behavior in soils, while attempting to minimize the complexity by developing an empirical approach to a predictive solution. This approach required the development of an experimental testing program that proved extremely sensitive to detail.

This study has shown the significant impact that environmental and inherent factors have on the behavior of frost susceptible soils exposed to freezing conditions. Based on this research, the following conclusions are provided:

- The fundamental conditions required for the initiation of frost heave and subsequent thaw-weakening are: 1) freezing temperatures, 2) source of groundwater available for capillarity migration of unfrozen water, and 3) frost susceptible soils based on grain-size distribution.
- The mechanistic frost heave theory discussed in this thesis applies to a one-dimensional transient frost front.
- A frost susceptible soil can be generally classified by its segregation potential (SP).
- The development of efficient and consistent testing procedures is critical in obtaining useful parameters from laboratory freezing tests.

- The warm-end boundary condition governs the rate and magnitude of frost penetration.
- A standardized procedure for the interpretation of laboratory freezing test results is required for the development of a predictive model.

Recommendations for Continued Research

This section contains suggestions for the continued research conducted on the frost heave theory. The work described herein falls into three main categories: 1) data collection at the field frost heave test facility, 2) laboratory testing procedures, and 3) interpretation of the results of these experiments.

Improvements to the Field Facility

The overall results of the first season of data collection at the field frost heave test facility were satisfying. However, some improvements should be made in order to optimize the operation and maintenance of the facility.

The simulated groundwater source that was installed proved to operate effectively, though it required a persistent and inefficient monitoring schedule. The only onsite water source available to refill the water supply tank became frozen during the winter months as the frost front penetrated to the depths of the pipeline. An offsite source and transportation tank was required to complete the process throughout the remainder of the winter season. An onsite water source that effectively operates throughout the entire cycle of data collection would greatly improve the operation of the facility during the cold winter months.

Installation of electronically calibrated piezometers - that automatically record the amount of water migrating from the supply tank, and the fluctuation of groundwater in the soil mass - would increase the efficiency of data collection.

Access into the insulated water supply shelter proved to be difficult and challenging at times. Additional space at the east end of the excavation would be useful to accommodate easy mobility into and out of the doorway. A stairwell should be constructed that leads from the ground surface down to the doorway for optimal access.

A survey transit system referenced to a pre-determined benchmark would increase the efficiency and accuracy of telltale displacements. A benchmark should be established at the site to implement a survey method for monitoring the displacement activity between the reference beams and the top plates of the telltales. An electronic caliper was used during the first season of operation, which likely introduced the potential for human errors.

As data collection continues to be conducted at the frost heave facility, some of the initial problems that were experienced should subside. For example, the unnatural displacement activity observed by the telltales was likely due to settlement of the disturbed ground, and redistribution of pore water pressures. As consolidation occurs, the soil mass should begin to demonstrate frost action behavior typical of an in-situ soil.

Laboratory Testing Procedures

The results of the seven laboratory freezing tests conducted on the S80K20 mix and the Post Farm CL proved to be generally inconsistent. In order to compile an accurate and reliable database of empirical evidence, more stringent test apparatus and protocol should be implemented.

The existing water supply system consisted of soft-rubber tubing that fed water from the Mariotte tube to the water reservoir in the testing cylinder inside the cold chamber. The task of keeping the rubber tubing properly insulated proved difficult and insufficient at times, as the water line often became frozen during the test. A copper water line could be insulated inside of the cold chamber using electrical heat tape. Furthermore, a fixed line would minimize leaks and the potential for damage.

Maintaining a constant warm-end boundary condition is essential in obtaining accurate results. The aluminum warm plate that was constructed simulates a geothermal gradient, which should not fluctuate during the test. The main problem encountered with the warm-end boundary control was maintaining a constant temperature of the ethanol glycol that was pumped through the radiant heating system. This could be improved by upgrading the immersion heater located in the external ethanol glycol tank. A larger heater and more consistent heat processor would better regulate the temperature of fluid being pumped out.

After numerous additions and modifications to the soil-testing cylinder, the author suggests the construction of a new apparatus. In general, the PVC (schedule 80) pipe used for the test cylinder proved durable enough and would be adequate for the new

device. The water reservoir and screw-plug immersion heater also worked well. However, the problem of most persistence concerned the preparation of a soil sample in the cylinder before freezing was induced. The apparatus was not constructed to allow for consistent compaction procedures due to sensitive instruments being exposed during the placement of soil in the test cylinder. This problem was further exacerbated during removal of the sample subsequent to the freeze cycle. Several instruments were damaged during these procedures. Therefore, the new testing device must implement an instrumentation set-up that is more durable, portable, and re-usable. Thermocouples should be placed throughout the soil column after compaction of the sample. This can be accomplished by drilling threaded holes at pre-determined depths and installing thermocouple “probes” from the outside of the cylinder. These probes should be durable enough to withstand damage throughout repeated installation/removal cycles.

The heat flux plates should be protected using the aluminum and Plexiglas casing system that was implemented for the last four tests. Along with providing durability, the aluminum increased the efficiency of heat transfer through the thin flux plate, resulting in more consistent thermal conductivity calculations. The heat flux instruments should consist of a durable conduit to house and protect the thin wires. The sensor should also be portable allowing for installation from the inside of the cylinder by inserting the wire conduit through a threaded hole, which would be tightened into place once the soil sample had been placed and compacted to the respective height.

In general, the construction of an improved laboratory-testing device (one that accommodates increased durability and portability of the instrumentation) would increase

the efficiency and accuracy of the testing protocol. The existing design and set-up provides the framework for new and improved testing methods.

Interpretation of the Results

The data collected thus far reflects the early stages of the ongoing frost heave research. The next phase of this study should include the further development of an accurate database to be used in obtaining empirical correlations between thermal and geotechnical index properties of frost susceptible soils.

The most significant challenge in interpreting the results of the laboratory freezing tests regarded the segregation potential (SP). For the purposes of developing a predictive model, the author chose to use the value of SP measured at the end of the freezing cycle. As discussed in Chapter 5, this value of SP was used as an input to the numerical model. As additional freezing tests continue and empirical data is gathered, the validity of this approach should be further examined.

Using test results from different soil types, supplemented with additional numerical analyses, correlation between geotechnical index parameters and thermal properties of a frost susceptible soil could be further addressed. Based on the results of this study, the author hypothesizes that an empirical correlation may exist between the Atterberg limits (liquid limit or plasticity index) and the segregation potential (SP). With this type of correlation, design engineers could simulate or predict the response of different soil types in freezing environments using the predictive model discussed herein.

REFERENCES CITED

- Andersland, O.B. and Ladanyi, B. (2004). *Frozen Ground Engineering, 2nd Ed.* John Wiley & Sons, Inc. Hoboken, New Jersey.
- ASTM (1999). *Annual Book of ASTM Standards*, Section 4, Volume 4.08, American Society for Testing and Materials, West Conshohocken, Pennsylvania.
- Boutonnet, M., Lerat, P., Pouliot, N., Savard, Y., and St-Laurent, D. (2003). "Thermal Aspect of Frost-Thaw Pavement Dimensioning." *Transportation Research Record*, No. 1821.
- Casagrande, A. (1932). "A New Theory of Frost Heaving." *Proceedings of the Highway Research Board*, Vol. 11, p. 168-172.
- Chamberlain, E. J. (1981). "Frost Susceptibility of Soil." *CRREL Monograph 81-2*, Hanover, New Hampshire.
- C-SHRP (2000). "Seasonal Load Restrictions in Canada and Around the World." *Canadian Strategic Highway Research Program*, Technical Brief No. 21, September, Ottawa, Ontario, pp. 1-8.
- Farouki, O.T. (1981). "Thermal Properties of Soils." *CRREL Monograph 81-1*, Hanover, New Hampshire.
- Ho, D.M., Harr, M.E., and Leonards, G.E. (1970). "Transient Temperature Distribution in Insulated Pavements: Predictions and Observations." *Canadian Geotechnical Journal*, Vol. 7, pp. 275-284.
- Ho, D.M. (1969). "Prediction of Frost Penetration Into a Soil-Water System." *A Thesis Submitted to the Faculty of Purdue University*, 154 pp.
- Holtz, R.D., Kovacs, W.D. (1981). *An Introduction to Geotechnical Engineering*. Prentice-Hall, Inc. Englewood Cliffs, New Jersey.

- Konrad, J.M. (1994). "Sixteenth Canadian Geotechnical Colloquium: Frost Heave in Soils: concepts and engineering." *Canadian Geotechnical Journal*, Vol. 31, pp. 223-245.
- Konrad, J.M. (1987). "Procedure for Determining the Segregation Potential of Freezing Soils." *Geotechnical Testing Journal*, Vol. 10, No. 2, pp. 51-58.
- Konrad, J.M. and Morgenstern, N.R. (1981). "The Segregation Potential of a Freezing Soil." *Canadian Geotechnical Journal*, Vol. 18, pp 482-491.
- Konrad, J.M. and Morgenstern, N.R. (1980). "A Mechanistic Theory of Ice Lens Formation in Fine-Grained Soils." *Canadian Geotechnical Journal*, Vol. 17, pp. 473-486.
- Mokwa, R.L., Newell, Z.A. and Eschbach, E. (2004). "Experimental Evaluation of the Frost Heave Phenomenon." *Proceedings of the 39th Annual Symposium on Engineering Geology and Geotechnical Engineering*, pp. 11-23.
- Mokwa, R.L. (2002). "Compressibility and Heave Characteristics of Subgrade Soils Exposed to Freeze/Thaw Conditions." *A Research Proposal Submitted to Western Transportation Institute*, pp. 1-12.
- Saarelainen, S. (1992). "Modelling Frost Heaving and Frost Penetration in Soils at some Observation Sites in Finland: The SSR Model." *Technical Research Centre of Finland*, 119 pp.
- Williams, P.J. and Smith, M.W. (1989). *The Frozen Earth – Fundamentals of Geocryology*. Cambridge University Press, New York City, New York.

APPENDICES

APPENDIX A

COMPLETE RESULTS FROM THE FIELD FROST HEAVE TEST FACILITY

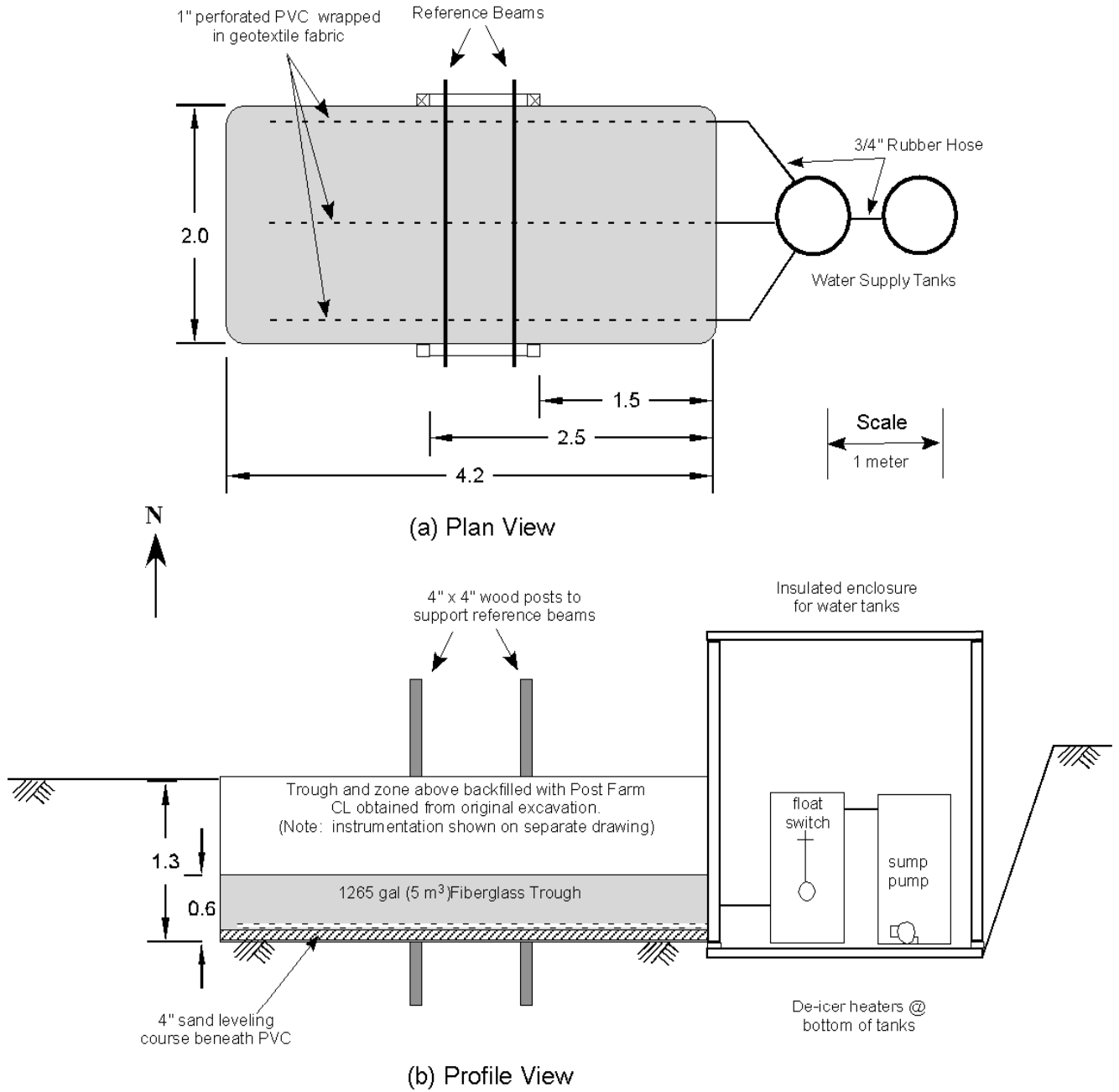


Figure A.1: Schematic illustrating the completed field frost heave test facility.

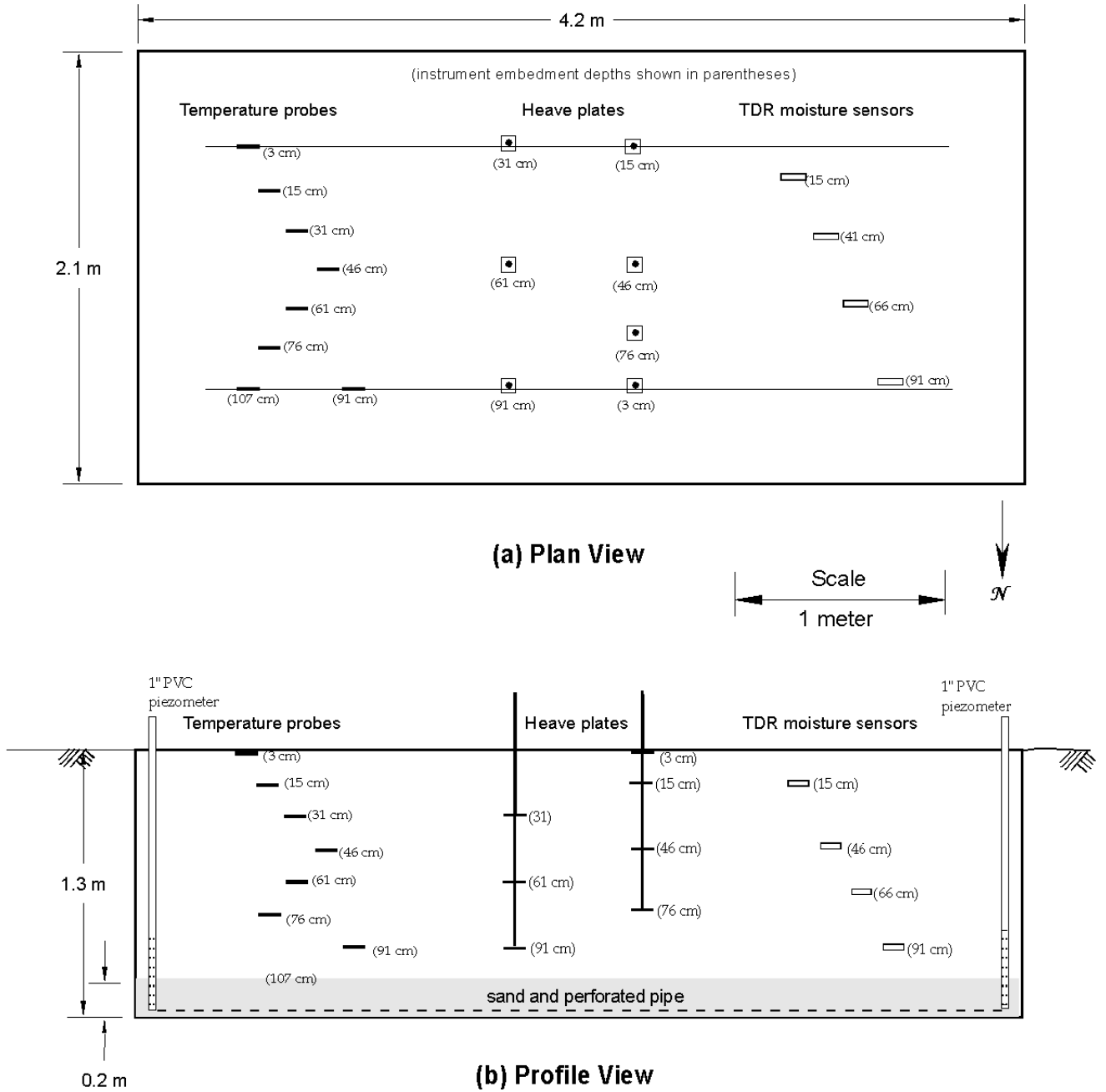


Figure A.2: Plan and profile views of the instrumentation and telltale construction at the field frost heave test facility.

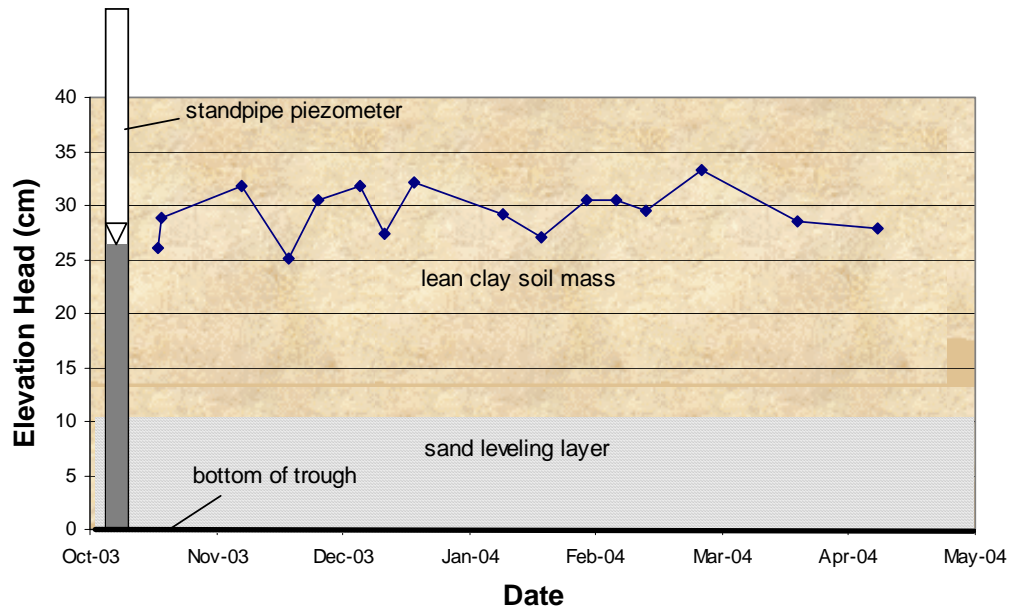


Figure A.3: Graphical illustration of piezometer readings taken at the field facility.

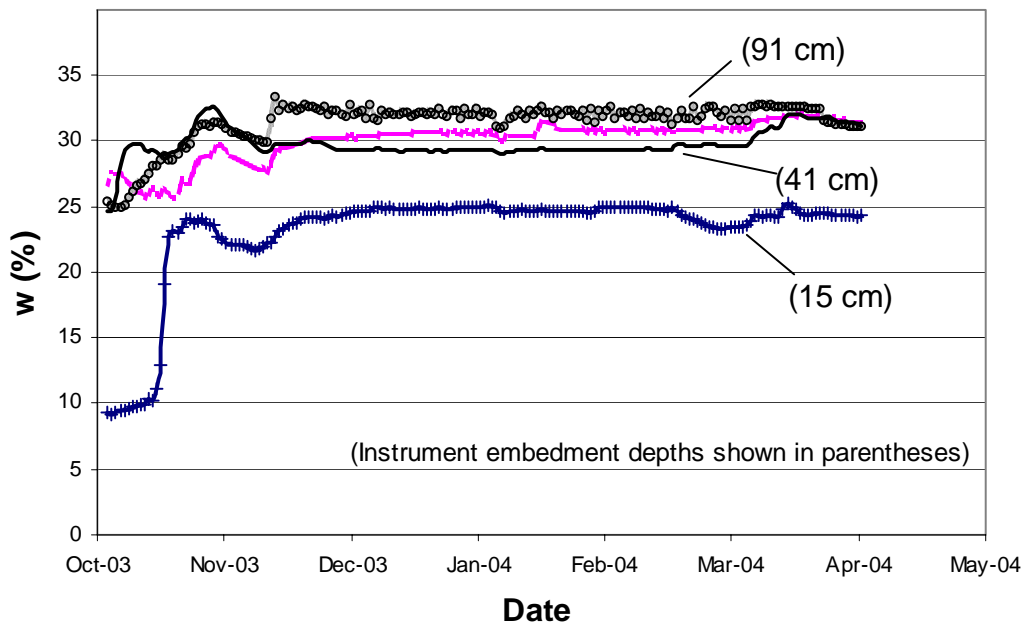


Figure A.4: Graphical illustration of water content profiles for the Post Farm lean clay.

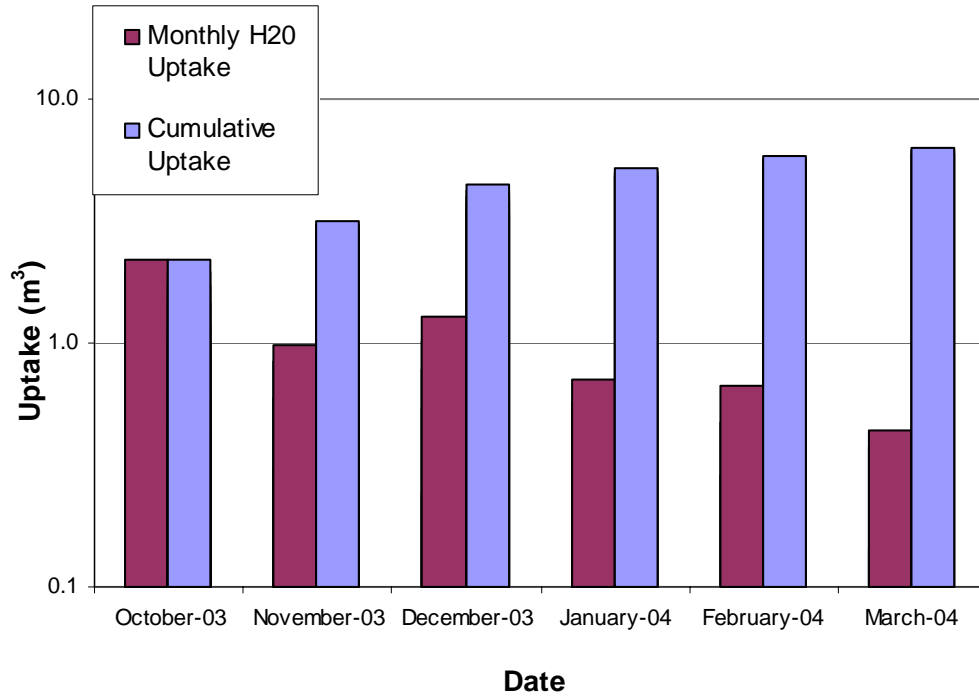


Figure A.5: Graphical illustration of cumulative water uptake at the field facility during 2003 – 2004 winter season.

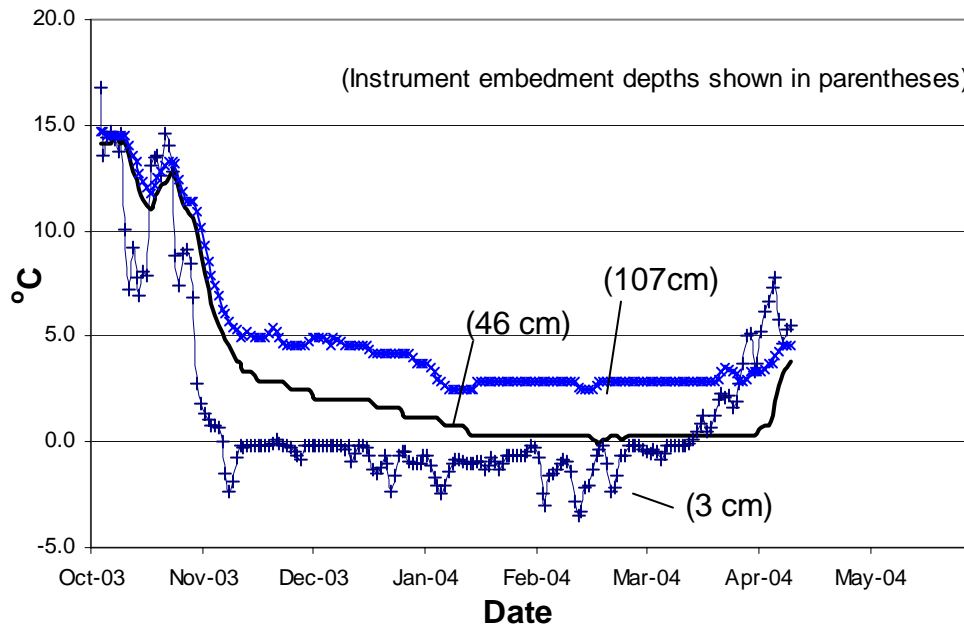


Figure A.6 Graphical illustration of temperature profiles for various instrument embedment depths at the field facility.

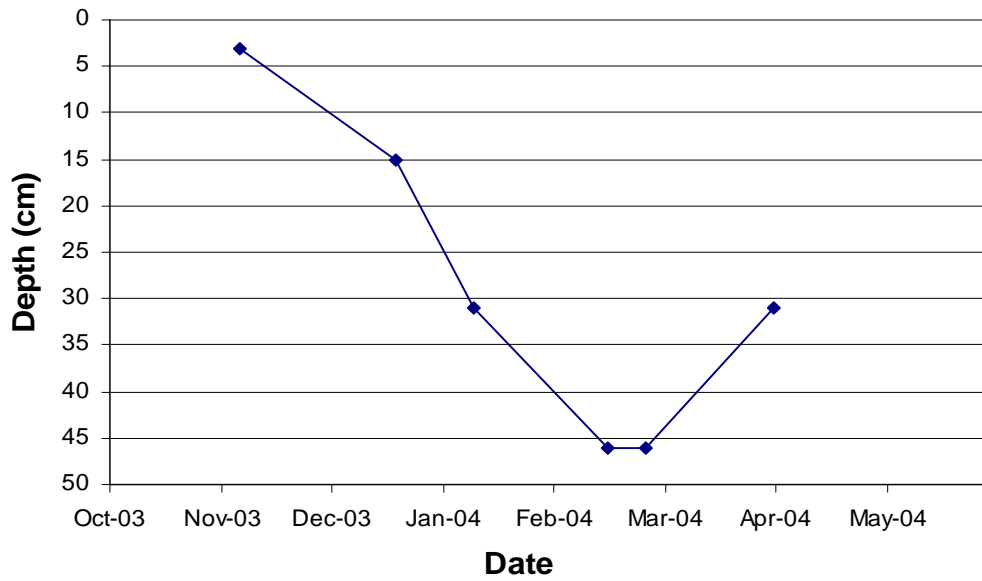


Figure A.7 Graphical illustration of the location of the frost front at the field facility.

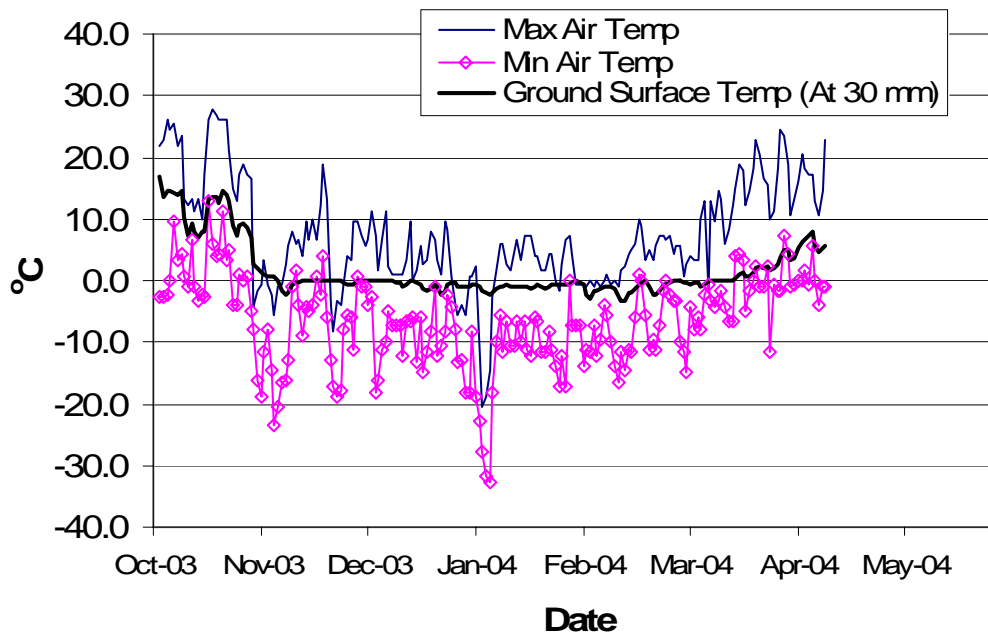


Figure A.8 Graphical illustration of maximum and minimum air temperatures compared to ground surface temperatures at the field facility.

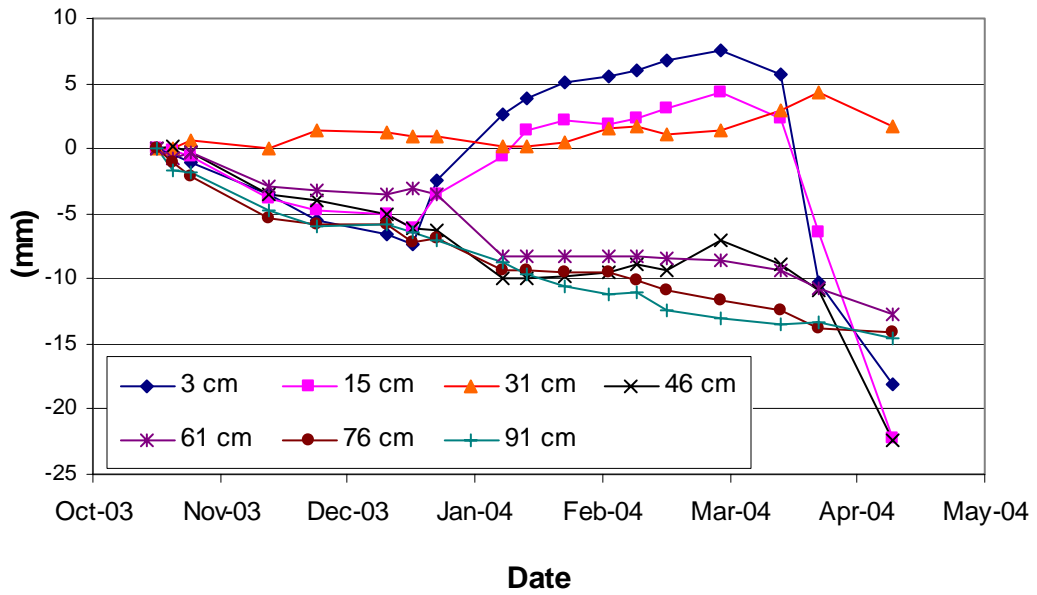


Figure A.9 Graphical illustration of telltale readings for various embedment depths at the field facility.

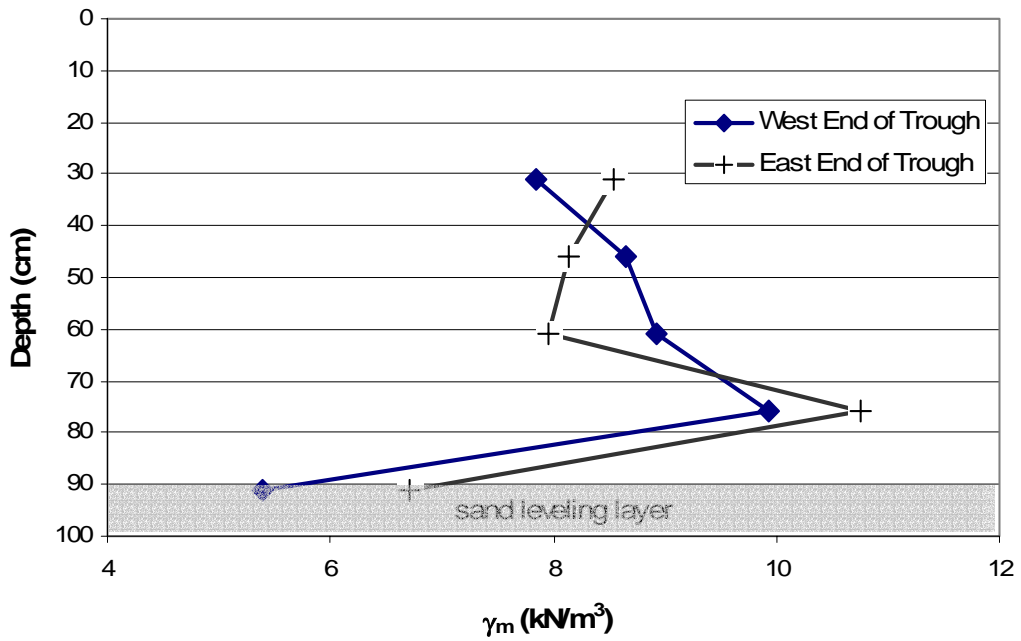


Figure A.10 Graphical illustration of in-place moist density results of the backfilled soil mass at the field facility.

APPENDIX B

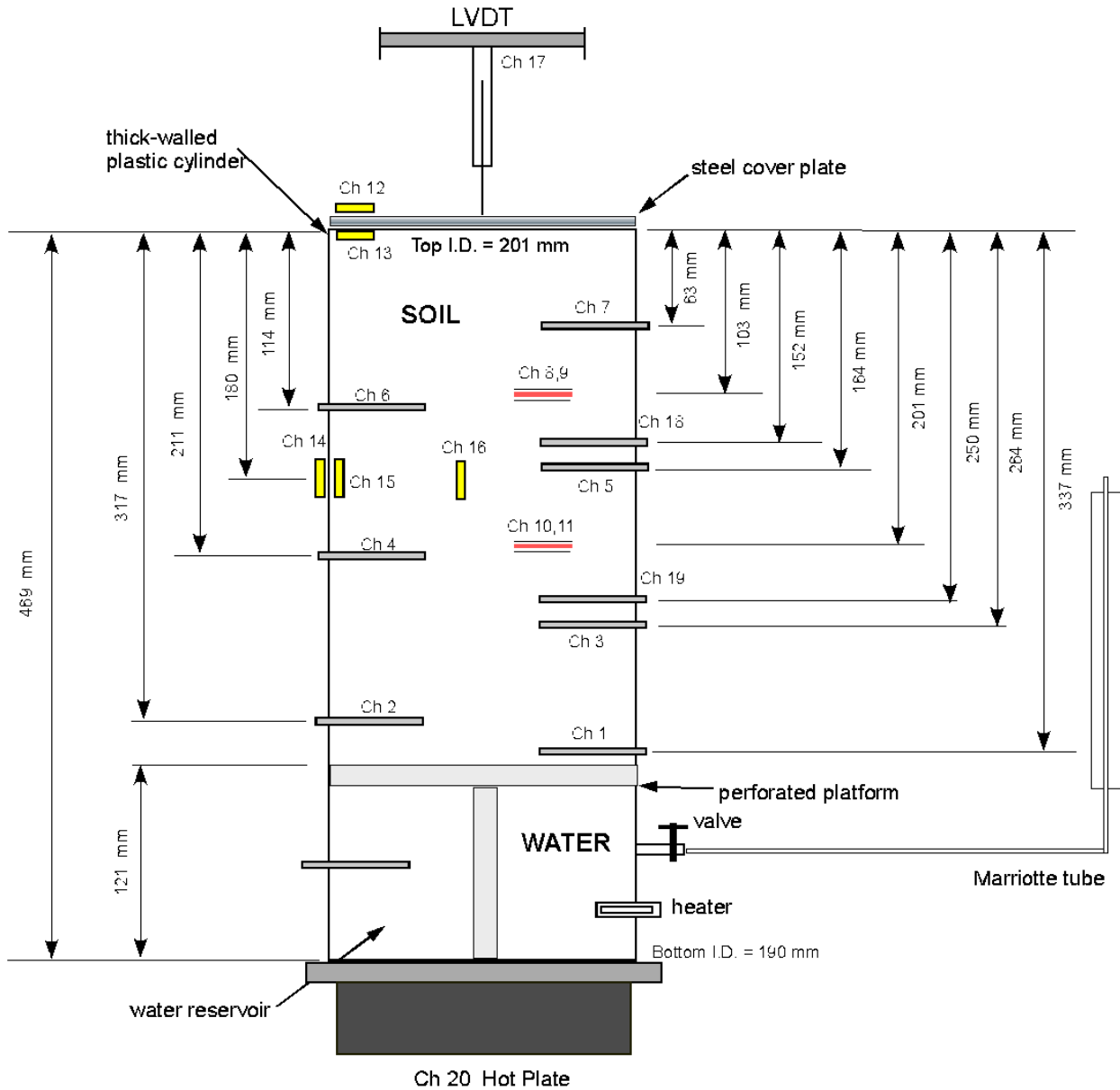
COMPLETE RESULTS FROM THE LABORATORY FREEZING TESTS

Table B.1 Laboratory Frost Heave Testing Schedule

Test No.	Date	Soil	Initial w(%)	Initial S(%)	Initial ρ_d (kg/m ³)
1	6/17-7/8/03	S80K20	13.4	46.3	1524
2	11/20-12/9/03	S80K20	11.5	42.7	1568
3	12/24 -1/4/04	P.F. CL	17.7	37	1205
4	2/25 - 3/3/04	P.F. CL No H ₂ O Uptake	16	36	1255
5	3/5 - 3/17/04	P.F. CL w/ H ₂ O Uptake	16	36	1255
6	3/24 - 4/1/04	P.F. CL; S=100% No H ₂ O Uptake	44.6	100	1255
7	4/5 - 4/12/04	P.F. CL; S=100% w/ H ₂ O Uptake	44.6	100	1255

Table B.2 Results to the Laboratory Frost Heave Testing Schedule

Test No.	Length of Test (hrs)	Total Heave (mm)	Total Vol. Heave (cm ³)	Total H ₂ O Uptake (cm ³)	Avg. Temp. Gradient (°C/mm)	Avg. Frozen Thermal Conductivity (W/m°C)	SP 10 ⁻⁴ (mm ² /s°C)
1	528	17.4	582	350	0.019	1.82	3.054
2	462	12.4	394	1003	0.024	N/A	7.919
3	263.5	8.4	266.5	830.5	0.03	N/A	9.197
4	165	0	0	N/A	0.033	0.4	N/A
5	285.5	0	0	1199	0.03	0.46	12.255
6	191	4.4	138.7	N/A	0.025	0.44	N/A
7	163	1.77	56.2	86.3	0.031	0.3	1.495



LEGEND

- Type T thermocouple
- Thermal flux plate & Type K thermocouple
- Adhesive Type T thermocouple

Notes:

- (1) Inside diameter taper begins 250 mm from top (taper not shown).
- (2) Cylinder encapsulated with insulation and placed inside of environmental cold chamber.
- (3) Agilent technologies data acquisition system used to record data.
- (4) Data acquisition channel indicated on drawing as Ch X, where X = channel number.

Figure B.1: Schematic illustrating the laboratory frost heave testing device.

Freezing Test #1

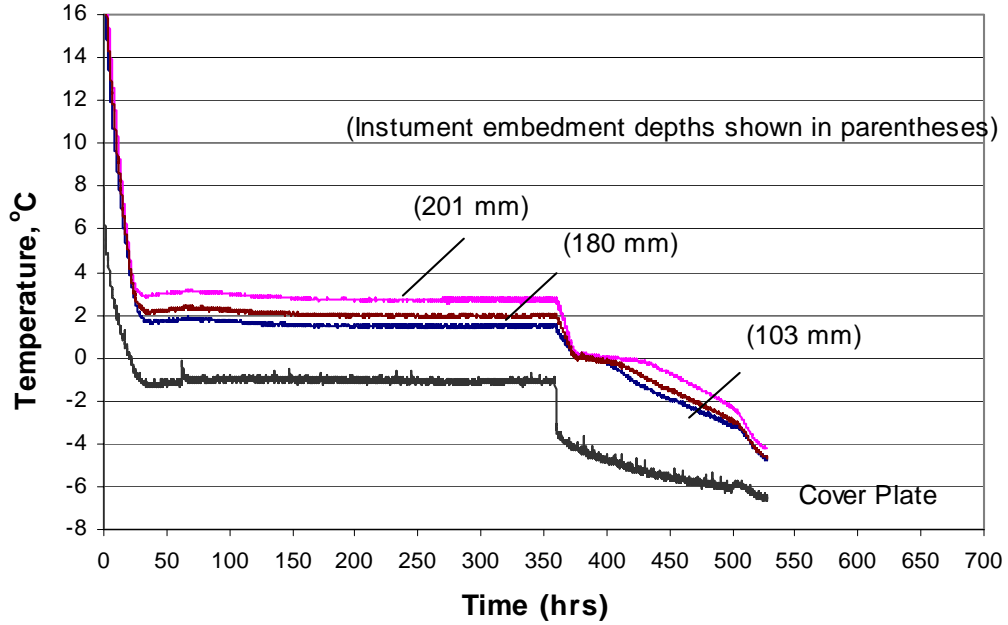


Figure B.2: Graphical illustration of temperature distributions throughout freezing Test #1.

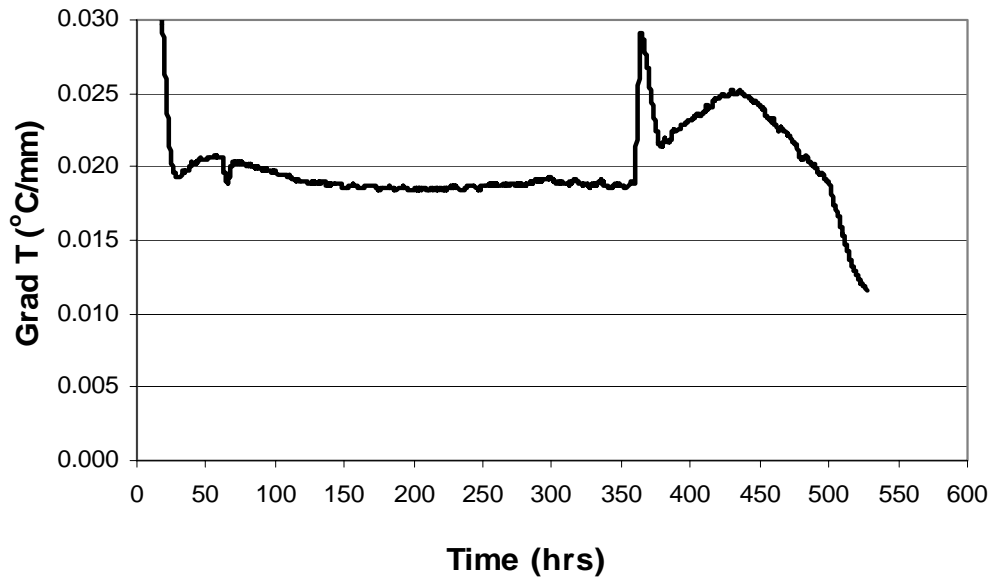


Figure B.3: Graphical illustration of overall temperature gradient throughout freezing Test #1.

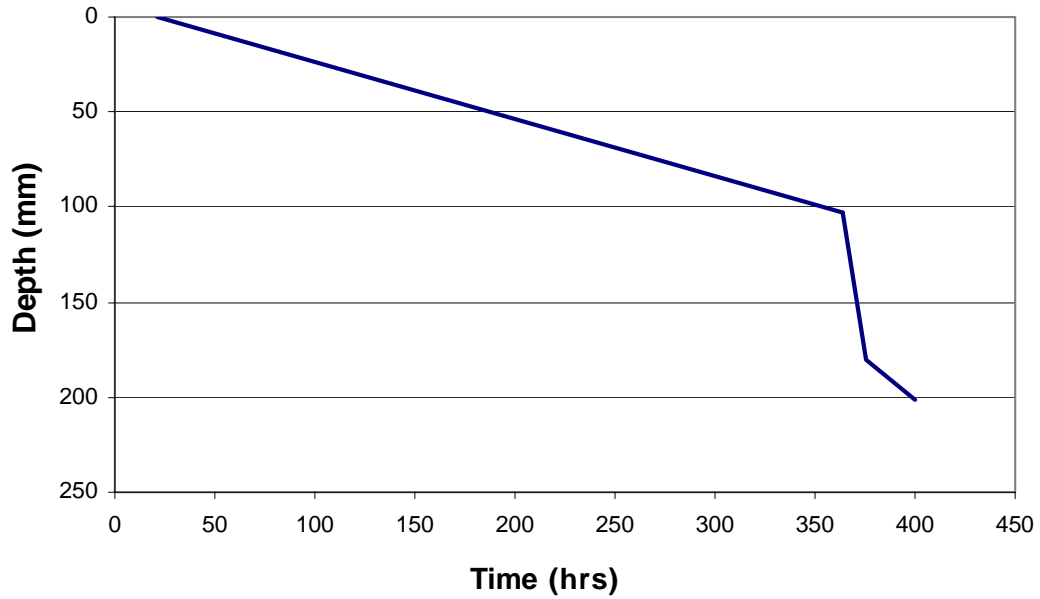


Figure B.4: Graphical illustration of the frost front location throughout freezing Test #1.

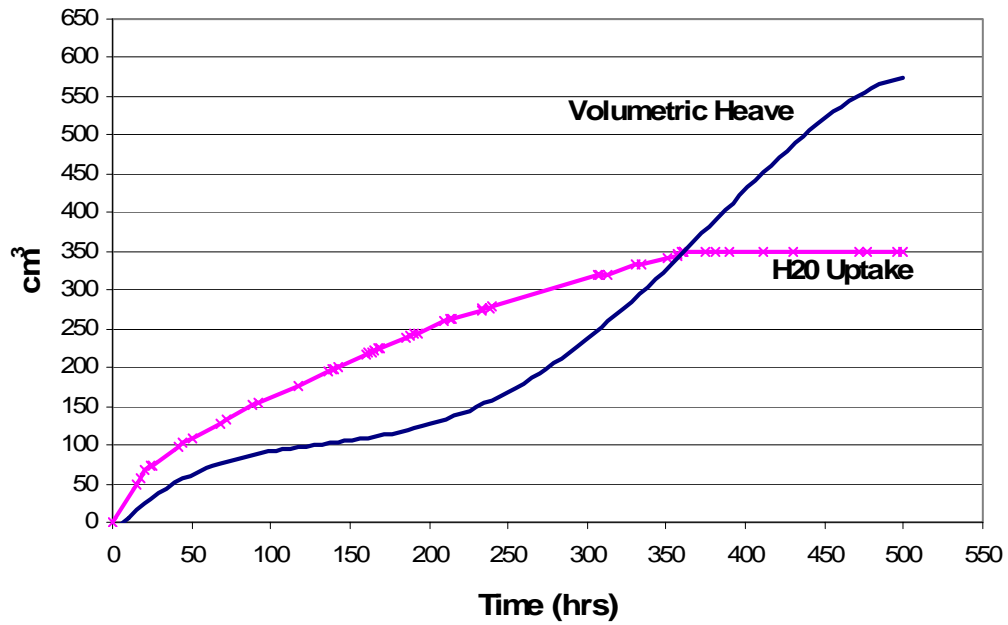


Figure B.5: Graphical illustration of volumetric heave and water uptake measurements throughout freezing Test #1.

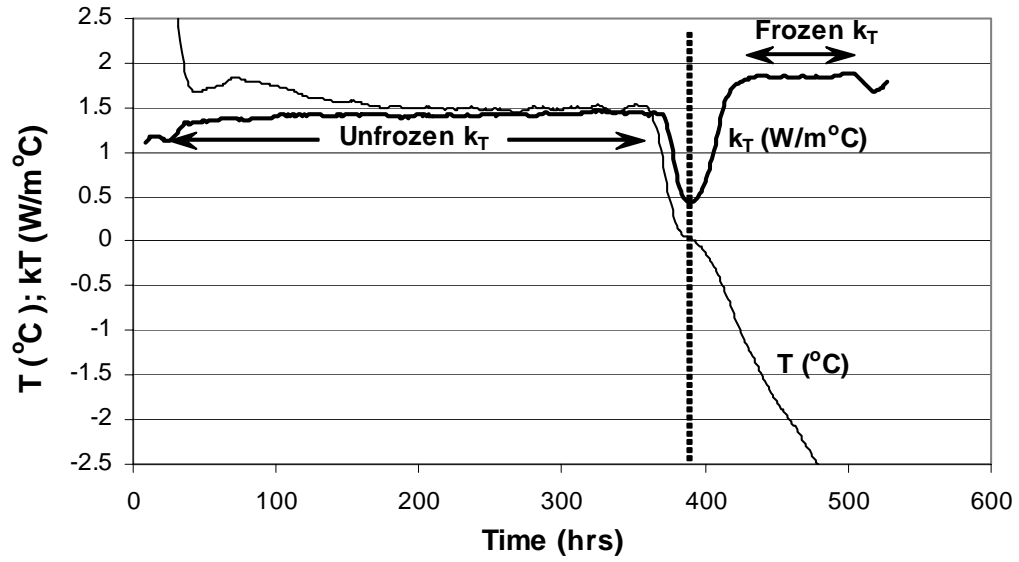


Figure B.6: Graphical illustration of calculated thermal conductivity values for freezing Test #.

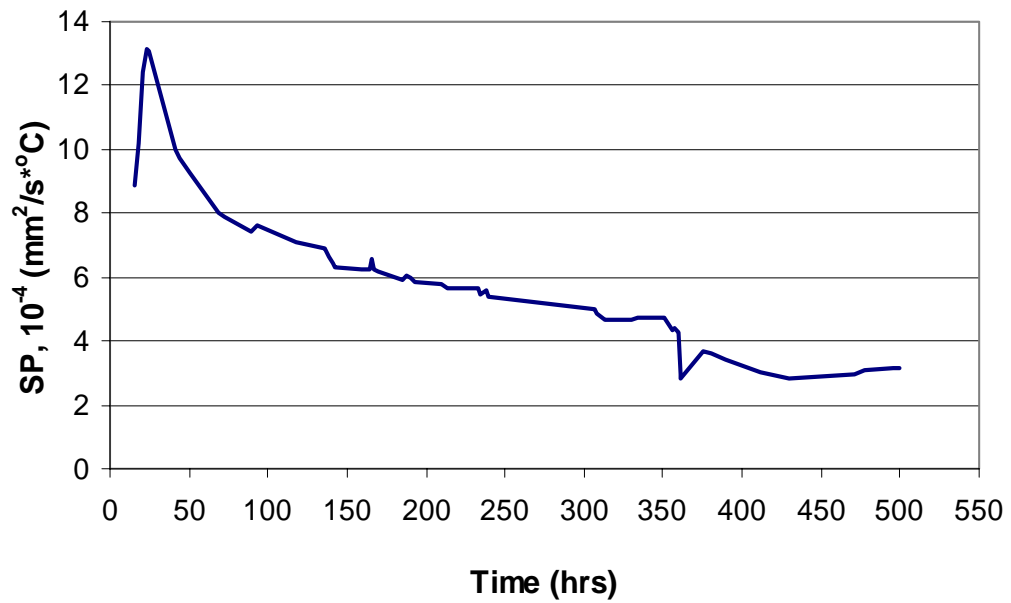


Figure B.7: Graphical illustration of calculated SP values for freezing Test #1.

Freezing Test #2

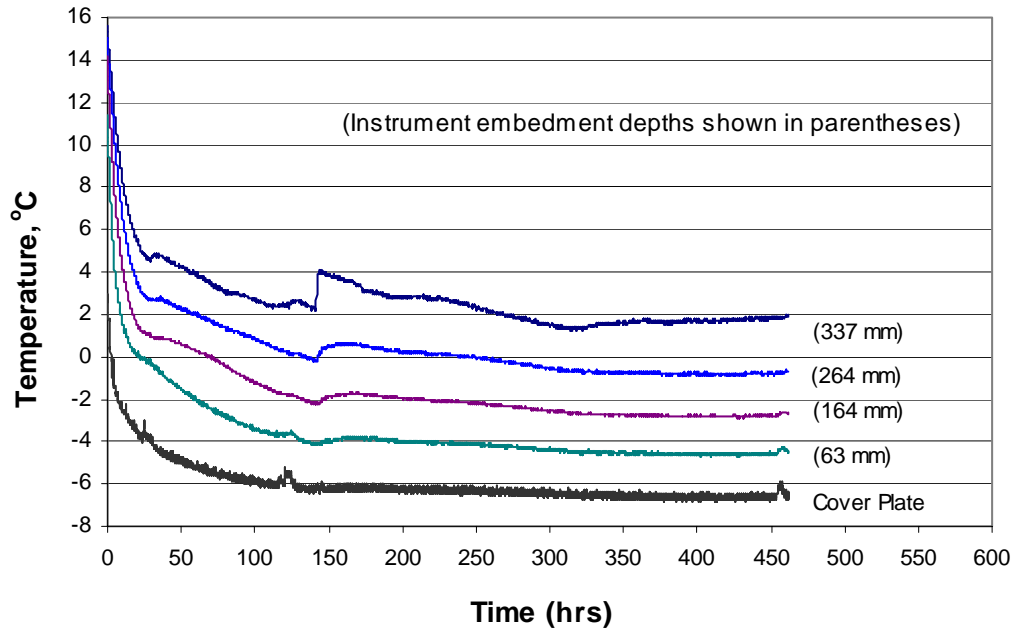


Figure B.8: Graphical illustration of temperature distributions throughout freezing Test #2.

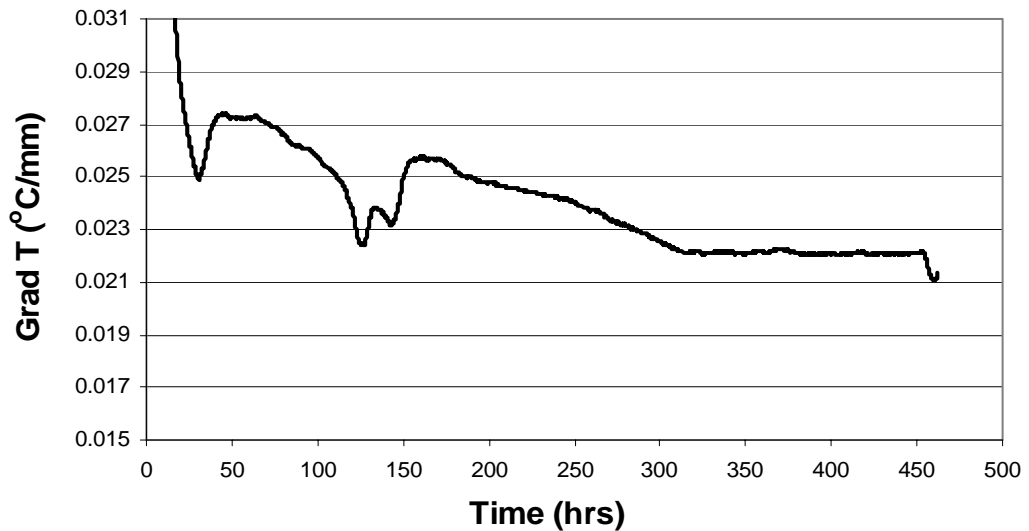


Figure B.9: Graphical illustration of overall temperature gradient throughout freezing Test #2.

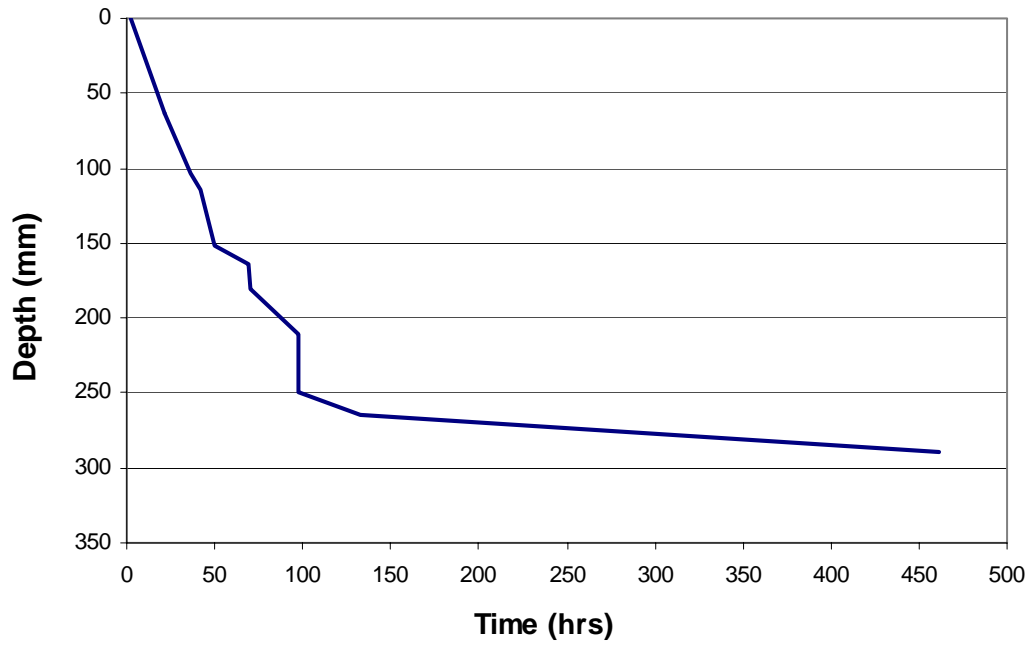


Figure B.10: Graphical illustration of the frost front location throughout freezing Test #2.

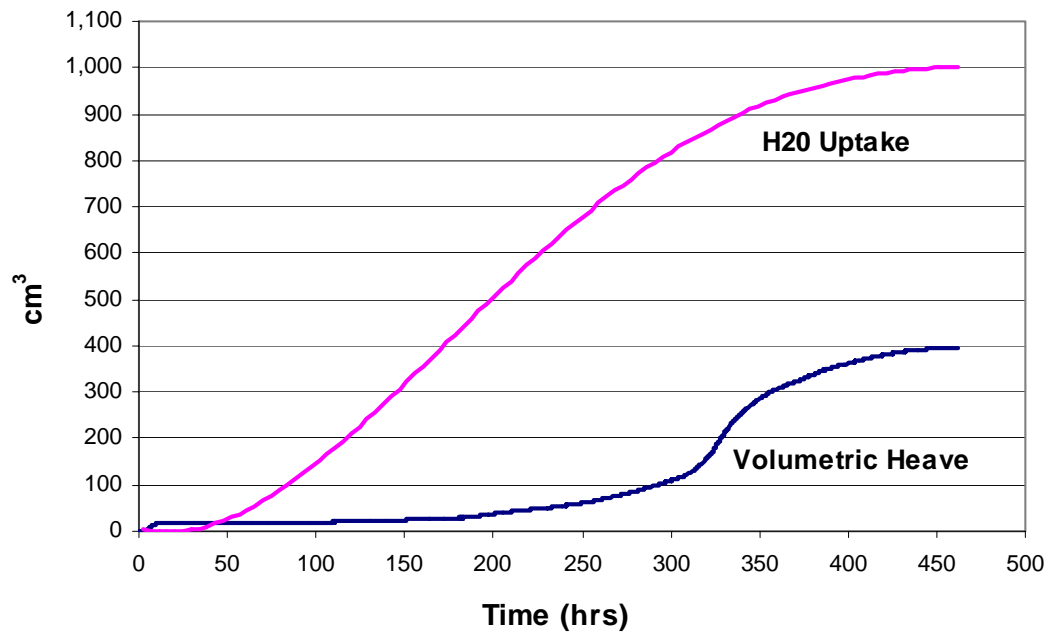


Figure B.11: Graphical illustration of volumetric heave and water uptake measurements throughout freezing Test #2.

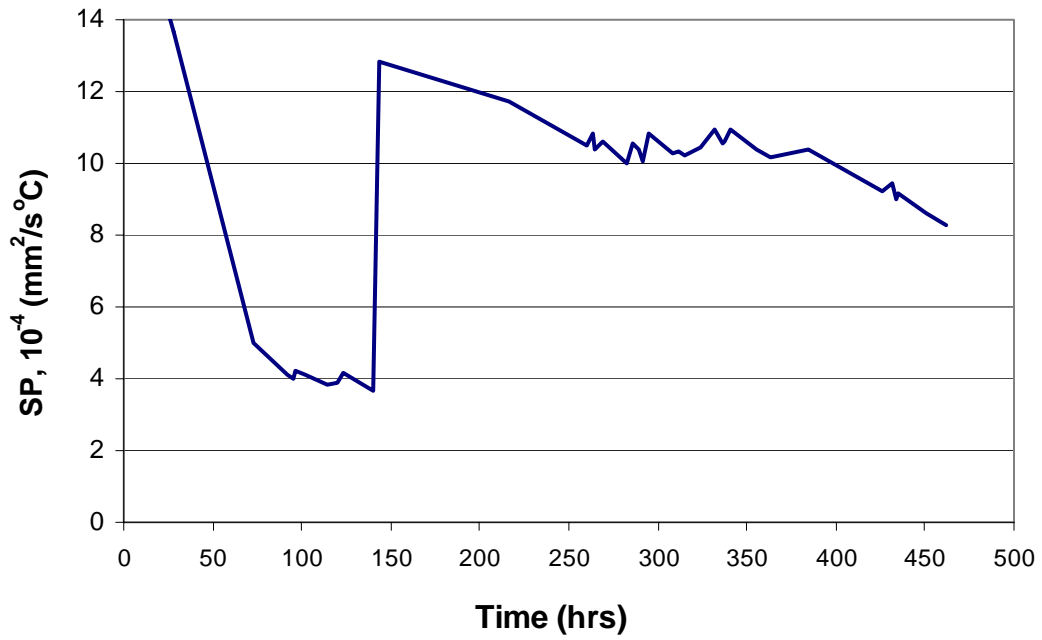


Figure B.12: Graphical illustration of calculated SP values for freezing Test #2.

Freezing Test #3

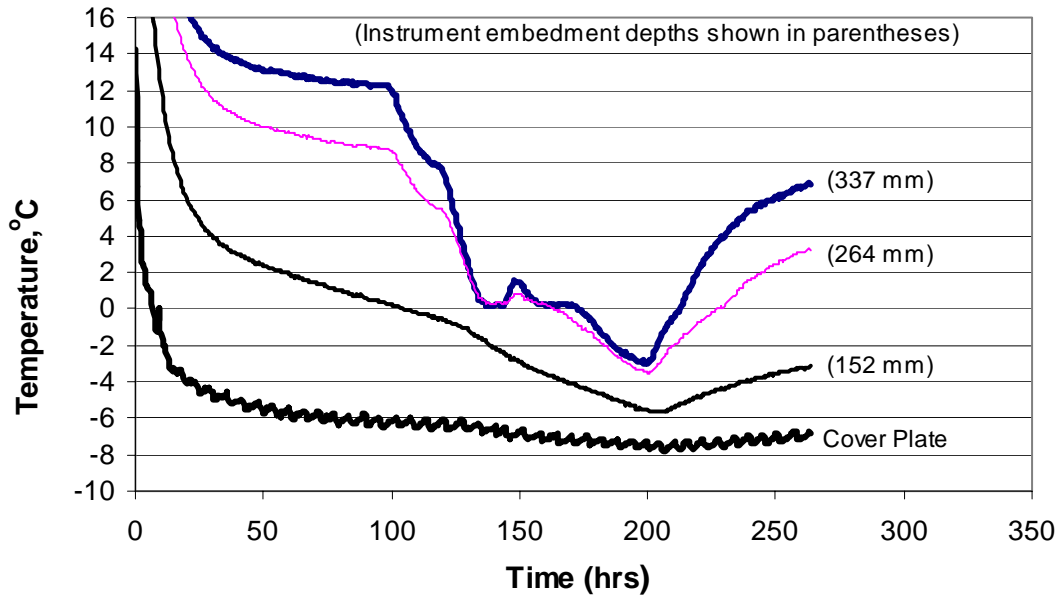


Figure B.13: Graphical illustration of temperature distributions throughout freezing Test #3.

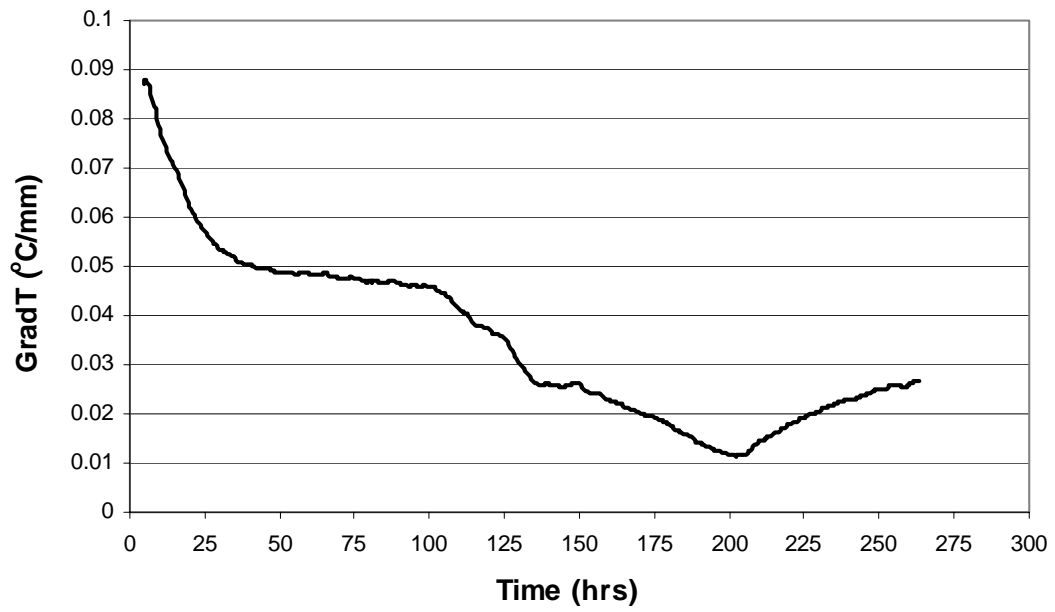


Figure B.14: Graphical illustration of overall temperature gradient throughout freezing Test #3.

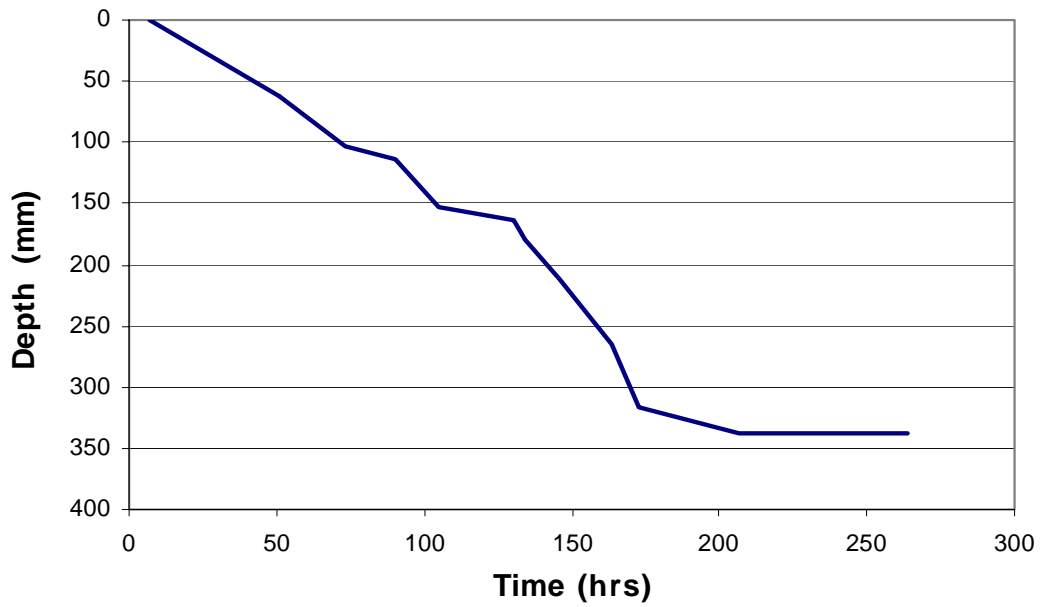


Figure B.15: Graphical illustration of the frost front location throughout freezing Test #3.

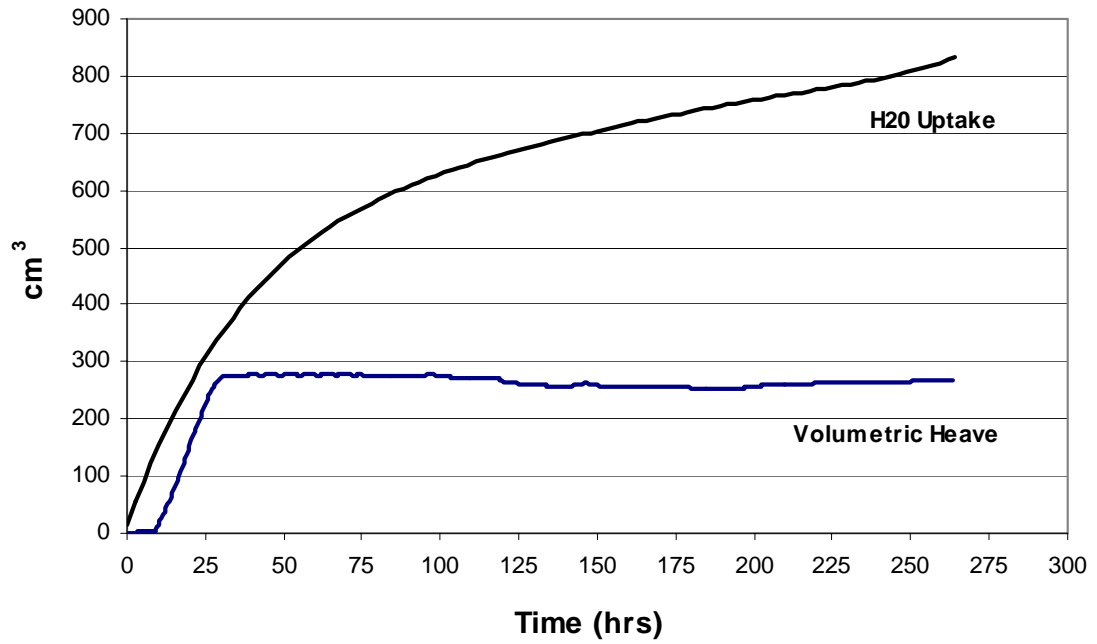


Figure B.16: Graphical illustration of volumetric heave and water uptake measurements throughout freezing Test #3.

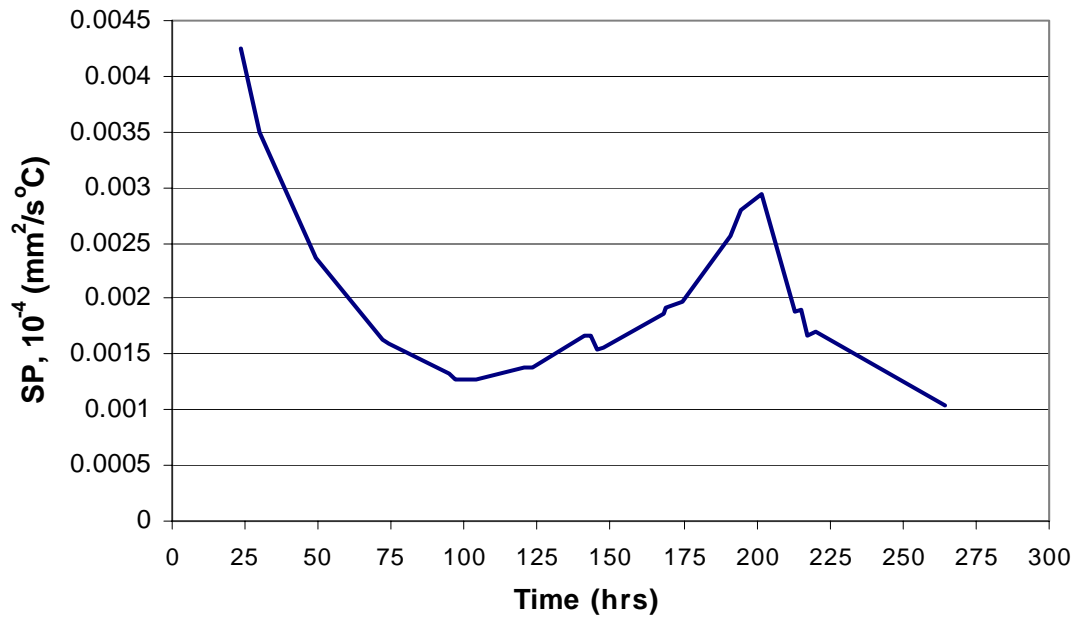


Figure B.17: Graphical illustration of calculated SP values for freezing Test #3.

Freezing Test #4

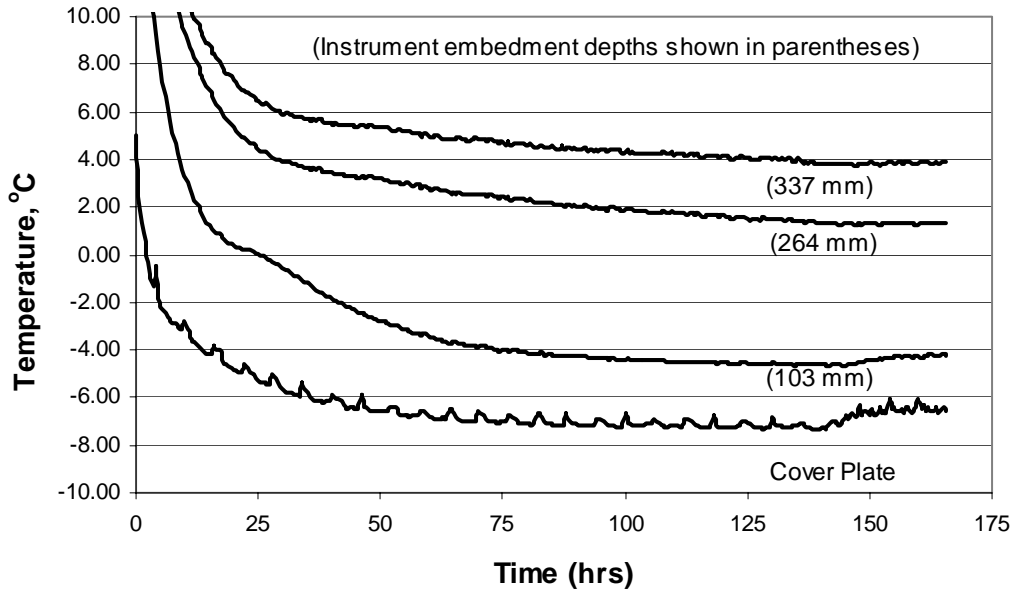


Figure B.18: Graphical illustration of temperature distributions throughout freezing Test #4.

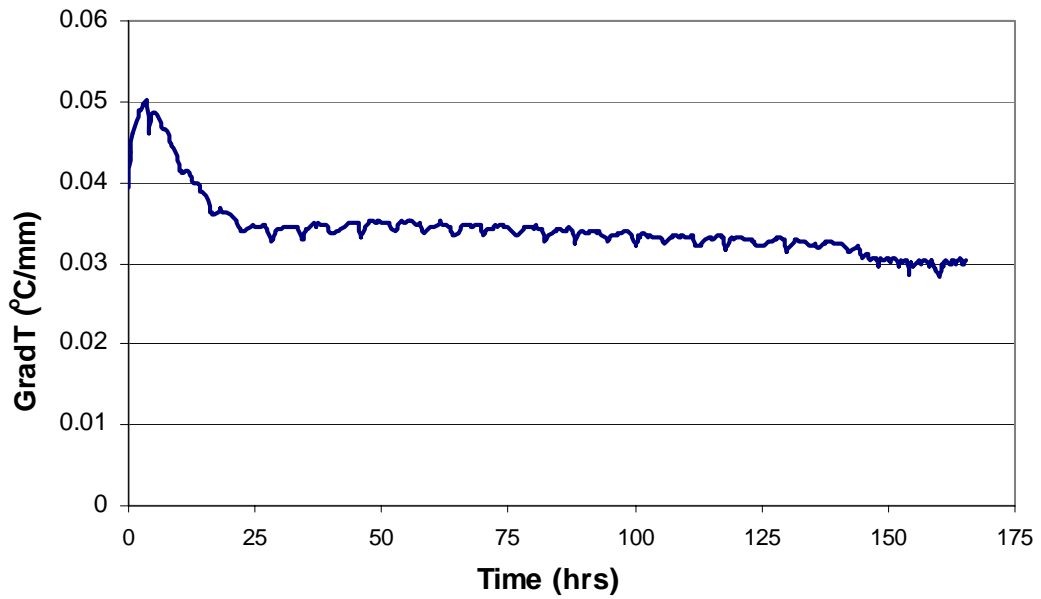


Figure B.19: Graphical illustration of overall temperature gradient throughout freezing Test #4.

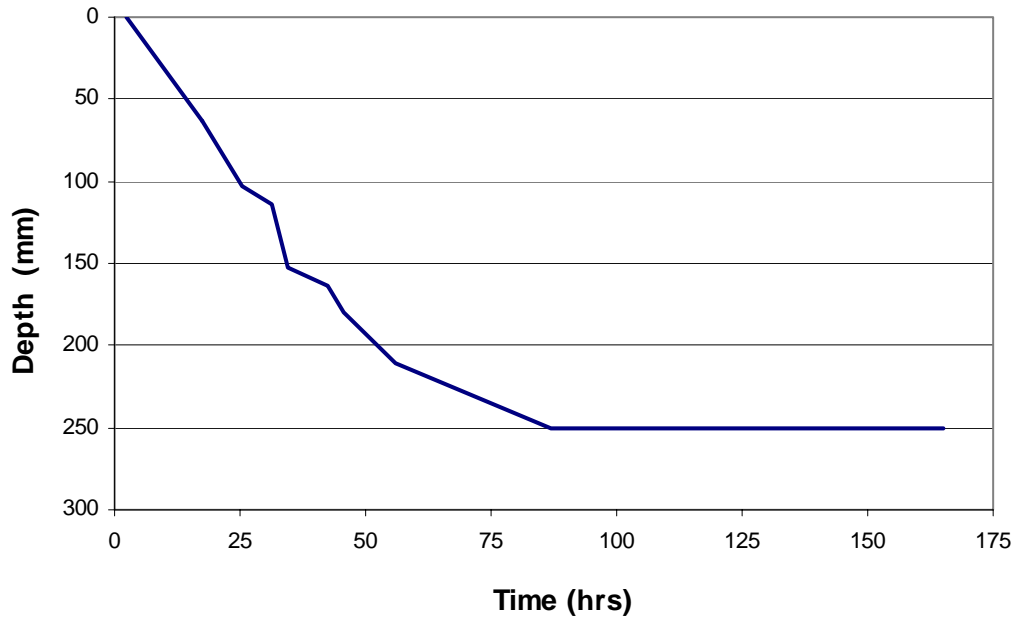


Figure B.20: Graphical illustration of the frost front location throughout freezing Test #4.

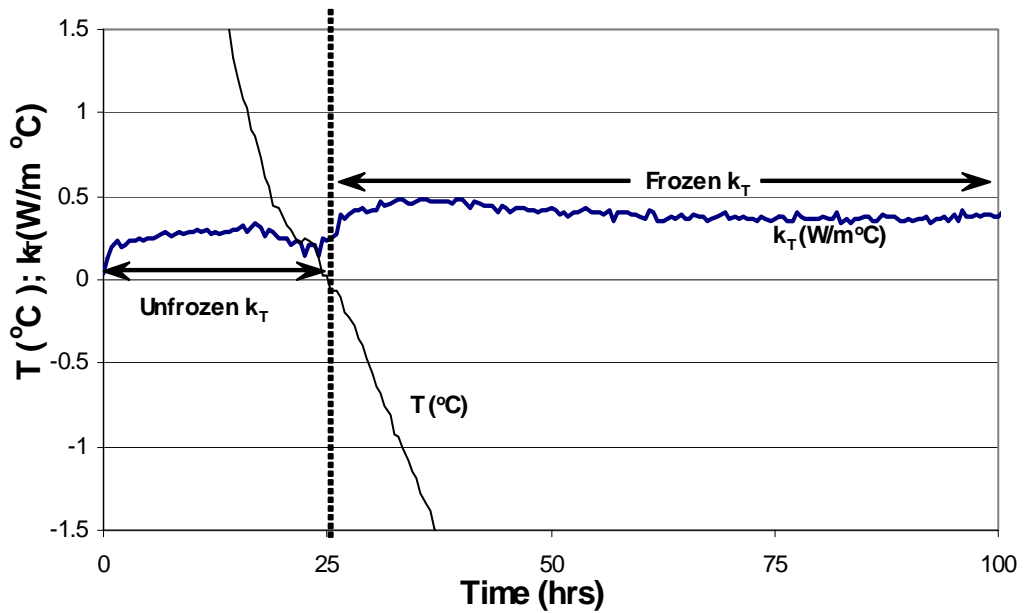


Figure B.21: Graphical illustration of calculated thermal conductivity values for freezing Test #4.

Freezing Test #5

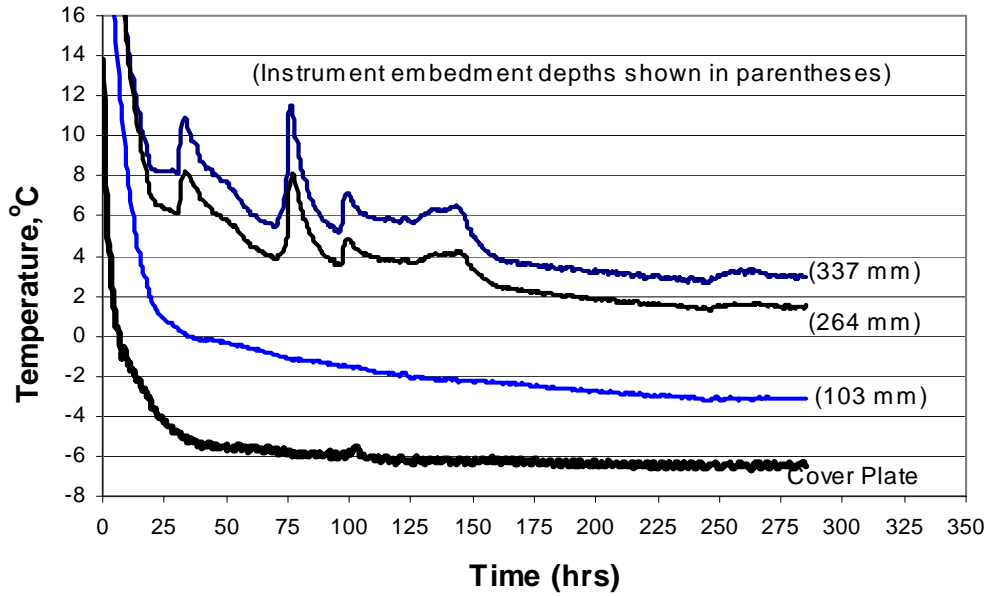


Figure B.22: Graphical illustration of temperature distributions throughout freezing Test #5.

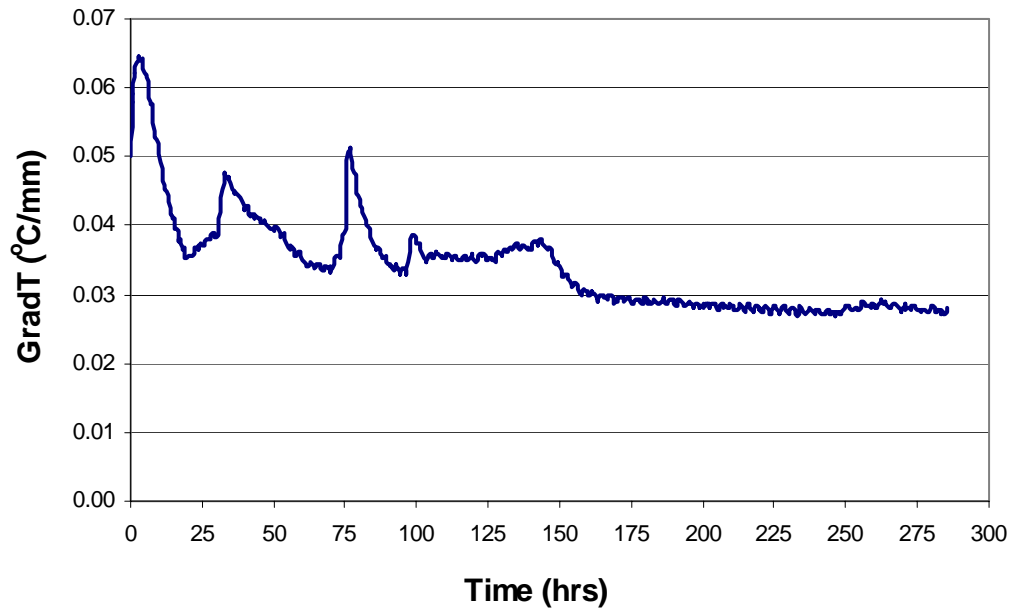


Figure B.23: Graphical illustration of overall temperature gradient throughout freezing Test #5.

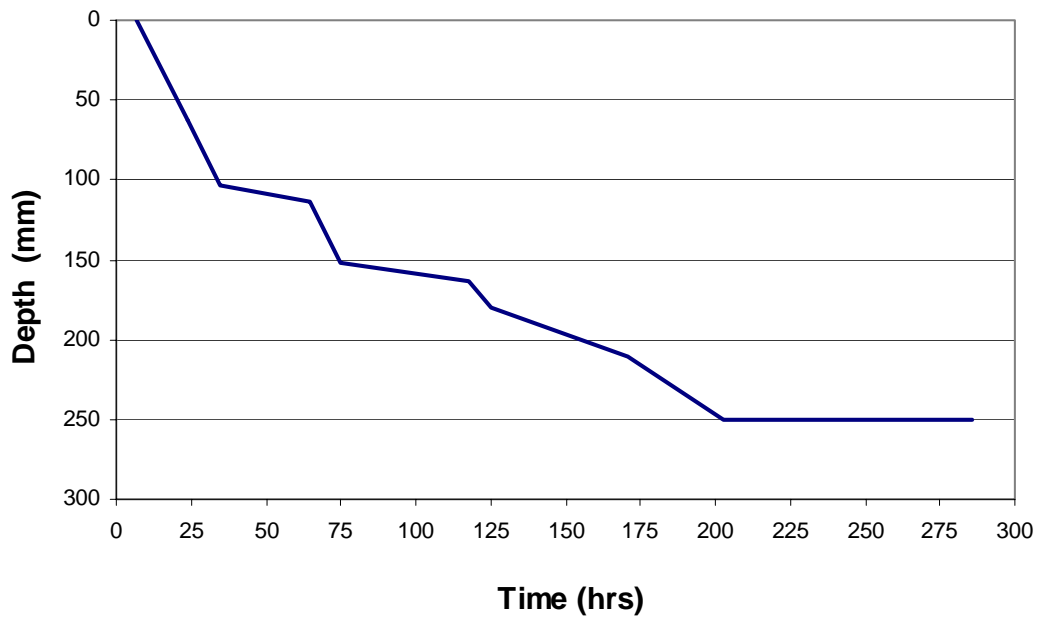


Figure B.24: Graphical illustration of the frost front location throughout freezing Test #5.

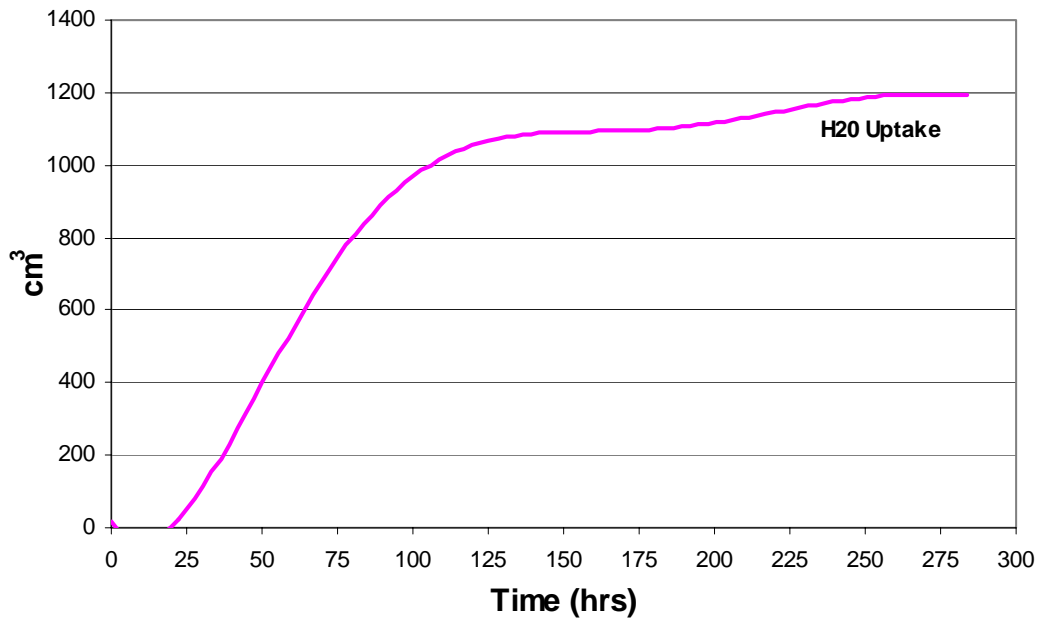


Figure B.25: Graphical illustration of volumetric heave and water uptake measurements throughout freezing Test #5.

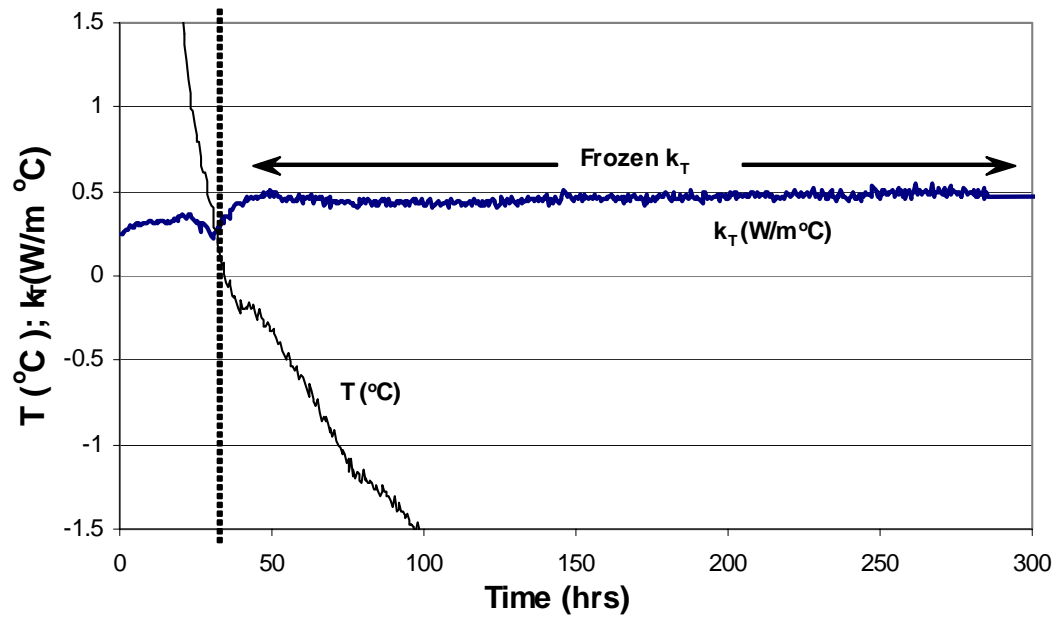


Figure B.26: Graphical illustration of calculated thermal conductivity values for freezing Test #5.

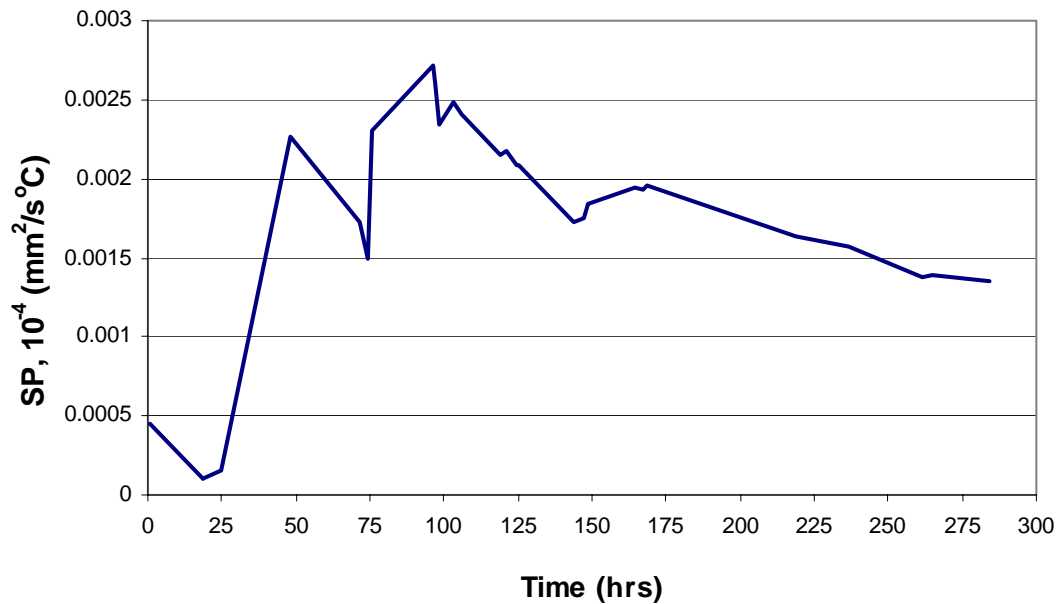


Figure B.27: Graphical illustration of calculated SP values for freezing Test #5.

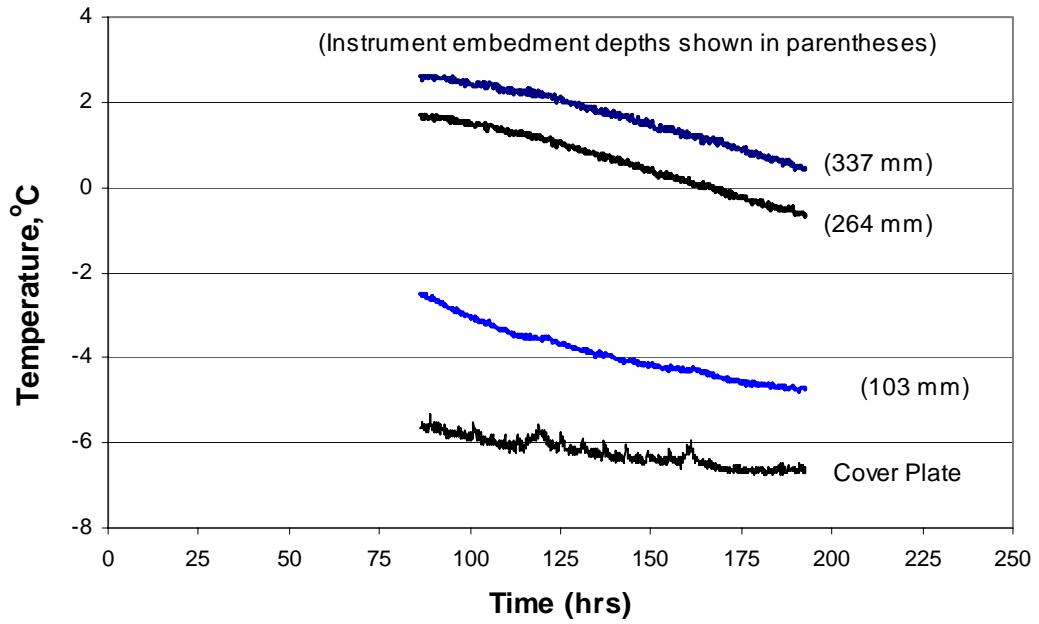


Figure B.28: Graphical illustration of temperature distributions throughout freezing Test #6.

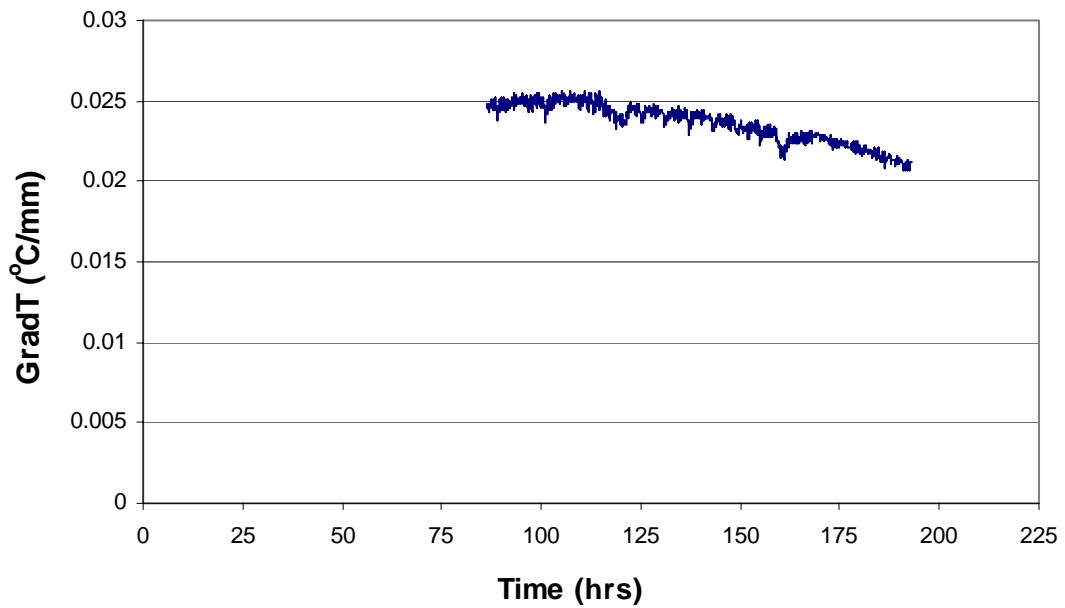


Figure B.29: Graphical illustration of overall temperature gradient throughout freezing Test #6.

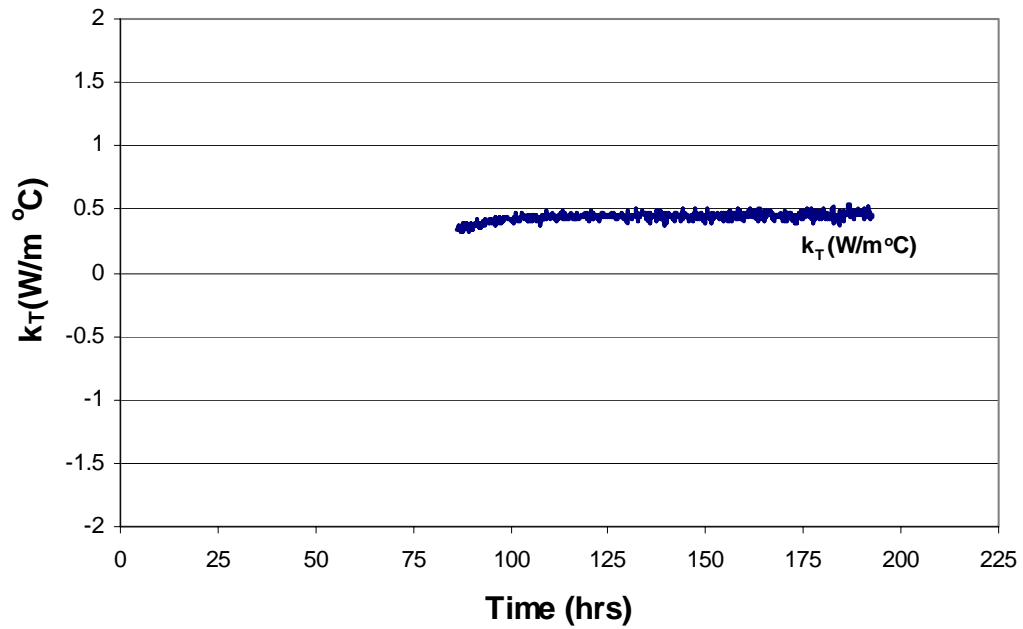


Figure B.30: Graphical illustration of calculated thermal conductivity values for freezing Test #6.

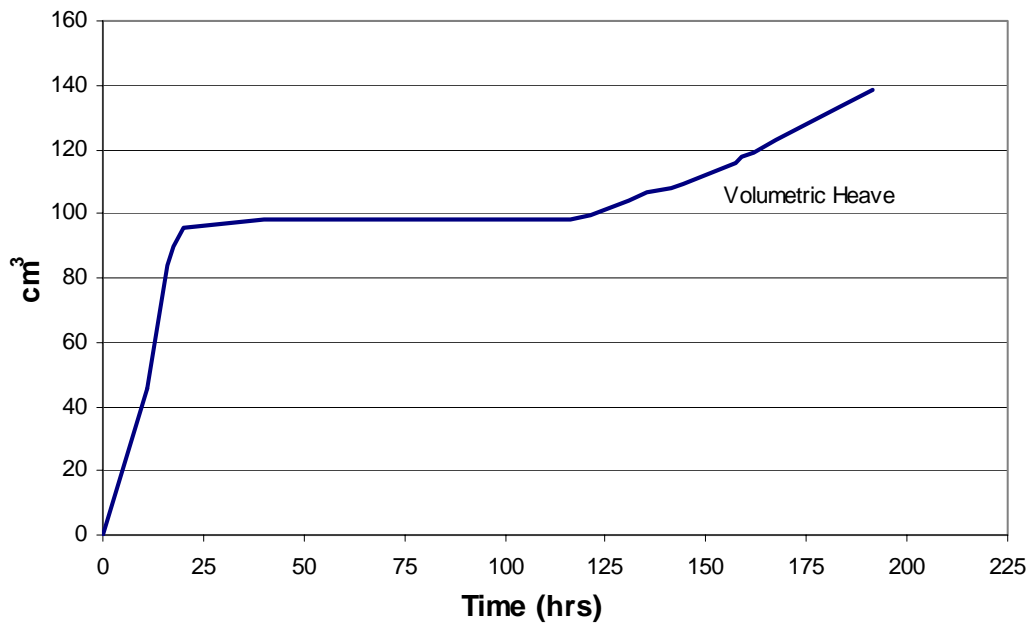


Figure B.31: Graphical illustration of volumetric heave measurements throughout freezing Test #6.

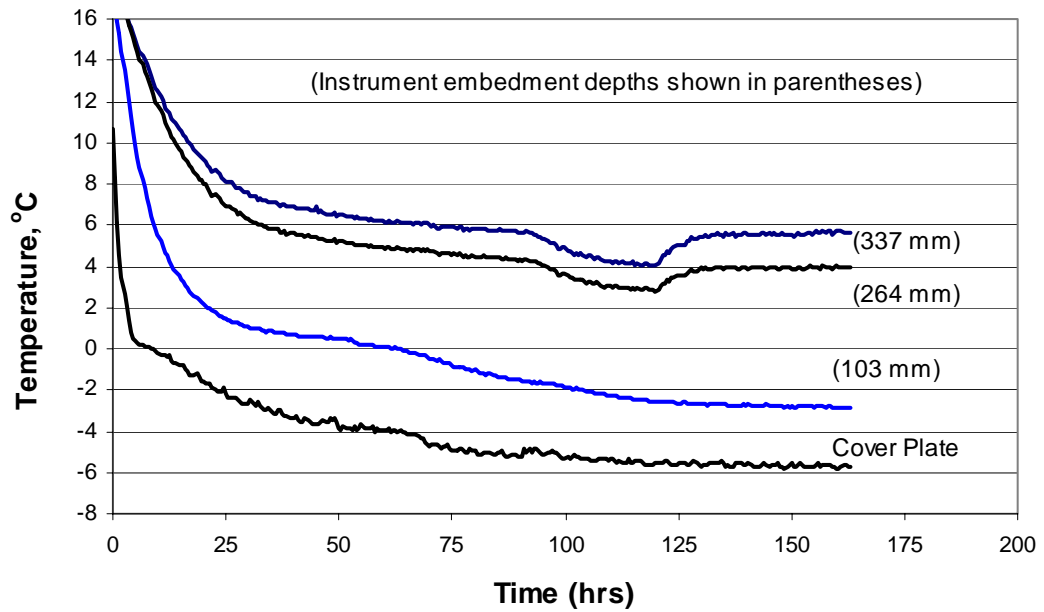


Figure B.32: Graphical illustration of temperature distributions throughout freezing Test #7).

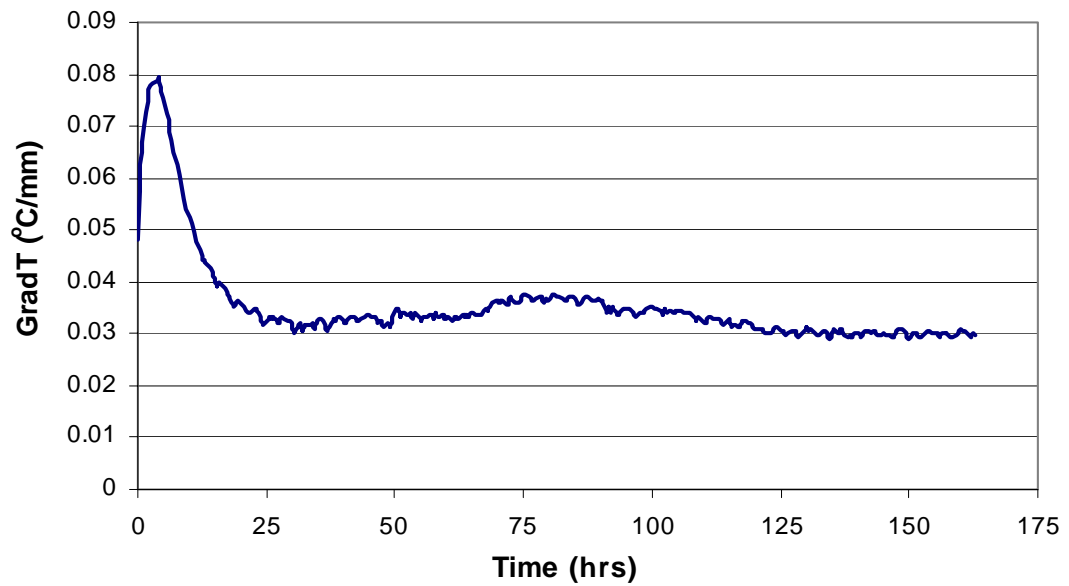


Figure B.33: Graphical illustration of overall temperature gradient throughout freezing Test #7.

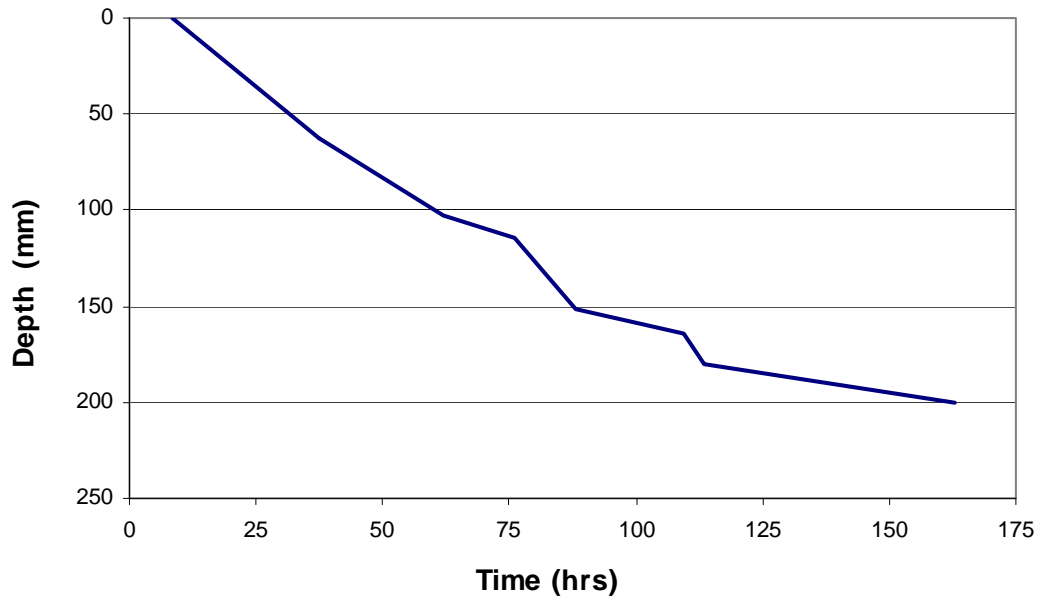


Figure B.34: Graphical illustration of the frost front location throughout freezing Test #7.

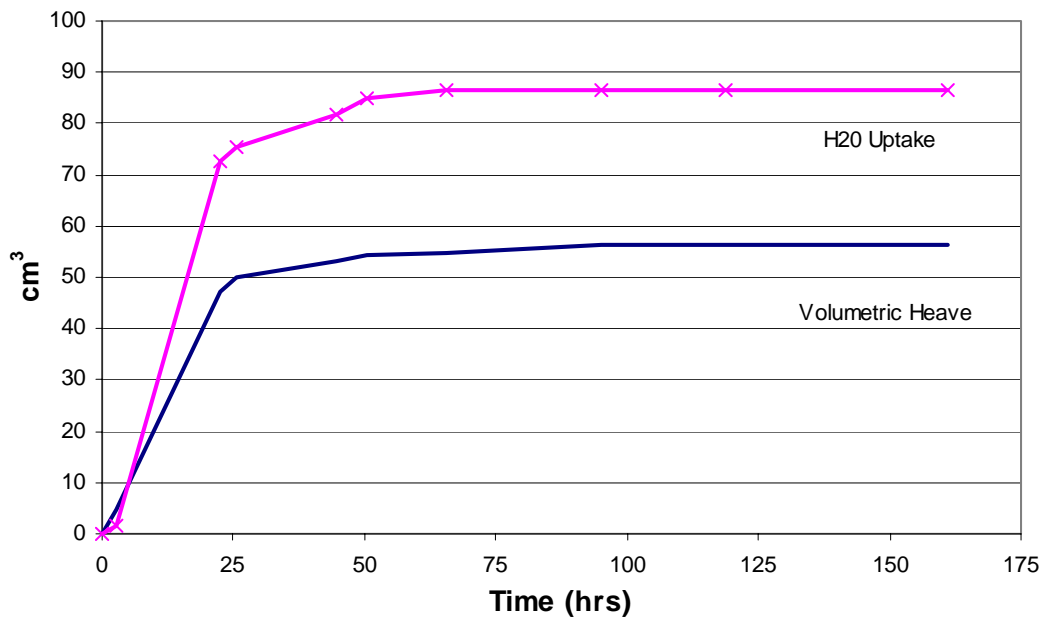


Figure B.35: Graphical illustration of volumetric heave and water uptake measurements throughout freezing Test #7.

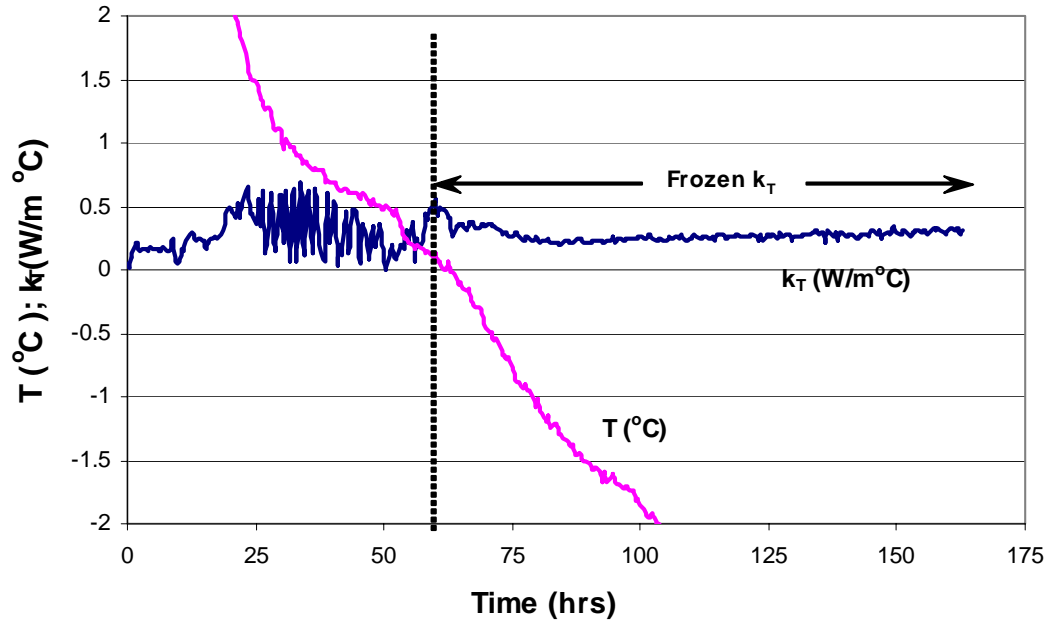


Figure B.36: Graphical illustration of calculated thermal conductivity values for freezing Test #7.

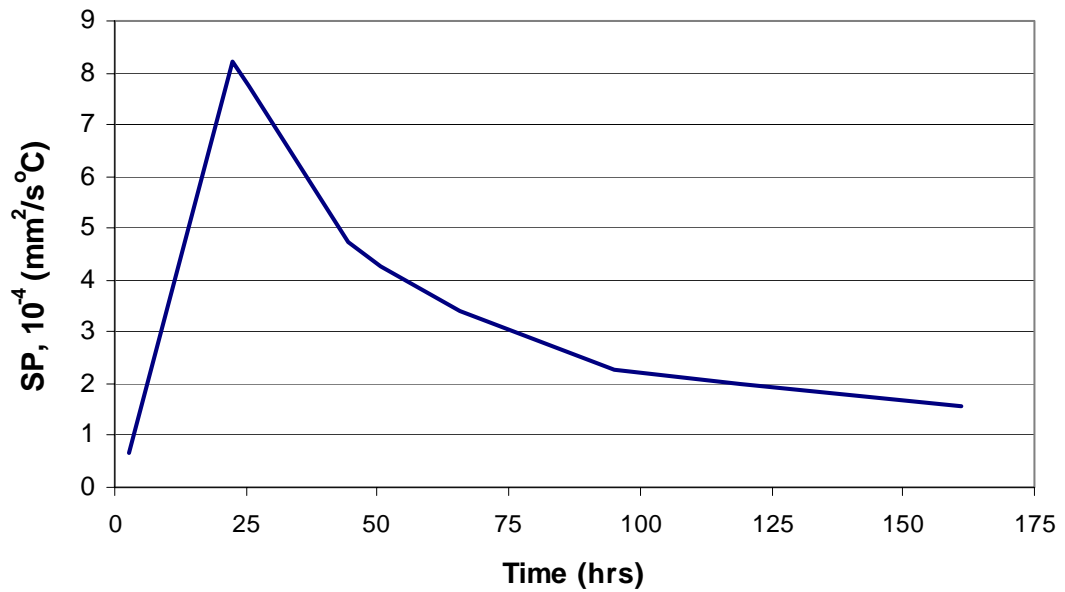


Figure B.37: Graphical illustration of calculated SP values for freezing Test #7.